DEPARTMENT OF CHEMISTRY

NOVA SCHOOL OF SCIENCE & TECHNOLOGY

CATARINA BARRADAS ANTUNES MARIA

BSc in Chemistry

EXPLORING SYNTHETIC APPROACHES OF PURINE NUCLEOSIDES AS POTENTIAL COPPER CHELATORS AND CHOLINESTERASE INHIBITORS

Dissertation for obtaining the Master's degree in Bioorganic Chemistry

MASTER IN BIOORGANIC CHEMISTRY

NOVA University Lisbon

October, 2022

NOVA SCHOOL OF SCIENCE & TECHNOLOGY

DEPARTMENT OF CHEMISTRY

EXPLORING SYNTHETIC APPROACHES OF PURINE NUCLEOSIDES AS POTENTIAL COPPER CHELATORS AND CHOLINESTERASE INHIBITORS

Dissertation for obtaining the Master's degree in Bioorganic Chemistry

CATARINA BARRADAS ANTUNES MARIA

BSc in Chemistry

Adviser: Amélia Pilar Grases dos Santos Silva Rauter
Full Professor, University of Lisbon, Faculty of Sciences

Co-adviser: Nuno Manuel Ribeiro Martins Xavier
Invited Assistant Professor, University of Lisbon, Faculty of Sciences

Examination Committee:

Chair: Luísa Maria da Silva Pinto Ferreira,
Assistant Professor, NOVA School of Science and Technology

Rapporteurs: Maria Manuel Martinho Sequeira Barata Marques,
Assistant Professor, NOVA School of Science and Technology

Adviser: Amélia Pilar Grases dos Santos Silva Rauter,
Full Professor, University of Lisbon, Faculty of Sciences

MASTER IN BIOORGANIC CHEMISTRY

NOVA University Lisbon
October, 2022

Exploring Synthetic Approaches of Purine Nucleosides as Copper Chelators and Cholinesterase Inhibitors

Dedicated to my grandmother Fernanda Alves Antunes.

ACKNOWLEDGEMENTS

First of all, I would like to acknowledge my supervisors, Professor Amélia Pilar Rauter and Professor Nuno Manuel Xavier, for giving me the opportunity to be part of this challenging project, for their guidance, for tirelessly supporting me and for being available to encourage me and to share their knowledge with me.

Centro de Química Estrutural and FCiênciasID are also gratefully acknowledge for funding my participation in several conferences this year and for always showing their availability.

I would also like to acknowledge Professor Maria João Ferreira and Professor Maria da Conceição Oliveira from Instituto Superior Técnico for their availability and interest to help me throughout this dissertation work.

I would like to acknowledge all my colleagues from the Carbohydrate Chemistry Group at Faculdade de Ciências da Universidade de Lisboa for all the support inside and outside the laboratory and for creating an amazing work environment, especially Dr. Ana Marta de Matos, Rafael Nunes, João Barros and Dr. Jaime Coelho that were always available to help and share their knowledge during this year.

To Duarte Clemente and Ana Rita Reis, I would like to thank all the support and both for the conversations about our concerns and successes during this year and for the conversations that simply helped us to relieve the stress of a day of work.

I would like to thank my friends, especially Rosana Lopes, for being by my side for the last 13 years and for always being available to listen to my concerns and to celebrate my successes, Rosana Neves, for the support and friendship even after 7 years of living 1700 km apart, and Carla Rebelo, for the support, friendship and for always having the right word to say.

Finally, I would like to thank my family, especially my sister Carolina, for staying up late with me to accompany me and cheer me up while I worked on this dissertation, and my cousin Inês, with whom I could share the experience of working on a master's thesis and for always staying by my side. I would also like to thank my grandparents, my uncles, aunts and, especially, my cousin Marta and my cats Stitch and Maui, for all the support and encouragement. At last, I would like to thank my parents for their unconditional support throughout my life, for always celebrating my successes, for all the patience to listen to my concerns and for all the efforts they made so I could follow my dreams.

ABSTRACT

Alzheimer's disease (AD), a neurodegenerative disease that is expected to affect 130 million people worldwide by 2050, is caused by multiple factors, such as the accumulation of amyloid-β (Aβ) plaques and the deposition of neurofibrillary tangles (NFT) of hyperphosphorylated tau protein, which lead to neuronal death and to a decrease of the levels of the neurotransmitter acetylcholine (ACh). The deregulation of biometals (Cu^{2+}, Zn^{2+}, Fe^{2+} and Al^{3+}) homeostasis is also characteristic of AD, being related to the formation of the aforementioned Aβ plaques and NFT. Currently, the therapeutic strategies, mainly based on treating AD patients with inhibitors of the two enzymes involved in ACh hydrolysis, namely acetylcholinesterase (AChE) and butyrylcholinesterase (BChE), were shown to have potential to promote disease modifying benefits. However, after long-term use, patients usually experience several side effects and these strategies have not been effective. Moreover, most of the single-target compounds against AD have failed in clinical trials. Some nucleosides synthesized in our group already showed potent AChE and/or BChE inhibitory activity and one has shown potential as a metal chelator. Inspired by these findings, in this dissertation, new nucleosides were prepared and tested. For the purpose, three synthetic methods were explored, including a new synthetic methodology for regio- and stereoselective preparation of nucleosides. Amongst the seven synthesized compounds, including five new nucleosides, two per-benzylated L-rhamnosylpurine nucleosides showed the most promising results, presenting metal chelation (one being a selective copper chelator and the other being a non-selective one) and potential as cholinesterase inhibitors, *in vitro*. Hence, this dissertation work opens opportunities for further research on nucleosides potential as dual- or multitarget compounds for disease modifying therapies against AD.

Keywords: Nucleosides, synthesis, cholinesterase inhibitors, metal chelators, Alzheimer's disease

RESUMO

A doença de Alzheimer (DA), uma doença neurodegenerativa que se espera que venha afetar 130 milhões de pessoas em 2050, é originada por múltiplos fatores como a acumulação de placas de amilóide-β (Aβ) e a deposição de novelos neurofibrilares (NNF) de proteína tau hiperfosforilada que levam à morte neuronal e à diminuição dos níveis do neurotransmissor acetilcolina (AC). A desregulação da homeostase de biometais (Cu^{2+}, Zn^{2+}, Fe^{2+} e Al^{3+}) trata-se também de uma característica da DA, estando relacionada com a formação das placas Aβ e dos NNF. Atualmente, as estratégias terapêuticas, principalmente focadas no tratamento de pacientes com DA com inibidores dos enzimas envolvidos na hidrólise da AC, a acetilcolinesterase (ACE) e a butirilcolinesterase (BCE), já demonstraram ter potencial para promover benefícios. No entanto, após toma prolongada, os pacientes sofrem frequentemente diversos efeitos secundários e, desta forma, estes fármacos não têm sido eficientes. Para além disso, a maior parte dos compostos de alvo único falharam em ensaios clínicos. Nucleósidos sintetizados no nosso grupo já demonstraram potente inibição de ACE e/ou BCE e um demonstrou potencial enquanto agente quelante de metais. Assim, com inspiração nestes estudos, nesta dissertação, novos nucleósidos foram preparados e testados. Para tal, três métodos sintéticos foram explorados, incluindo um novo método de síntese regio- e esterosseletiva de nucleósidos. Entre sete nucleósidos sintetizados, incluindo cinco novos compostos, duas L-ramnosilpurinas demonstraram os resultados mais promissores, apresentando quelação de metais (um sendo quelante seletivo de Cu^{2+} e outro sendo não seletivo) e potencial enquanto inibidores de colinesterase, *in vitro*. Desta forma, esta dissertação abre a oportunidade para futura investigação acerca do potencial de nucleósidos deste tipo enquanto compostos que atuam em dois ou mais alvos como terapias que modificam o desenvolvimento da doença contra a DA.

Palavras chave: Nucleósidos, síntese, inibidores de colinesterase, quelação de metais, doença de Alzheimer

CONTENTS

LIST OF FIGURES

LIST OF TABLES

LIST OF SCHEMES

LIST OF ABBREVIATIONS AND SYMBOLS

δ	Chemical shift
^{13}C NMR	Carbon Nuclear Magnetic Resonance
^{1}H NMR	Proton Nuclear Magnetic Resonance
A	Alanine
Ac	Acetyl group
ACh	Acetylcholine
AChE	Acetylcholinesterase
ACN	Acetonitrile
ACo-A	Acetylcoenzyme-A
ACP	2-acetamido-6-chloropurine
AD	Alzheimer's disease
APP	Amyloid Precursor Protein
ATOX1	Antioxidant protein-1
Aβ	Amyloid-β
Aβo	Amyloid-β oligomers
BBB	Blood Brain Barrier
BChE	Butyrylcholinesterase

Bn	Benzyl group
br s	Broad singlet
br t	Broad triplet
BSA	*N*, *O*- Bis(trimethylsilyl)acetamide
Bz	Benzoyl group
c	Concentration
CAS	Catalytic Active Site
ChAT	Choline-acetyltransferase
COSY	Correlation Spectroscopy
CTR1	Copper Transporter 1
D	Aspartic Acid
d	Doublet
DCM	Dichloromethane
dd	Double doublet
DMAP	4-dimethylaminopyridine
DMF	*N*, *N*-dimethylformamide
DMT	Disease Modifying Therapy
DMT1	Divalent Metal Transporter 1
DTNB	5,5'-dithiobis(2-nitrobenzoic acid)
E	Glutamate
***ee*AChE**	Electric eel acetylcholinesterase
***eq*BChE**	Horse serum butyrylcholinesterase
Et	Ethyl group
F	Phenylalanine
FDA	US Food and Drug Administration

FPN	Ferroportin
Glu	Glutamate
GSK3	Glycogen Synthase Kinase 3
H	Histidine
***h*AChE**	Human acetylcholinesterase
***h*BChE**	Human butyrylcholinesterase
Hex	Hexane
His	Histidine
HMBC	Heteronuclear Multiple Bond Correlation
HMDS	Hexamethyldisilazane
HRMS	High resolution mass spectrometry
HSQC	Heteronuclear Single Quantum Coherence
IC_{50}	Half-maximal Inhibitory Concentration
IUPAC	International Union of Pure and Applied Chemistry
J	Nuclear magnetic resonance coupling constant
K_i	Inhibitory Constant
L	Leucine
m	Multiplet
m/z	Mass to charge ratio
mAChR	Muscarinic Acetylcholine Receptor
MCI	Mild Cognitive Impairment
Me	Methyl
nAChR	Nicotinic Acetylcholine Receptor
NFT	Neurofibrillary Tangles
NMR	Nuclear Magnetic Resonance

OS	Oxidative Stress
PAS	Peripheral Anionic Site
PrP^C	Cellular Prion Protein
qd	Quartet of doublets
r.t.	Room temperature
ROS	Reactive Oxygen Species
S	Serine
s	Singlet
Ser	Serine
SPD1	Superoxidant Dismutase 1
t	Triplet
Tf	Trifluoromethanesulfonate group
THF	Tetrahydrofuran
TLC	Thin Layer Chromatography
TMS	Trimethylsilyl
TMSCl	Trimethylsilyl group
TNB	5-thio-2-nitrobenzoic acid
V	Valine
VAChT	Vesicular Acetylcholine Transporter
W	Tryptophan
Y	Tyrosine
ZIP	Zinc Importing Protein
ZnT	Zinc Transporter

1

INTRODUCTION

Dementia is the most prevalent neurodegenerative pathology among the elderly community. In 2015, it is estimated that there were about 45 to 50 million people living in this condition, a number that is expected to increase up to 130 million by 2050 [1].

1.1 Alzheimer's disease

Alzheimer's disease (AD) is the most common form of dementia, counting with 60 to 70% of cases of dementia worldwide [2]. AD is a neurodegenerative pathology that can be characterized by multiple factors, such as the neurons' death caused by the extracellular accumulation of amyloid-β (Aβ) plaques and by the intracellular deposition of neurofibrillary tangles (NFT) of hyperphosphorylated tau protein [2, 3]. There are more factors that contribute for this disease being, for example, the neuroinflammation, the oxidative stress, the deposition of metal ions and the neurotransmitter imbalance, namely, the acetylcholine imbalance [3].

A healthy adult brain has about a 100 billion neurons that communicate with each other, originating a 100 trillion synapses [4]. This communication is made through the release of a chemical, or, in other words, a neurotransmitter, by a neuron, that crosses the synaptic gap, and, finally, binds to the receptors of another neuron (Figure 1.1) [5].

Each of the factors above mentioned contributes, therefore, to the brain death. The extracellular accumulation of Aβ plaques and the decrease of the synthesis of acetylcholine interfere with the neuron-to-neuron communication at synapses and the abnormal forms of tau protein block the transport of nutrients inside the neurons [4].

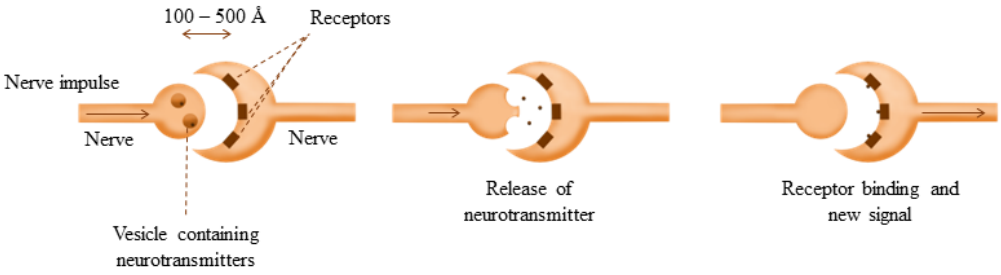

Figure 1.1. Signal transmission in a synapse (original image, inspired from [5])

Hence, these factors lead to a cellular loss that, macroscopically, is translated into a brain atrophy and a decrease on its size Figure 1.2 [4].

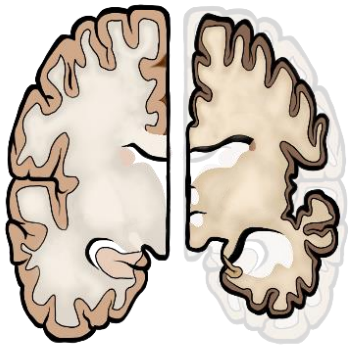

Figure 1.2. Comparison between a healthy brain, on the left side, and a brain with AD, on the right side (original image, inspired from ©*2020 Alzheimer's Association, www.alz.org. Illustrations by Stacy Jannis*)

1.1.1 Symptoms and stages of Alzheimer's disease

There are three identified stages of AD, which are distinguished by the changes in the brain and by the symptoms that result from them.

Firstly, there is the preclinical AD, a stage in which it is already possible to measure and quantify some biomarkers that might be indicative of the earliest signs of the disease [4]. AD is thought to begin 15 to 20 years before the first symptoms arise, which means that small brain changes and biomarkers appearance start years before individuals experience noticeable symptoms, namely language issues and memory loss [3, 4].

This stage is followed by the mild cognition impairment (MCI) due to AD, in which patients show evident AD biomarkers and symptoms that should not interfere with their daily life, being only noticeable to close family and friends, but not to others [4].

Finally, the most severe stage of the disease is reached, being this the dementia due to AD, which can be divided in three different stages, according to the evolution of the severity of the symptoms. The first stage is the mild stage of dementia and patients may still be able to function independently, however, they may start to require assistance in some activities. Then, the moderate stage is reached, being the longest one. Patients may lose abilities to daily life activities, such as communication, and might develop behavioral and personality changes. Finally, in the last stage, the most severe one, brain changes are evident, with the neurons involved in learning and memory as well as in movement being compromised, so that simple actions, such as talking or swallowing, become impossible, leaving patients totally dependent on external care. This condition may lead to blood clots and skin and lung infections, ultimately, leading to death [4].

1.2 Hypotheses for Alzheimer's disease drug development

As mentioned, AD is a multifactorial pathology and, as such, there are also multiple theories that seek to explain the underlying pathogenesis of this disease.

1.2.1 The cholinergic hypothesis

The cholinergic hypothesis is the oldest [6] and the clinically most popular theory related with AD [7], arising from cognitive impairment of patients that results from the loss of cholinergic neurons. This loss leads to a decrease in the synthesis of acetylcholine (ACh, Scheme 1.1), an important neurotransmitter, thus compromising the cholinergic transmission [3, 8, 9].

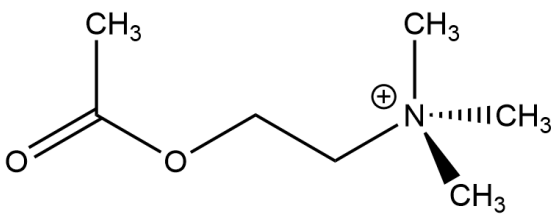

Scheme 1.1. Structure of acetylcholine

ACh is involved in several cognitive functions, such as memory, learning and attention [8, 9], being synthesized by a chemical reaction between choline and acetylcoenzyme A (ACo-A), catalyzed by choline-acetyltransferase (ChAT). The synthesis is followed by the transport of the neurotransmitter by the vesicular acetylcholine transporter (VAChT) and by its storage in synaptic vesicles. ACh is then released by the presynaptic neuron into the synaptic cleft, where it binds to its specific receptors, the nicotinic and the muscarinic acetylcholine receptors (nAChR and mAChR, respectively). Excess ACh is then degraded to choline and acetic acid through the action of acetylcholinesterase. The choline obtained after this process is transported back to the presynaptic neuron where it reacts again with ACo-A to generate ACh [9].

Synthesis, transport and reception of ACh, as well as the transport of choline back to the presynaptic neuron are represented in Figure 1.3.

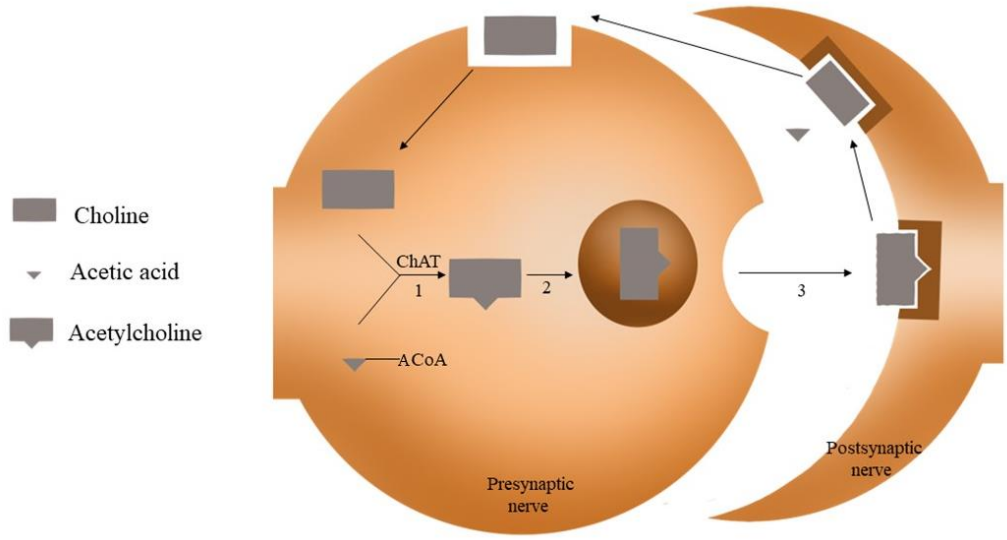

Figure 1.3. Synapse and synthesis of acetylcholine, acting as a neurotransmitter (original image, inspired from [5])

ACh may be hydrolyzed by two cholinesterases, namely, acetylcholinesterase (AChE) and butyrylcholinesterase (BChE) [7, 8].

Under normal conditions and in the early stages of AD, AChE plays the main role in the hydrolysis of ACh in the brain, with BChE showing a marginal role [7], as it is a non-specific enzyme that is mainly involved in the hydrolysis of other substrates such as the succinylcholine and the butyrylcholine [7, 8].

Unlike AChE, which is mainly located in the nervous system, BChE has a restricted neuronal distribution, being mainly synthesized in the liver and secreted into the plasma. In advanced stages of the pathology, AChE levels progressively decrease reaching about 10% of its normal values, due to the degradation of the cholinergic neurons. To compensate this loss,

BChE activity increases up to 105-165 % of the normal condition, becoming the main metabolic enzyme in the degradation of ACh [7].

Both cholinesterases have three main structural units: a catalytic active site (CAS), where the catalytic triad, consisting of the amino acid residues Serine (Ser or S), Histidine (His or H) and Glutamate (Glu or E), is found, a gorge region and a peripheral anionic site (PAS) [8, 10, 11].

In AChE, the CAS can be found at the bottom of the gorge and contains the catalytic triad S200-H440-E327 and the aromatic amino acid residues W84 and F330 (Tryptophan 84 and Phenylalanine 330, respectively). The PAS is located at the entrance of the gorge, having three amino acid residues: Y70, Y121 (Tyrosine 70, Tyrosine 121, respectively) and W279. The gorge, 20 Å deep and 5 Å wide, contains fourteen aligned amino acid residues, two of these being the F288 and the F290. These residues are constituents of an acyl pocket and are quite bulky groups that only allow the passage of ACh and other small substrates [8, 10, 11]. It is noteworthy that one AChE molecule is able to degrade about 25.000 ACh molecules per second [7]. Figure 1.4 shows the binding of ACh to the CAS of AChE.

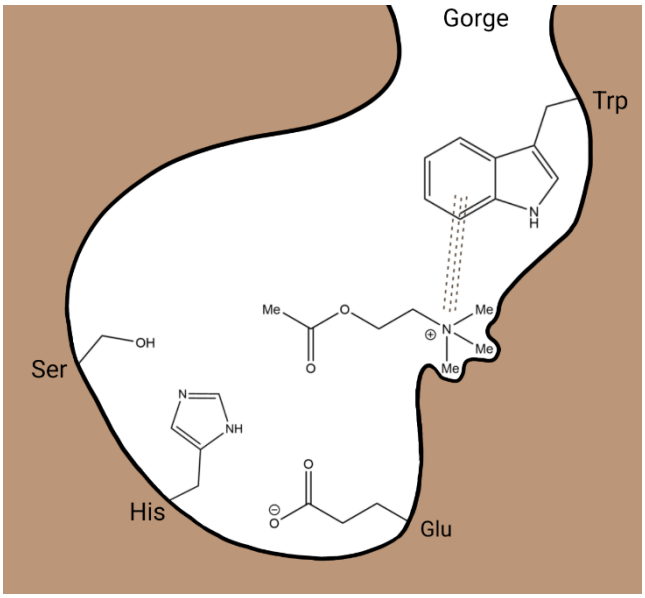

Figure 1.4. Key amino acid residues within the AChE binding site (original image, inspired from [5])

In BChE, the CAS shows a constitution similar to that of AChE, with a catalytic triad S198-H438-E325 and an important amino acid residue A328, being less bulky residue than the F330 found in AChE. In this enzyme, the gorge region has only six aligned aromatic amino acid residues and the PAS has only two, D70 and Y332. Finally, the acyl pocket has two less

bulky amino acids than those found in AChE, these being the L286 and the V288, which allow the passage of substrates larger than ACh. The aforementioned differences are probably the most important ones to explain the different substrate features of the two cholinesterases [8, 10].

By the analysis of Scheme 1.2, it is possible to understand the mechanism by which ACh is hydrolyzed by the catalytic triad. Since only amino acids serine and histidine play a role in this reaction, glutamate is not represented.

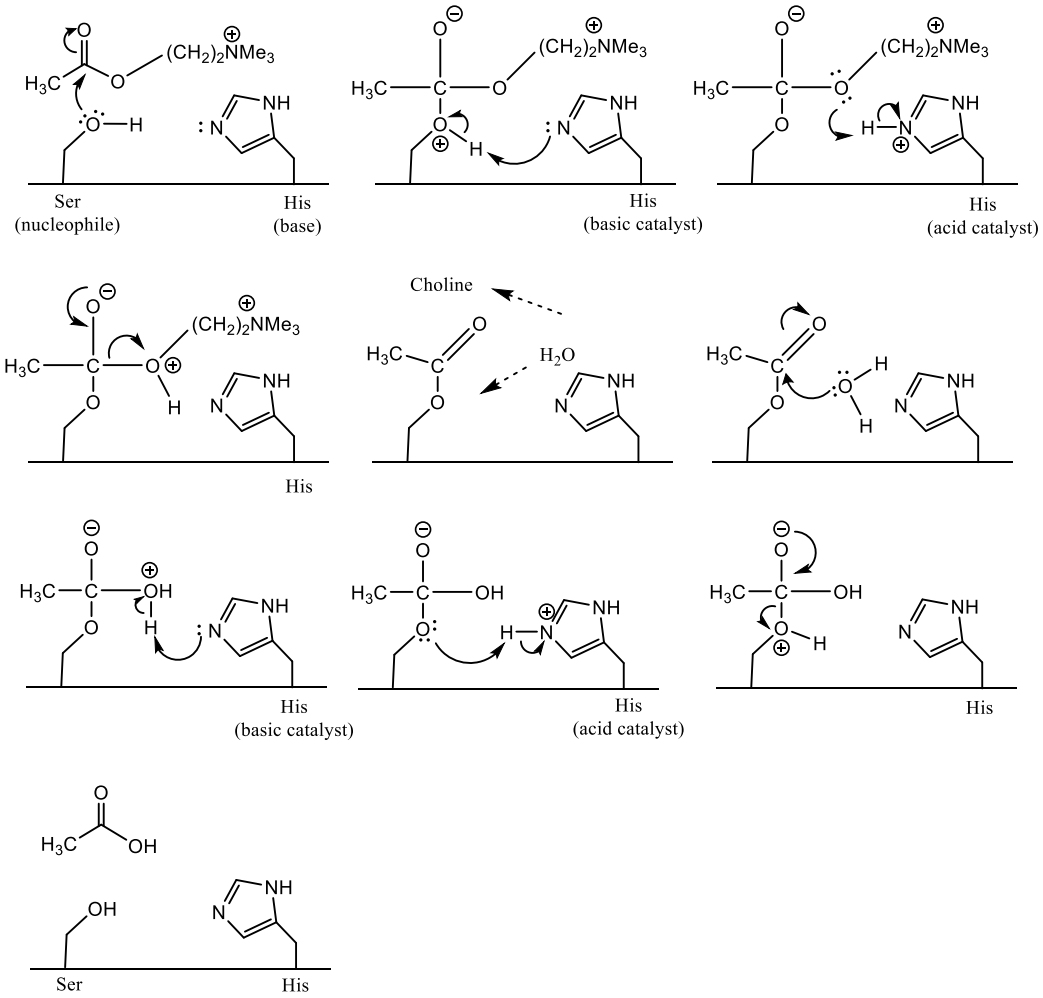

Scheme 1.2. Hydrolysis of acetylcholine by the catalytic triad

At first, after the binding of ACh to the binding site of the enzyme, Ser acts as a nucleophile and, by using a pair of unshared electrons from the hydroxy group oxygen, forms a bond with the ester of ACh, opening the carbonyl group. His then catalyzes the reaction by acting

as a base and capturing a proton, thus neutralizing the positive charge previously formed on the oxygen of Ser, making it more nucleophilic. His starts acting as an acid and promotes the protonation of the alkoxy group of the intermediate, making it a better leaving group. The oxygen negative charge delocalizes forming, again, the carbonyl group, allowing the elimination of choline, which leaves the active site and allows the entry of water that, then, acts as a nucleophile and attacks the acyl group, using the unshared pair of electrons of its oxygen, opening the carbonyl group. Histidine, again acting as a base, removes a proton from the formed ion, catalyzing the process and, in a similar way to the one already described, His returns to act as an acid, allowing the protonation of the formed intermediate, making it a better leaving group. Finally, the carbonyl group is formed, releasing the Ser residue. The formed acetic acid leaves the active site and the process can be repeated [5].

To conclude, it was possible to verify that the balanced synthesis of ACh is an important process to the maintenance of the cholinergic transmission and, consequently, for the maintenance of the healthy cognitive function. AD leads to the loss of the cholinergic neurons and, therefore, to the reduced synthesis of the neurotransmitter ACh. Hence, targeting AChE and BChE, which promote ACh hydrolysis, is an interesting strategy to overcome the symptoms related to the pathology.

1.2.2 The Aβ cascade hypothesis

Aβ cascade hypothesis was postulated in 1999 [12], describing the aggregation and the deposition of Aβ peptides as the main cause of AD [13].

Aβ peptides exist naturally in the healthy human brain, being produced in the intracellular environment and in the cell membrane and being then released into the extracellular environment [12]. In addition, healthy individuals also have antibodies against Aβ that are responsible for its elimination and for the maintenance of the balance between its production and clearance [14].

Amyloid precursor protein (APP), a transmembrane protein, under physiological conditions, is involved in important processes such as synaptogenesis, synaptic plasticity and cell survival [14].

APP can be cleaved by two pathways, the non-amyloidogenic and the amyloidogenic pathways (Figure 1.5), being the second one the origin of the pathogenic forms of Aβ [12–14]. Thus, cleavage by the amyloidogenic pathway, by the sequential action of β- and γ-secretases,

results in the generation of Aβ peptides, with lengths comprising 37 to 49 amino acids [12]. The most toxic forms are $A\beta_{1-42}$, prone to aggregation [12] and the predominant constituents of AD's characteristic plaques, although $A\beta_{1-40}$ forms are also toxic [14].

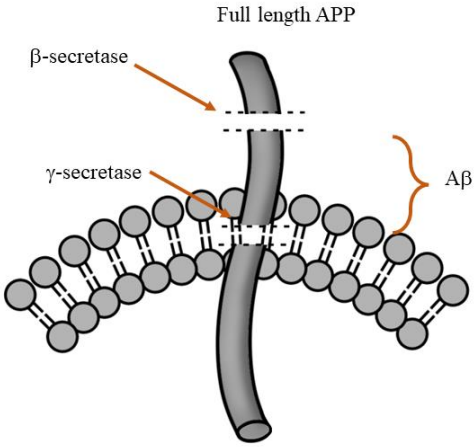

Figure 1.5. APP cleavage by the amyloidogenic pathway (original image, inspired from [15])

The two mentioned Aβ forms are the most investigated ones due to their importance in the diagnosis of AD. $A\beta_{1-40}$ remains unchanged with disease evolution, while the levels of $A\beta_{1-42}$ decrease, which may be a reflection of aggregates formation and further deposition in the brain. Hence, the ratio ($A\beta_{1-42}$/ $A\beta_{1-40}$) is a suitable marker for the plaque pathology [12].

Aβ exists in the brain of AD patients in different forms, such as monomers, oligomers, fibrils and amyloid plaques, being the oligomeric and the plaque forms the most toxic. The origin of this toxicity is not yet fully understood, however, some cellular mechanisms have been proposed [14]. The aggregation of peptides into oligomers triggers oxidative stress and induces intraneuronal phosphorylation of tau protein and its aggregation into NFT, promoting neuronal death and, consequently, the loss of synapses and ACh, leading to the cognitive decline [12].

Although this hypothesis for AD pathology contemplates the multifactorial nature of the disease, the high rate of failure (99%) obtained in clinical trials for compounds targeting the Aβ pathway makes it a controversial theory that has raised questions about the possibility of this pathway explaining the pathology by itself [13, 14].

1.2.3 The tau protein hypothesis

Due to the questions raised about the Aβ as the origin of AD, another theory was formulated, the tau protein hypothesis, in which the deposition of NFT, formed by hyperphosphorylated tau, is described as contributing to the loss of neuronal mass characteristic of AD [14].

Tau is a protein predominantly expressed in the central and the peripheral nervous systems [14], being found mainly in the axonal compartments of neurons and, to a lesser extent, in the dendrites and in the pre- and post-synaptic terminals of healthy neurons. Its main functions are the stabilization of neuron microtubules and axonal transport [16], and it can also play several other roles in physiological processes, such as myelination, neurogenesis, motor functions, learning, memory and DNA protection [14].

This protein's toxicity is associated with its abnormal forms [14, 16, 17]. Unlike Aβ, which is a unique feature of AD, toxic forms of tau, caused by post-translational mutations or modifications, can be found in a group of neurodegenerative diseases called tauopathies [14, 16]. There are different possible post-translational modifications such as phosphorylation, acetylation, methylation and isomerization that lead to conformational changes of the protein. These lead to tau's aggregation and the formation of NFT that promote synaptic dysfunction [16].

Of all post-translational modifications, phosphorylation is the most investigated one since tau deposits found in lesions of several tauopathies were hyperphosphorylated tau deposits [14].

Figure 1.6 shows the process of generation of the characteristic NFT.

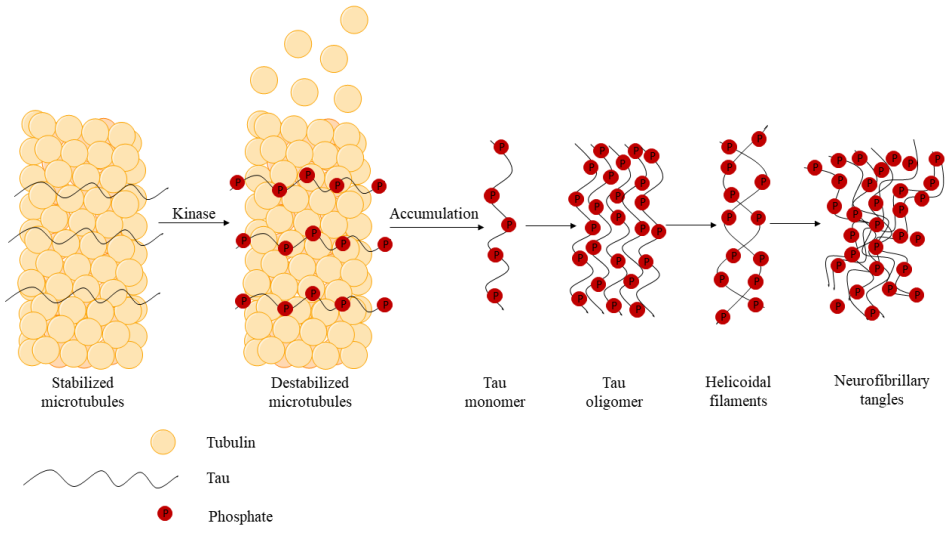

Figure 1.6. Formation of neurofibrillary tangles, caused by hyperphosphorylation of tau (original image, inspired from [17])

At first, the protein is phosphorylated at different positions by the action of kinases [17], which decreases its affinity for the microtubules [16], leading to their depolymerization [17]. Then, the accumulation of hyperphosphorylated tau monomers occur, aggregating and forming protomers. The latter aggregate, in groups of two, forming helical filaments that, in turn and at last, form the NFT [17].

The hypothesis that the aggregated form of tau is first formed in a reduced number of brain cells and that, from these, it spreads to other regions, giving rise to neurodegeneration, has become particularly relevant since it is proved that the protein proliferates and propagates between cells, however, the transmission mechanisms are still unclear [18].

1.2.3.1 The connection between the Aβ cascade and the tau protein hypotheses

Hyperphosphorylation of tau is related to the Aβ signaling pathway. Studies performed in mice models showed that Aβ accelerates the hyperphosphorylation of tau and influences its aggregation in tangles. In addition, tau protein can also mediate and increase Aβ toxicity. Thus, the peptides and the protein work in parallel and synergically, strengthening each other's destructive impact [19, 20].

There are several pathways that explain the Aβ-induced phosphorylation of tau, two of them being the glycogen synthase kinase 3 (GSK3) and the Fyn kinase pathways. After the synthesis of the Aβ peptides and their subsequent oligomerization, a high affinity binding between the oligomers and the cellular prion protein (PrP^C) occurs, triggering the transmembrane receptor mGluR5-signaling cascade that activates both GSK3 and Fyn, two kinases involved in the hyperphosphorylation of tau protein [21–25].

In Figure 1.7, there is a schematic representation of Fyn kinase pathway. This kinase is recognized as a key mediator of the neuronal damage induced by the interaction between the Aβ oligomers (Aβo) and the PrP^C, having studies shown that the genetic depletion of this kinase could prevent the induced cell death in the hippocampus and its inhibition could be able to promote restorage of the synaptic density and memory function in transgenic mice [23].

Thus, the excessive generation of Aβ, caused by the imbalance between its formation and its clearance, also induces excessive tau phosphorylation through signaling cascades and, therefore, Aβ, Fyn, GSK3 and tau could all be considered as potential drug targets for the AD cure research.

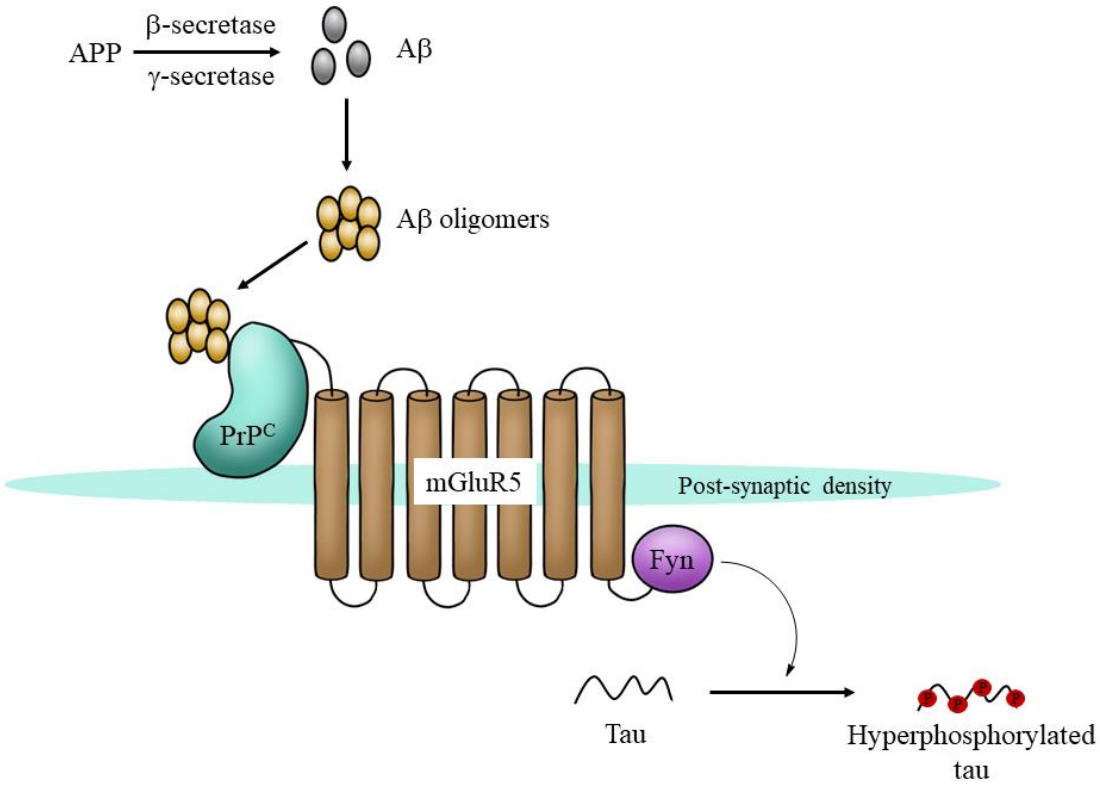

Figure 1.7. Tau hyperphosphorylation via Fyn kinase pathway (original image, inspired from [22])

1.2.4 The oxidative stress and the biometal hypotheses

In living organisms, the oxygen molecule, O_2, can be converted to reactive oxygen species (ROS), which can be partially reduced [superoxide radical ($O_2^{\cdot-}$)], hydrogen peroxide (H_2O_2) and hydroxyl radicals ($OH^{\cdot}$)] or excited [singlet oxygen ($^1O_2$)] forms that have the ability to rapidly oxidize proteins, lipids and the DNA [26]. The state in which there is an imbalance between ROS production and the cellular mechanism that allows the reduction of their destructive impact, namely, the action of antioxidant defenses, is called oxidative stress (OS) [27–29].

OS has been reported as a crucial event in AD. In the stage of MCI due to AD, there is an extensive oxidative damage, which suggests that OS is an early event in the progression from the normal aging to the AD pathology, with neurons being particularly vulnerable cells to the damage caused by the action of ROS [7, 28 ,29].

There are several mechanisms that might induce OS, being the deregulation of the homeostasis of biometals, namely copper, zinc and iron one of them. Under normal conditions,

the blood-brain barrier (BBB) regulates the concentration of these metals, however, in AD patients, their levels were found significantly increased [7, 27]. These biometals can be found in the core and the rims of senile plaques and are co-located with Aβ. Thus, by interfering with these biometals' homeostasis, in other words, by inducing an alteration in their baseline, the production of free radicals occurs and also the induction of Aβ aggregation and of tau hyperphosphorylation and aggregation [28, 30].

The production of oxidizing agents increases the expression of APP and the action of β- and γ-secretases, thus increasing the intracellular and secreted levels of Aβ. In turn, Aβ reduces Fe^{3+} and Cu^{2+}, inducing the production of H_2O_2, contributing to the OS [28].

The connection between Aβ and OS is represented in Figure 1.8.

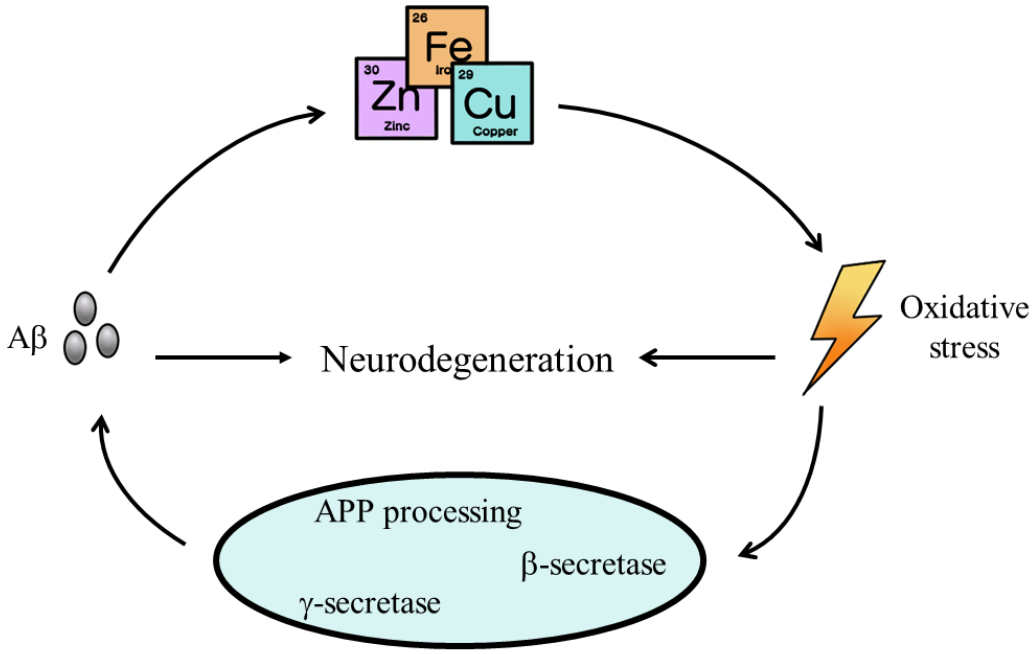

Figure 1.8. Connection between Aβ and OS (original image inspired from [28])

1.2.4.1 Copper

Copper is an essential micronutrient, playing an important role in several metabolic processes and being necessary for the Superoxidant Dismutase 1 (SPD1), a vital cellular antioxidant [30]. It is also a redox-active metal with greater relevance in the induction and in the increase of OS, due to the two copper binding sites on the Aβ plaques (Figure 1.9), which promote the production of ROS [30–32].

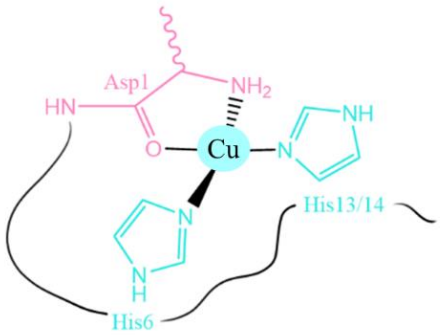

Figure 1.9. Copper (II) binding site in Aβ (original image, inspired from [31])

The role of copper in AD is shown in Figure 1.10. It is possible to verify that the copper divalent ions, Cu^{2+}, enter the cell through the divalent metal transporter 1 (DMT1), while the monovalent ions, Cu^{+}, penetrate the cell membrane via copper transporter 1 (CTR1). By the action of the antioxidant protein-1 (ATOX1), Cu^{+} is imported into synaptic vesicles that facilitate its exit from the cellular environment, through vesicle fusion, where it interacts with Ab, generating Cu^{+}-Aβ extracellular complexes. In turn, excessive Cu^{2+} levels activate the Fenton-like reaction and oxidize biomolecules, generating ROS. In addition, these ions can activate the GSK3 kinase, inducing tau hyperphosphorylation, and can interact with APP, inducing the excessive production of Aβ and, consequently, its aggregation in senile plaques [33].

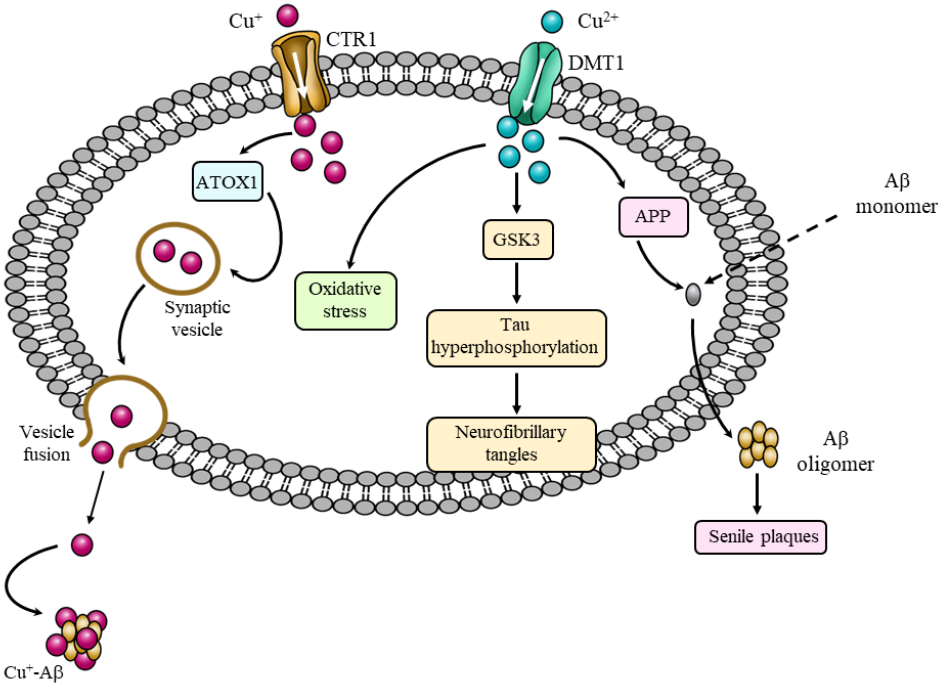

Figure 1.10. The role of copper in AD (original image, inspired from [33])

1.2.4.2 Zinc

Zinc, like copper, supports SOD1 [30] and binds to a binding site of Aβ (Figure 1.11) [31].

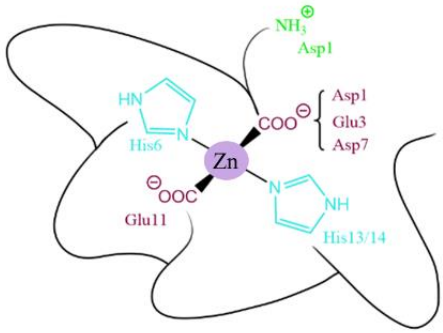

Figure 1.11. Zinc (II) binding site in Aβ (original image, inspired from [31])

The entry of divalent ions, Zn^{2+}, into the plasma membrane is carried out through the zinc importing protein (ZIP), while its efflux is regulated by the zinc transporter (ZnT) [33]. There are negative consequences for either excess or lack of zinc ions in the brain. First, excessive concentrations of Zn^{2+} can inhibit APP cleavage via the non-amyloidogenic pathway, resulting in an excessive processing of APP by β- and γ-secretases, thereby increasing Aβ production. In addition to increasing the production of these peptides, the ions promote the aggregation and stabilize the toxic oligomers generated, both *in vitro* and *in vivo*. Like copper, zinc ions activate GSK3's activity [34] and induce the production of ROS [33]. Furthermore, the lack of Zn^{2+} leads to synaptic dysfunction and reduces Aβ clearance [33] and, therefore, leads to an increase in Aβ concentration in the brain (Figure 1.12).

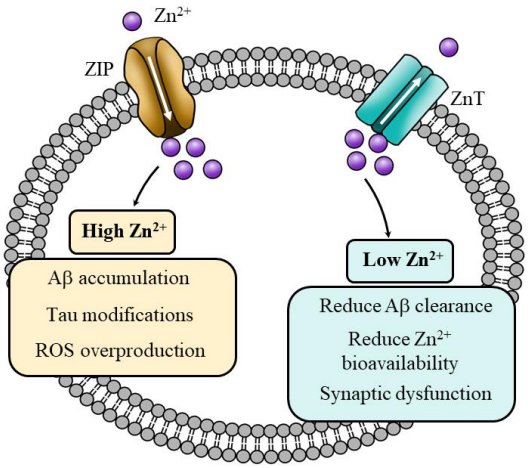

Figure 1.12. The role of zinc in AD (original image, inspired from [33])

Molecules designed to chelate copper and zinc ions from Aβ promoted its solubilization and, therefore, reduced its deposition, in mice models [30].

1.2.4.3 Iron

Iron, in normal levels, is involved with several vital neuronal functions, namely, the synthesis of myelin and the cellular respiration [33].

In AD patients, there is an overload of iron in different areas of the brain, being the divalent ion form, Fe^{2+}, the one with most toxicity. These ions pass the cell membrane through the DMT1 and leave via iron exporter ferroportin (FPN). In excessive levels, they stimulate the Fenton reaction, generating hydroxyl radicals that result in OS. Moreover, Fe^{2+} induces the formation of NFT by activation of GSK3 [33] and increases Aβ production (Figure 1.13) [30].

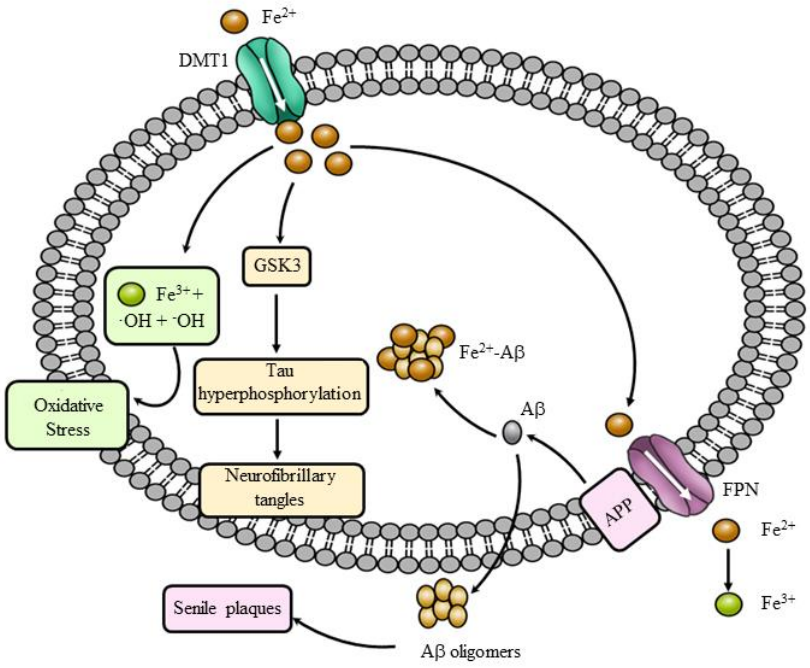

Figure 1.13. The role of iron in AD (original image, inspired from [33])

1.2.4.4 Aluminum

Aluminum is a metal with evident associated neurotoxicity and has been related to behavioral changes, when in chronic exposure. Furthermore, it has been studied due to its connection to AD. Studies have revealed that aluminum, under the ionic form Al^{3+}, may induce the aggregation of Aβ and its accumulation and also activate GSK3. In addition to activating the mechanism that leads to the achievement of two essential characteristics of AD, it is co-located with them, suggesting the formation of complexes with Aβ and tau [34].

1.3 Alzheimer's disease treatment

AD is a devastating disease that does not yet have an efficient treatment. Finding a therapy that prevents or delays and slows down the progression of the disease and, at the same time, allows the improvement of the symptoms is therefore necessary [35].

Until 2021, therapeutic strategies focused only on the disease's symptomatic relief through AChE and BChE inhibitors (donepezil, rivastigmine and galantamine) and through a modulator of the *N*-methyl-D-aspartate receptor (memantine), since, until then, most attempts to obtain a disease modifying therapy (DMT), targeting tau and Aβ, had failed [1, 13, 35].

In order to block tau's aggregation, stabilize microtubules and manipulate kinases and phosphatases responsible for tau's post-translational modifications, several vaccines have been tested, however, most of them failed in clinical trials. There are currently four vaccines in phases I and II of clinical trials, these being ADDvac and AC125, as active vaccines, and RG6100 and ABBv-8E12, as passive vaccines [36].

Targeting Aβ, as already mentioned, there is a 90% failure rate, however, on June 7, 2021, Aducanumab was approved by the US Food and Drug Administration (FDA) as the first disease-modifying therapy (DMT), this being a monoclonal antibody of Aβ, with a view to its clearance. This drug's approval was carried out through an accelerated regulatory mechanism based on amyloid plaque lowering that was considered reasonably likely to predict benefit, which was a decision that gave rise to controversy. A randomized controlled clinical trial will be conducted and should be complete by 2030 [13, 35, 36].

In 2020, a set of specific copper chelators was synthesized in order to regulate the copper homeostasis in the brain and to inhibit the damage from the OS caused by copper-amyloid complexes. The oral treatment with one of these compounds, TDMQ20, was able to fully reverse the cognitive and the behavioral impairments in different murine models representing the early and the more advanced stages of AD [37].

There are currently 143 agents being evaluated in 172 clinical trials, 83.2% of which being DMTs and 16.8% being agents for symptomatic treatment targeting cognitive enhancement and intending to treat neuropsychiatric behavioral symptoms [36].

1.3.1 Donepezil

Donepezil (Scheme 1.3) is the most effective and the best tolerated AD drug, having been approved by the FDA in 1996, to relieve AD symptoms in all stages, particularly, in the mild and the moderate stages [3, 38–40].

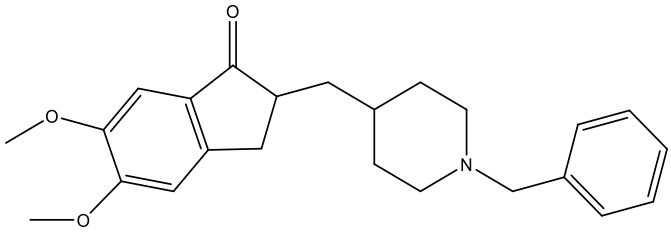

Scheme 1.3. Structure of donepezil

Being a selective AChE inhibitor, the benzyl group in its structure interacts with the enzyme's CAS and the dimethoxy indanone part interacts with its PAS, thus inhibiting its activity. This drug also shows activity against the neurotoxicity induced by the Aβ oligomers and against the effects of OS in mice models [7].

Despite being well-tolerated and safe in a wide range of concentrations, it is associated with several side effects, mainly, gastrointestinal disorders [41]. Donepezil has favorable pharmacokinetic properties, namely its long half-life of approximately 70 hours and its slow clearance, which allow the drug concentration to remain stable during the day with a single daily intake. It is metabolized in the liver through the action of cytochrome P450 3A4 enzymes and excreted in a percentage of 80% of the administrated dose by the kidneys, being the remainder eliminated by biliary excretion [39].

Moreover, the drug has hydrophilic properties that make it difficult to penetrate the BBB and, in addition, studies suggest that the beneficial effects that come from the treatment with donepezil only last between 6 to 12 months [7, 41], therefore, a study of possible alteration of its structure that allow an increase in its concentration in the brain and an increase in the longevity of its therapeutic effects is necessary.

1.3.2 Rivastigmine

Rivastigmine (Scheme 1.4) is a drug approved in 2000 by the FDA [3] for the treatment of mild to moderate stages of Alzheimer's and Parkinson's diseases, being a pseudo-irreversible inhibitor of the activities of AChE and BChE [42]. The drug is a small molecule, with lipophilic and

hydrophilic properties, developed for administration through a transdermal patch. It can also be administered orally, however, the transdermal route is preferred since the drug avoids the gut cholinesterases, increasing its bioavailability [43]. Additionally, the administration by this route is smooth and continuous and the incidence of side effects is lower [44].

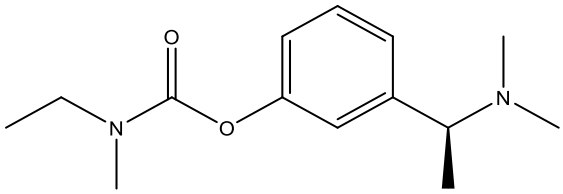

Scheme 1.4. Structure of rivastigmine

Once absorbed, this drug exhibits a behavior similar to that of ACh, binding to AChE and undergoing hydrolysis, however, after this step, it does not immediately dissociates, leaving the esteratic site, where the catalytic triad is found, carbamylated, inhibiting its action [42]. The compound is then rapidly metabolized to its inactive metabolite NAP 226-90 (Scheme 1.5), via cholinesterase-mediated decarbamylation, and has a short half-life of about 1 hour. Finally, the drug is eliminated, under the metabolite form, via renal excretion [42, 43].

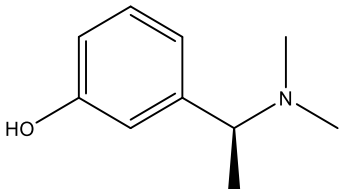

Scheme 1.5. Structure of NAP 226-90

Rivastigmine is a well-tolerated and safe drug that offers several benefits to AD patients, such as the appetite regulation, since lack of appetite affects 50 to 70% of patients and leads to weight loss [44]. Furthermore, studies have shown that starting this drug's administration after, for example, the loss of efficacy or tolerance to donepezil may offer benefits, possibly due to the fact that it is a dual cholinesterase inhibitor [42].

1.3.3 Galantamine

Galantamine (Scheme 1.6) is an alkaloid from the family *Amarylidaceae* that was approved as an AD drug by FDA, in 2001 [45, 46]. This compound is a selective, competitive, reversible and long-acting AChE inhibitor [47–49], interacting with the anionic subsite and the aromatic gorge [7] and having been originally developed for the treatment of mild to moderate AD, however,

it was already shown that it could improve cognition in patients with severe stage AD, by promoting neurogenesis in the hippocampus region [46, 47].

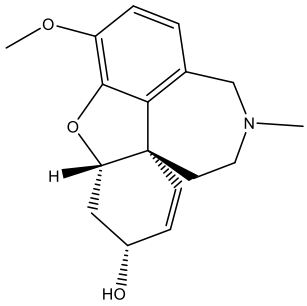

Scheme 1.6. Structure of galantamine

Although the inhibition mechanism of ACh degradation by galantamine is not known yet [46], it is known that it is well-tolerated and safe for the recommended doses [45], however, it seems to cause more side effects than the other cholinesterase inhibitors [7]. Moreover, this compound is not only able to improve cognitive and behavioral symptoms, but it may actually have disease-modifying properties due to its neuroprotective effects, such as the delay of the production of Aβ plaques, showing inhibitory activity of AChE and activity as an allosteric modulator of the nAChR [47–49].

1.4 Cholinesterase inhibitors: connection to AD hypotheses and neuroprotective effects

As aforementioned, cholinesterase inhibitors have been approved for AD's symptomatic treatment, nonetheless recent studies have shown that the long-term use of this drugs may lead to disease-modifying benefits [50].

Although there is a decrease of the AChE activity in AD brains, its levels seem to be increased around the Aβ plaques and in tangle-bearing neurons [51]. Thus, this enzyme, in addition to its cholinergic functions, has been associated with the AD plaques for inducing and accelerating the Aβ fibril formation and for forming AChE-Aβ complexes that are highly toxic, triggering neurodegeneration both *in vitro* and *in vivo* [52, 53]. This effect has been associated with the PAS of the enzyme, specifically, with its amino acid residue W297 and, as such, it was shown to be sensitive to drugs that blocked this site of the enzyme [52]. Moreover, BChE may also be related to the Aβ plaques accumulation, since studies showed that when the BChE gene is knocked out in AD mouse models, a reduction in fibrillar Aβ plaque deposition occurs [54].

Donepezil, rivastigmine and galantamine already showed action against several targets and pathways involved in the AD pathology, thus promoting neuroprotection. Several studies conducted in cell cultures, animal models and AD patients showed that the three cholinesterase inhibitors were able to promote neuroprotection, to reduce the Aβ deposits and to enhance cognitive and behavioral functions. Moreover, these drugs showed neuroprotective effects against GSK3 activity, a tau hyperphosphorylation inducer. In addition, the treatment of rat cortical neuron cultures with donepezil showed protective effects against ischemic damage while the treatment with rivastigmine and galantamine did not promote the same effects. *In vitro*, the pre-treatment with donepezil has protected endothelial cells against damage induced by hydrogen peroxide and, in neuronal cultures, galantamine promoted protective effect against oxidative damage. Furthermore, other studies demonstrated that the three compounds could promote neuronal differentiation and neurite outgrowth, both *in vitro* and *in vivo* [8].

Hence, although AChE and BChE inhibitors are not developed to promote a DMT, focusing only on relieving AD symptoms, they still have the ability to promote this type of benefits, acting on several targets and thus promoting neuroprotection and neurogenesis, being, for this reason, relevant compounds in the study of the AD treatment.

1.5 Purine nucleosides, Alzheimer's disease and objectives

Purine nucleosides (Figure 1.14) are highly functionalized molecules that are essential in diverse biological events, namely the nucleic acid synthesis, the cell division and signaling and the metabolism [51–53].

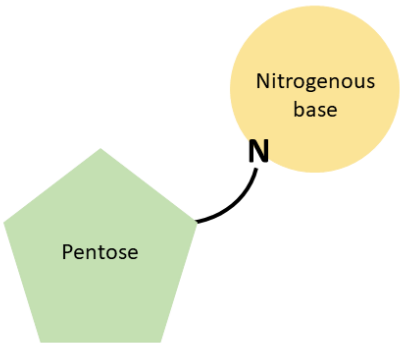

Figure 1.14. General structure of a purine nucleoside

1.5.1 Nucleoside analogues as pharmaceutical agents

The DNA structure, discovered in the 1950s, has attracted the attention of researchers to nucleosides, these being the starting compounds for the synthesis of nucleotides (Figure 1.15) and both, thorugh processes of polymerization and phosphorylation, being transformed into nucleic acids, DNA and RNA [54, 55]. In the 1960s, the idea of native nucleoside analogues, such as, for example, uridine, guanosine and adenosine analogues, inhibiting viral replication, has arisen and multiple libraries of these compounds have been synthesized [58], becoming indispensable for the treatment of different health complications. These compounds have been considered as the cornerstone of antiviral therapies against herpesviruses, HIV, hepatitis viruses [60], and various types of cancer.

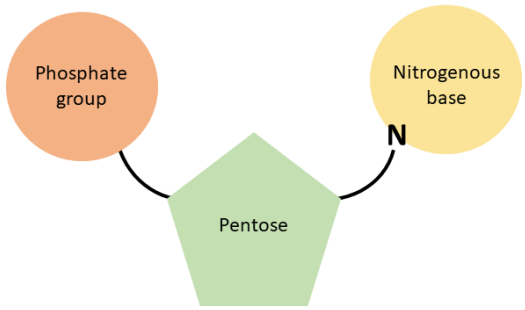

Figure 1.15. General structure of a nucleotide

As antiviral therapies, these compounds have caused an early stop of the hepatitis B virus replication and sofosbuvir (Scheme 1.7), an uridine nucleotide prodrug, was one the most successful discoveries for the treatment of the hepatitis C virus (HCV), the most relevant cause of chronic liver disease in the world. The approval of direct-acting antivirals, including sofosbuvir and other nucleoside/nucleotide analogues revolutionized the treatment of HCV infections, providing the possibility of almost all patients being cured as these are highly effective and well tolerated, with few or none side effects [61]. More recently, for the infections caused by SARS-CoV-2, the RNA virus that originates COVID-19, remdesivir (Scheme 1.7), a modified adenosine *C*-nucleotide, was the first FDA approved drug for the treatment of this disease and, currently, molnupiravir (Scheme 1.7), another nucleoside analogue, is approved by the FDA for the emergency use for the treatment of adults in risk of severe progression of the disease [59, 61, 62].

The antimicrobial resistance, another major threat to public health, is a growing problem that urgently needs the investigation of new antimicrobial drugs. Therefore, nucleoside/nucleotide analogues, playing essential roles in the cellular metabolism, also show capability of

targeting different enzymes, including the ones that are involved in bacterial peptidoglycan biosynthesis and in fungal chitin biosynthesis [64]. Furthermore, these analogues have shown efficacy against cancer diseases, which lead millions of people worldwide to death. There are currently 15 FDA and European Medicines Agency approved anticancer nucleoside analogues, such as, for example, cytarabine (Scheme 1.7), the first approved nucleoside against acute myeloid leukemia which led to an increase of the research of these compounds as antitumoral therapies [65].

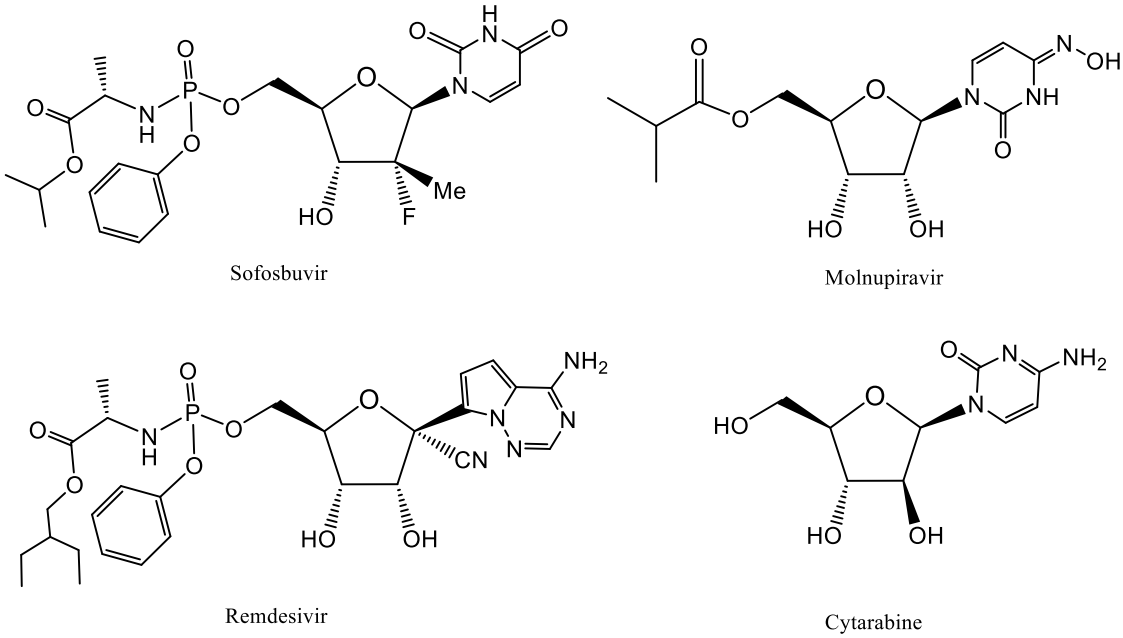

Scheme 1.7. Structures of sofosbuvir, remdesivir, molnupiravir and cytarabine

Finally, despite having already shown promising bioactivities over relevant AD targets, there are no approved drugs for AD based on nucleosides, thus encouraging further investigation of these molecular entities.

1.5.2 Investigation of nucleoside synthesis and pharmaceutical properties

The synthesis of nucleosides may be achieved by several routes and reagents, however it is usually achieved by a convergent method via *N*-glycosylation of a nucleobase, with coupling of a ribosyl moiety with a heterocyclic base [56]. This type of reactions seems simple, however they are accompanied by several issues such as the challenging regio- and diastereoselectivities due to factors such as the base's low nucleophilicity and the functional groups in the ribosyl moiety. Moreover, it may be challenging to achieve the desired linkage of the

nucleobase to the anomeric center of the sugar moiety since several side reactions may occur such as the non-stereoselective nucleophilic attack that leads to the formation of both α- and β-anomers and the nucleophilic attack by other base groups which leads to obtaining complex mixtures of products [56].

In 2014, the carbohydrate chemistry group of Faculdade de Ciências, Universidade de Lisboa, presently integrating the Centro de Química Estrutural, Institute of Molecular Sciences, reported the synthesis of the first series of purine nucleosides showing a promising cholinesterase inhibition, the most potent nucleoside being the N^7-linked-2-acetamido-α-D-mannosylpurine (**1**, Scheme 1.8) with a dissociation constant of enzyme-inhibitor complex in competitive inhibition (K_i) of 50 nM and a selectivity factor of 340-fold for BChE over AChE [66].

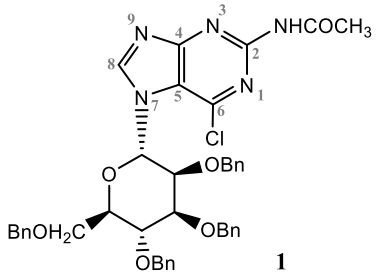

1

Scheme 1.8. Structure of compound **1**

Inspired by these studies and in view of the multifactorial nature of AD and of the fact that most of the single-target compounds were not well succeeded as AD therapies in the last years, a new set of purine nucleosides, still to be published, was synthesized by the same group aiming to achieve compounds with potential to act both as AChE and BChE inhibitors and as relevant biometal chelators, namely copper, zinc, iron and aluminum chelators. These compounds were synthesized to study structure modifications, such as the glycosyl donor and the purine base, the anomeric stereochemistry (α or β), sugar D or L configuration, sugar 6-deoxygenation and also the glycosyl group regioligation to the purine base at positions N^7 and N^9, and their role in compounds' bioactivity.

The synthetic results of these new studies are summarized in Scheme 1.9 and for the reaction of the per-benzylated methyl α-D-mannopyranoside, as the substrate, with the N^6-benzoyladenine purine base, following a procedure elsewhere described [66], no selectivity was achieved. Four isomers [N^9-linked α (**2**, Scheme 1.9), N^9-linked β (**3**, Scheme 1.9), N^7-linked α (**4**, Scheme 1.9), N^7-linked β (**5**, Scheme 1.9)] were obtained for this reaction, being noteworthy that the N^9-linked β isomer has a non-usual conformation, which was confirmed by

computational methods. In the opposite side, the coupling reaction of the per-benzylated methyl α-D-rhamnopyranoside with the same purine was selective for the N^9 isomers (**6** and **7**, Scheme 1.9). Finally, compound **8** (Scheme 1.9), a N^9-linked a compound, was selectively obtained by the same method through the reaction of the per-acetylated α-L-rhamnose with the same heterocyclic base.

Another interesting finding was that amongst the seven synthesized compounds, only **8** showed activity as a metal chelator, namely, a copper chelator, having shown no activity towards zinc, iron and aluminum. Furthermore, anticholinesterase assays, against electric eel AChE and horse serum BChE, were carried out for all the nucleosides and some interesting conclusions were found. Compounds exhibiting β-D-configuration seemed to be dual inhibitors regardless of the N^7 or the N^9 purine ligation. Moreover, the selective AChE inhibition seemed to be related with the N^9 ligation, while the selective BChE inhibition seemed to be related with the N^7 one. Finally, in these assays, nucleoside **8**, the only acetylated compound, showed no activity towards any of the enzymes which suggested that this activity could be related with the aromatic rings found in the other compounds' structures.

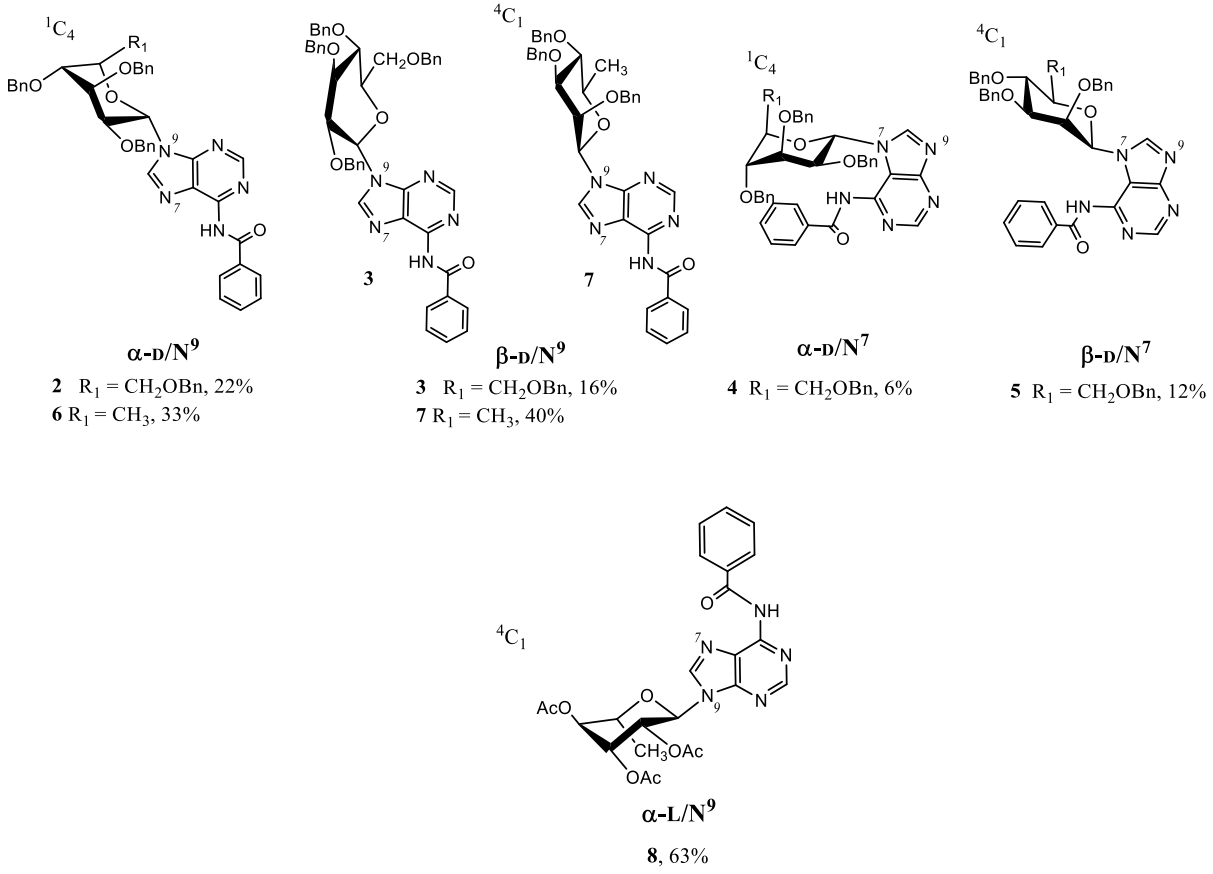

Scheme 1.9. Structures of the synthesized compounds (**2**-**8**)

The obtained results gave rise to a set of questions, such as: would it be possible to selectively synthesize compounds **2** and **3** (N^9 isomers) or **4** and **5** (N^7 isomers)? Would it be possible to synthesize nucleoside **3** with the usual $^4C_1$ configuration? May the chelating activity only be achieved through compounds with no aromatic rings in their structure? Is this kind of activity really related to the glycone L-configuration? Could a nucleoside bearing a L-configurated sugar moiety with benzyl protecting groups be a dual target drug against cholinesterases and the biometals accumulation?

Hence, inspired by these findings, the present work was accomplished aiming to answer these questions, with its first objective being the synthesis of new nucleosides, to complete the previously synthesized library, using the methyl L-rhamnopyranoside (**9**, Scheme 1.10), protected with either benzyl or benzoyl groups, and *N*^{6}-benzoyladenine as the purine base. The reaction using the per-benzylated methyl α-D-mannopyranoside was also tested and will be described. Furthermore, attempting to provide a regio- and stereoselective method for the latter reaction, in this dissertation, a new method was explored, inspired by a 2020 study [67], aiming to control the reaction conditions either for N^7 or N^9 selectivity, using phenyl α-D-thiomannopyranoside (**11**, Scheme 1.10) as the substrate and *N*^{6}-benzoyladenine or 2-acetamido-6-chloropurine, either silylated or non-silylated (Scheme 1.11), as bases. Finally, the spectroscopic characterization of all synthesized compounds will be described as well as the evaluation of compound's chelating and anticholinesterase activities.

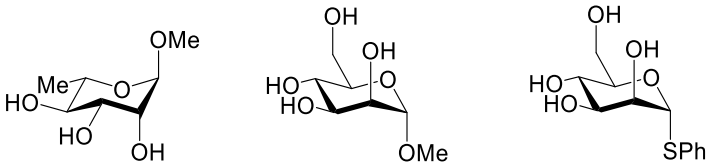

9 **10** **11**

Scheme 1.10. Structures of the unprotected glycosyl donors (**9**-**11**)

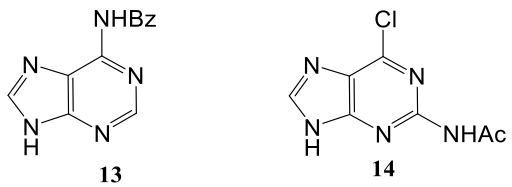

13 **14**

Scheme 1.11. Structures of the purine base (**13** and **14**)

2

RESULTS AND DISCUSSION

In the past years, the synthesis of purine nucleosides has been achieved by different methods, some being selective for the N^9 or the N^7 isomers and some showing no selectivity, in the case of adenosine derived nucleosides. Moreover, work has been done focusing on nucleoside properties as anti-AD and antitumor agents, showing promising results. Hence, it is interesting to study new synthetic methods to design and synthesize new nucleosides and to prepare already known compounds through simpler and stereo- and/or regioselective methods and look for biological properties that have never been reported for them.

In 2020, the synthesis of thiofuranoside *N*-glycosides bearing an adenine nucleobase was published. This publication reported an acyclic approach to synthesize these compounds using acyclic dithioacetal substrates and N^6-benzoyladenine in the presence of iodine. The followed procedures were shown to provide the ability to control N^7 or N^9 selectivity, by reacting the substrates with either the silylated or the non-silylated purine base [67].

In this work, different purine nucleosides (**2**, **19**-**24**) were synthesized aiming to achieve a dual-target compound against AD, targeting the cholinergic system by inhibiting AChE and/or BChE, and targeting the metal chelation, namely, copper, zinc, iron and aluminum chelation. To synthesize these nucleosides, four intermediates, three per-benzylated (**15**-**17**) and a per-benzoylated (**18**) sugars, were synthesized and three different *N*-glycosylation methods were tested. All compound structures were elucidated by nuclear magnetic resonance (NMR) spectroscopy and by high resolution mass spectrometry (HRMS). Furthermore, nucleosides' properties as anticholinesterase agents and metal chelators were studied.

2.1 Intermediates

2.1.1 Per-benzylated intermediates

2.1.1.1 Synthesis

Intermediates **15**, **16** and **17** were synthesized following a reported procedure [68] with some modifications previously carried out by our group. In the original methodology, the substrate was dissolved in anhydrous dimethylformamide (DMF) under inert nitrogen (N_2) atmosphere and the mixture was then cooled to 0ºC. Sodium hydride [NaH (60% dispersion in mineral oil)] was then added and the mixture stirred for 10 minutes prior to the dropwise addition of benzyl bromide (BnBr). The reaction was left under stirring at room temperature for 18 hours and an aqueous saturated solution of ammonium chloride (NH_4Cl) was added to quench the reaction. Hereinafter, the modifications applied to this procedure by our group are described in the preparation of these compounds followed in this work. The synthesis was achieved by a two-step reaction as described in Scheme 2.1. Deprotonation for OH-2 is illustrated for compound **15** (Scheme 2.2) being carried out by reacting the starting material (**9**, **10** or **11**) with sodium hydride, in dry tetrahydrofuran (THF). Sodium hydride is a strong base, which undergoes dissociation forming the ions Na^+ and H^-. In contact with water, it releases a flammable gas, H_2, that might spontaneously ignite, making it challenging to handle safely. During the deprotonation of the hydroxy groups of the starting material, the release of H_2 occurs and, for this reason, this reaction was carried out at 0ºC, under N_2 atmosphere, and NaH was slowly added to the solution, to prevent the formation of a large amount of flammable gas. Moreover, the NaH used was purchased as a 60% mineral oil dispersion, which made it safer to use.

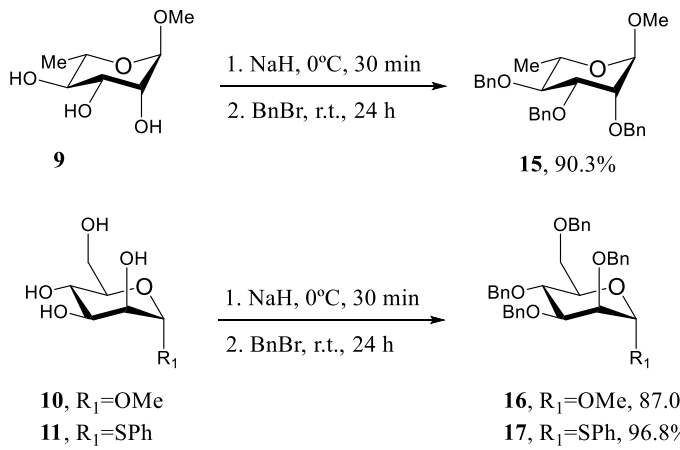

9

15, 90.3%

10, R_1=OMe
11, R_1=SPh

16, R_1=OMe, 87.0%
17, R_1=SPh, 96.8%

Scheme 2.1. Syntehesis of compounds **15**, **16** and **17**

After the deprotonation step, the mixture was heated up to room temperature and BnBr was added to the mixture. At this step, the deprotonated hydroxy groups react with BnBr by a S_N2 mechanism, as described in Scheme 2.2. It is noteworthy that BnBr is a compound with a pungent odor, releasing gases that cause severe skin and eyes irritation, therefore, it was handled carefully in the fume hood.

To quench the reaction, methanol (MeOH) was added to the mixture to react with the remaining NaH, once this reagent was added in excess. Finally, after the work-up and the isolation steps, compounds **15**, **16** and **17** were obtained with 90.3, 87.0 and 96.8% as the best isolated yields found for each compound, respectively. Benzylation reactions were carried out with the mentioned conditions several times (5, 3 and 9 times for obtaining **15**, **16** and **17**, respectively) and the results were reproducible with the isolated yields ranging from 89.4 to 90.3%, from 86.6 to 87.0% and from 90.2 to 96.8%, for the three intermediates, respectively.

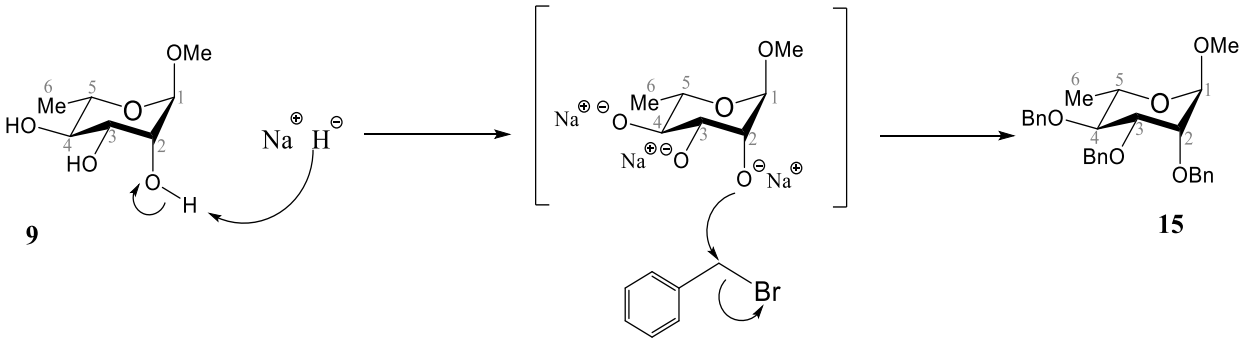

Scheme 2.2. Synthesis of the intermediate **15**

2.1.1.2 Structure characterization

The three compounds were fully characterized by NMR spectroscopy (^{1}H NMR, ^{13}C NMR, COSY, HSQC and HMBC experiments) and HRMS.

Compound **15**'s ^{1}H NMR spectrum shows a multiplet signal (δ 7.31-7.18 ppm), integrating for 15 protons, in the aromatic region. Moreover, the spectrum presents three AB systems. These results then confirm that the three initial hydroxy groups were replaced by benzyloxy groups. Furthermore, HRMS results confirmed the compound structure with the three benzyl groups.

There are two possible conformations for the structure of this intermediate, the $^1C_4$ and the $^4C_1$ conformations, as shown in Scheme 2.3.

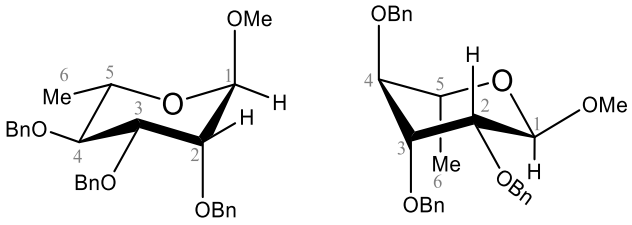

15, $^{1}C_{4}$ conformation **15**, $^{4}C_{1}$ conformation

Scheme 2.3. Compound **15**'s possible conformations, highlighting the positions of protons 1 and 2

Looking at the two structures, the $^{1}C_{4}$ conformation shows most of its voluminous groups, the -OBn groups, in equatorial positions, while the $^{4}C_{1}$ conformation has most of its voluminous groups in axial positions, therefore, the first conformation is the preferred one, as confirmed by the coupling constants in the ^{1}H NMR spectrum, showing a small $^{3}J_{1,2}$ coupling as detected through the H-2 signal.

For compounds **16** and **17** (Scheme 2.4), the same rational was used. Both of them showed multiplet signals at the aromatic region, integrating for 20 and for 25 protons, respectively, and both showed the presence of four AB systems, confirming that the initial hydroxy groups were replaced by the benzyloxy groups. HRMS also confirmed their structure since the molecular weights found were correspondent to the structures with the benzyl protecting groups.

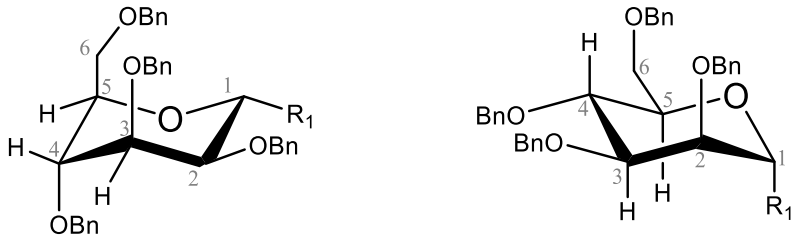

16, R_1=OMe, $^{1}C_{4}$ conformation **16**, R_1=OMe, $^{4}C_{1}$ conformation

17, R_1=SPh, $^{1}C_{4}$ conformation **17**, R_1=SPh, $^{4}C_{1}$ conformation

Scheme 2.4. Possible conformations for compounds **16** and **17**, highlighting protons 3,4 and 5 positions

For these compounds, it was not possible to analyze the coupling constant for protons 1 and 2, however, it was possible to verify that both showed $^{3}J_{3,4}=^{3}J_{4,5}$, with values of 9.18 and 9.57 Hz for **16** and **17**, respectively. These results suggest that for both compounds, protons 3 and 4 and protons 4 and 5 are in *trans*-diaxial positions, indicating that both adopted the $^{4}C_{1}$ conformation (Scheme 2.5), as it would be expected by the voluminous groups' positions.

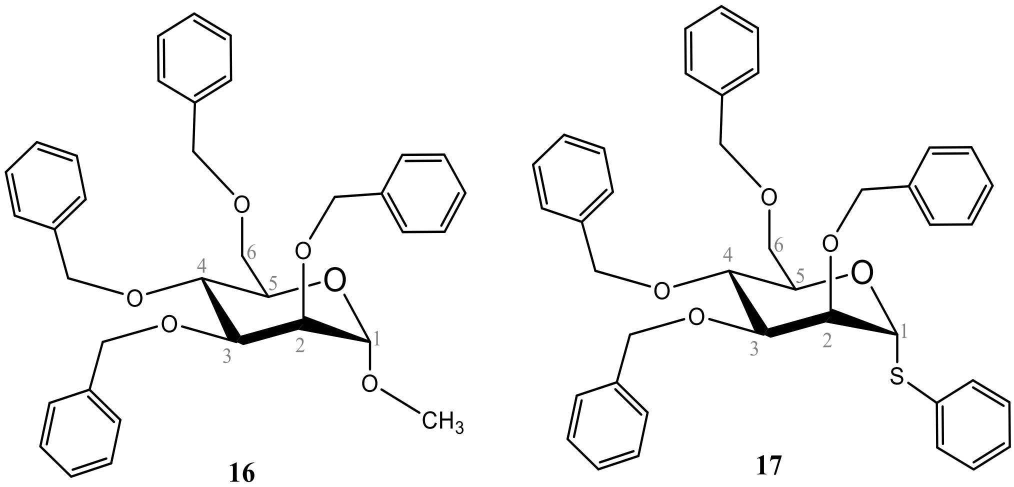

Scheme 2.5. Intermediates **16** and **17** final conformations

2.1.2 Per-benzoylated intermediate

2.1.2.1 Synthesis

Synthesis of intermediate **18** was carried out following a reported procedure [68] with some modifications previously carried out in our laboratory. By the original procedure, 4-dimethyl-aminopyridine (DMAP) and triethylamine (NEt_3) should be added to a solution of the substrate in dry dichloromethane (DCM). Then, the benzoyl chloride should be added and the reaction carried out overnight at room temperature. The procedure followed by our group was similar, however without the addition of DMAP and with an alteration of the solvent from DCM to THF and is described as follows: the substrate should be dissolved in dry THF and NEt_3 and benzoyl chloride (BzCl) added dropwise to the mixture at room temperature. The reaction should then be carried out for about 2 hours with thin layer chromatography (TLC) control. Following the latter methodology, as shown in Entry 1 (Table 2.1), 2 mmol of the starting material **9** were dissolved in 10 mL of THF, followed by the addition of 2.00 equiv./-OH of NEt_3 and of BzCl. Then, after the 2 hours period, the reaction did not occur, therefore, another 2.00 equiv./-OH of NEt_3 and of BzCl were added. After 2 hours, the reaction was not complete and DMAP was added to the reaction, in a catalytic amount, to catalyze the process. The reaction was then carried out overnight (17 hours), until the complete reaction was achieved. The product was obtained with a 96.5% isolated yield.

Since the addition of DMAP and of a larger amount of NEt_3 and BzCl was successful, some alterations to this modified procedure were made. NEt_3 (3.00 equiv./-OH) and BzCl (3.00 equiv./-OH) were added to the solution of the starting material **9** (2 mmol) in THF (10 mL). DMAP was added to the solution in the beginning of the reaction, again in a catalytic amount, and the reaction was carried out overnight, for 20 hours, until the reaction was complete. By this method, intermediate **18** was obtained in a 99.8 % isolated yield (Entry 2, Table 2.1).

Having the latter method been successful, a scale-up was attempted, using twice of the starting material **9** and twice of the volume of the solvent and of the remaining reagents. By this method, **18** was obtained at a 91.3% isolated yield (Entry 3, Table 2.1), which confirmed that this methodology was efficient for the protection of methyl α-L-rhamnopyranoside (**9**) with benzoyl groups.

Table 2.1. Preparation of intermediate **18**

Entry	S. m. [a] (mmol)	NEt_3 (equiv./-OH)	BzCl (equiv./-OH)	DMAP	Time (h)	Isolated yield (%)
1	2.00	2 .00	2.00	-	2	0.0
2	2.00	3.00	3.00	c.a.[b]	20	99.8
3	4.00	3.00	3.00	c.a.[b]	20	91.3

[a] S. m. -Starting material

[b] c.a. - catalytic amount

The mechanism of nucleophilic addition-elimination behind this reaction is described in Scheme 2.6. In this scheme, it is possible to understand the importance of using DMAP as a reaction catalyst. The pair of unshared electrons from the heterocyclic nitrogen of DMAP attacks the carbonyl group of BzCl, eliminating the chloride ion (step 1) and making the compound more vulnerable to nucleophilic attack by the starting material (step 2). After step 3, **18** is formed as well as hydrochloric acid. In step 4, the importance of NEt_3 is highlighted since it will deprotonate the acid, originating the salt $NHEt_3Cl$, which will be separated from the starting material after the work-up.

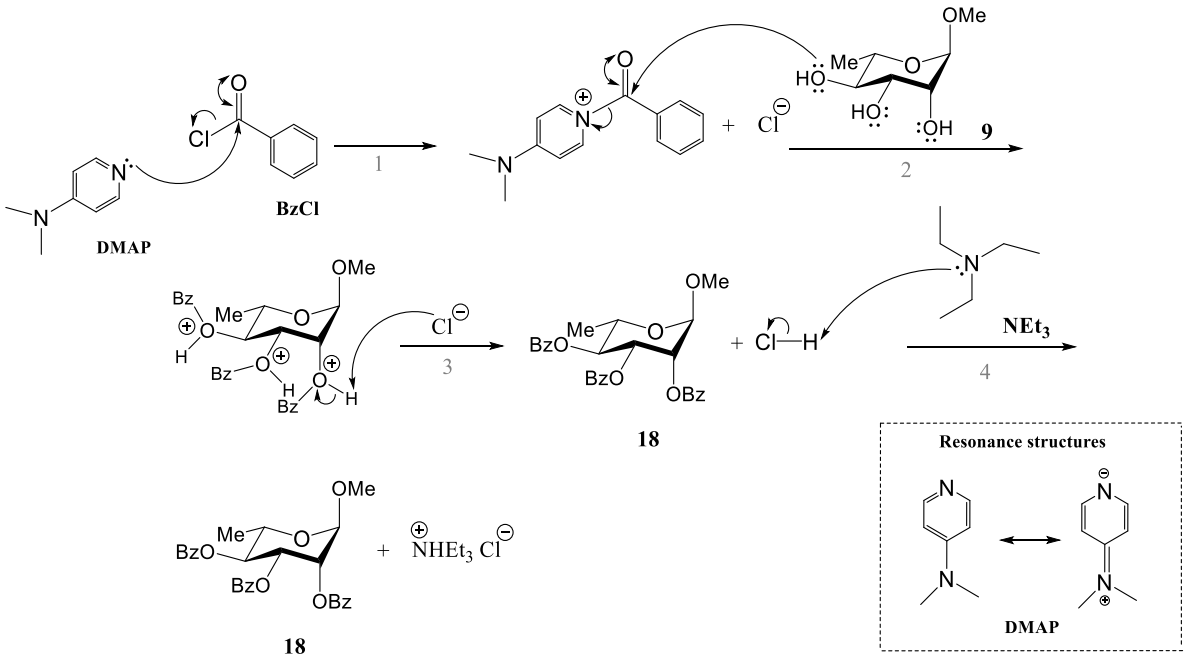

Scheme 2.6. Benzoylation mechanism for preparation of intermediate **18**

2.1.2.2 Structure characterization

Intermediate **18** was fully characterized by NMR spectroscopy and HRMS.

By analysis of the ^{1}H NMR spectrum, it was possible to identify 15 protons, in the aromatic region, corresponding to the aromatic rings from the benzoyl groups of the molecule. Moreover, in the ^{13}C NMR spectrum it was possible to observe 3 signals (δ 165.9, 165.7, 165.6 ppm) corresponding to the three carbonyl group carbons, which confirms the formation of the ester groups.

To find out which conformation was adopted by this compound, a method similar to the one already described in section 2.1.1.2 was used. The coupling constants $^{3}J_{3,4}$ and $^{3}J_{5,4}$ were found to have values above 8.00 Hz, suggesting that protons 3 and 4 and 4 and 5 are in *trans*-diaxial positions, which is in agreement with the $^{1}C_{4}$ conformation (Scheme 2.7), as expect by the equatorial position of two of the benzoyl groups.

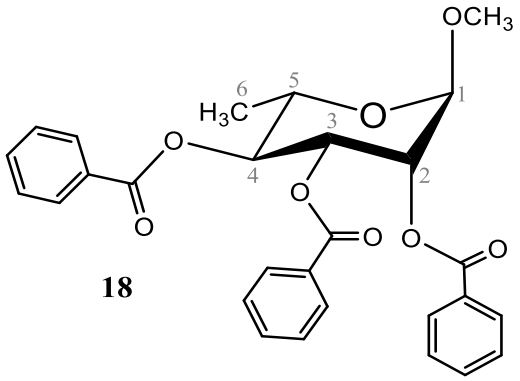

18

Scheme 2.7. Final conformation of intermediate **18**

2.2 Nucleosides

With all the necessary intermediates in hand, the *N*-glycosylation reactions of the purine bases N^6-benzoyladenine and 2-acetamido-6-chloropurine with the synthesized compounds were started. These reactions, carried out by different methods, led to obtaining 7 different nucleosides (**2**, **19**-**24**).

2.2.1 Microwave assisted *N*-glycosylation (method 1)

2.2.1.1 Synthesis

The microwave assisted *N*-glycosylation was carried out following a reported methodology [66] with no modifications in the procedure and the mechanism behind this reaction is exemplified in Scheme 2.8. In the first step, *N*,*O*-Bis(trimethylsilyl)acetamide (BSA) was added to a solution of the purine base, N^6-benzoyladenine, in dry acetonitrile (ACN), reacting for 50 minutes at room temperature. During this period, the N-H ligations of the base are protected with trimethylsilyl (TMS) groups, which, by analysis of our group's former findings, facilitates the reaction, making the purine more reactive. It is noteworthy that the purine is not soluble in the chosen solvent, although, after addition of BSA, it starts to dissolve as the protection reaction is carried out. Obtaining a clear solution is therefore indicative that the TMS protection reaction is complete. In the second step, a solution of the protected sugar in the same solvent and trimethylsilyl trifluoromethanesulfonate (TMSOTf) were added to the reaction solution, and the mixture submitted to microwave irradiation (150 W, 65ºC,15 PSI) for 60 minutes. TMSOTf acts as a catalyst, making the -OMe a better leaving group, facilitating the reaction between the sugar and the purine, that occurs in the last step, originating the nucleosides. This methodology should conduct to four nucleosides, namely the N^9 thermodynamic

regioisomers and the N^7 kinetic regioisomers, with the possible formation of both the α- and β-anomers.

In Scheme 2.8, it is possible to observe the reaction of purine base *N*^{6}-benzoyladenine and intermediate **15** that leads only to the formation of two nucleosides being both of them N^9 isomers. This reaction allowed us to obtain N^9 selectivity, in line with our group previous findings, although with not such good yields (unpublished results).

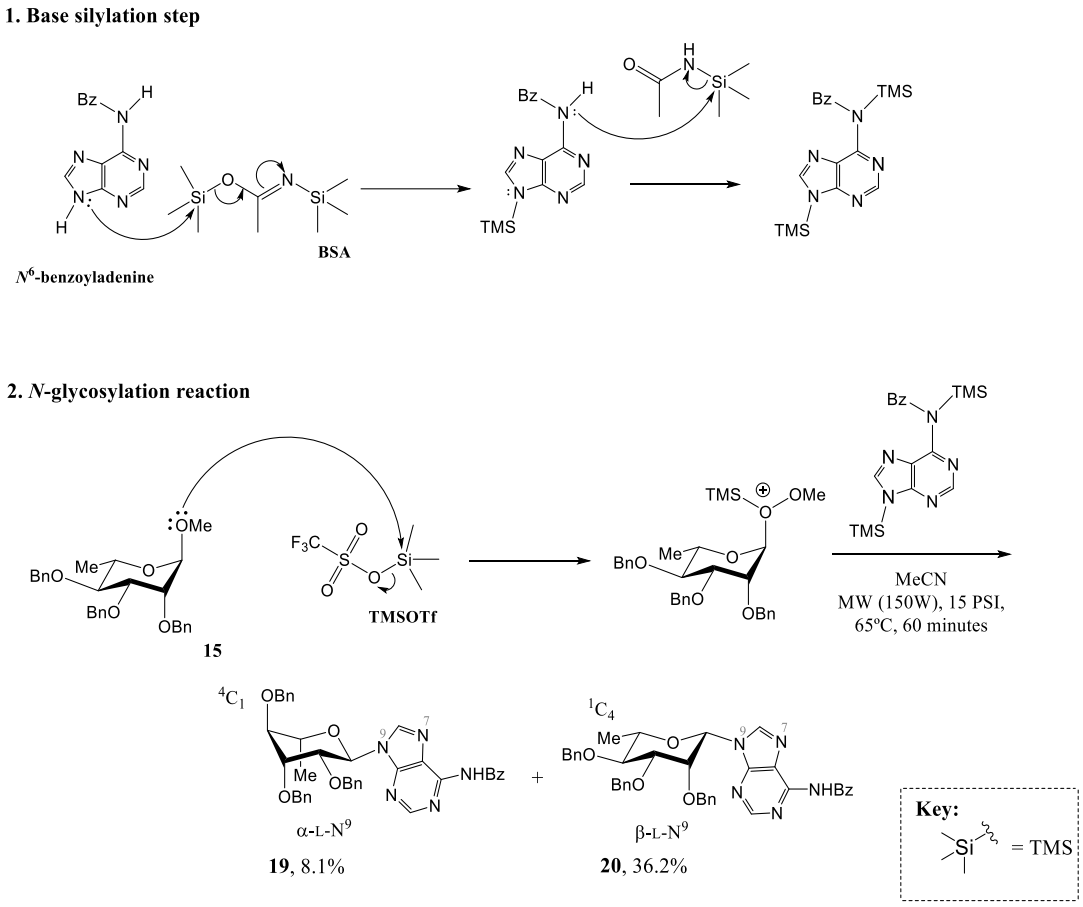

Scheme 2.8. Microwave assisted synthesis of nucleosides **19** and **20**

Following this method, another two reactions were experimented, having **16** and **18** as the starting materials. In Scheme 2.9, the synthesis of nucleosides **2** and **21** is represented. It is possible to notice that this reaction allowed us to obtain N^9 selectivity with low yields. However, this result is not in agreement with our group previous findings that, for the reaction with the same intermediate, showed no selectivity (unpublished results).

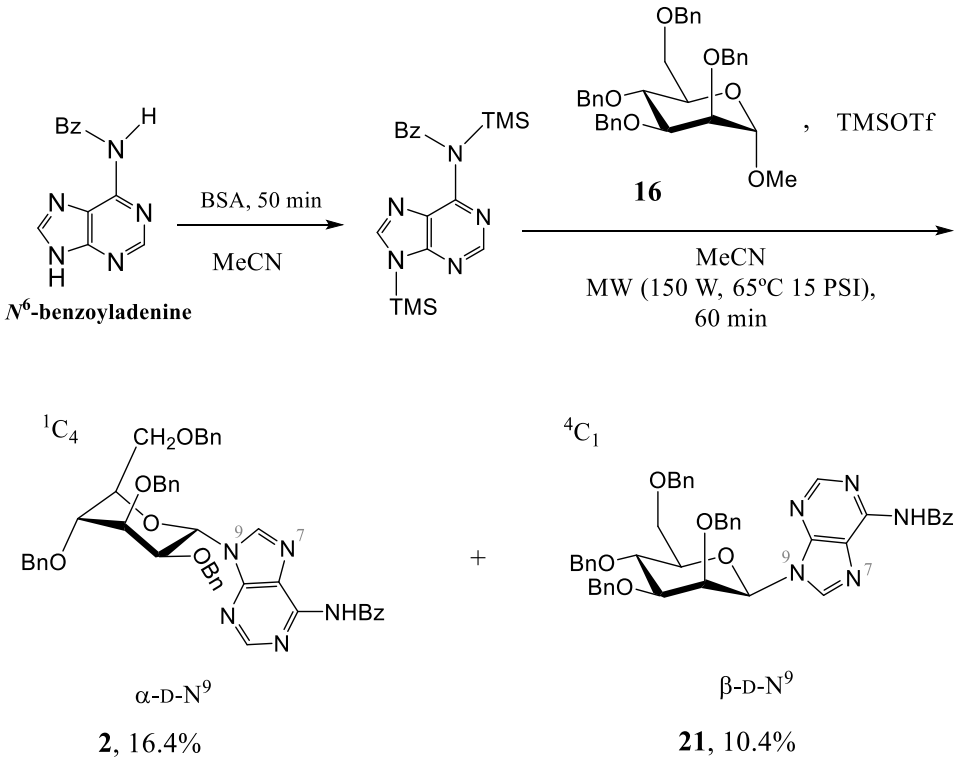

Scheme 2.9. Microwave assisted synthesis of nucleosides **2** and **21**

In order to test a different protecting group, we attempted to react the purine *N*6-benzoyladenine with the intermediate **18**, following the same procedure. Nevertheless, for this reaction, no results were obtained, as it is described in Scheme 2.10.

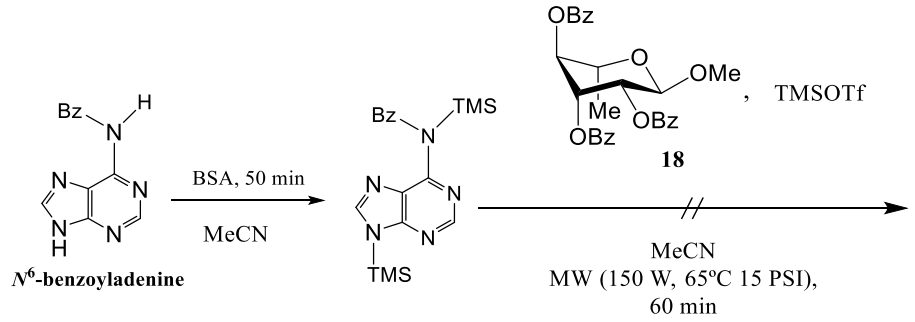

Scheme 2.10. Microwave assisted reaction between intermediate **18** and *N*6-benzoyladenine

During the development of this work, we faced technical problems in the microwave reactor that most likely interfered with the reaction results. Reactions of **15**, **16** or **18** with *N*6-benzoyladenine were attempted several times, however, no consistent results were obtained. For the intermediate **15**, only the first two attempts led us to obtain similar results and those were the ones that were considered for this work. After that, the reaction yields lowered: for **19** from 8.1% to 4.5% and for **20** from 36.2% to 9.0 %. For **16**, only the first attempt led us to

obtain products. For **18**, none of the attempts gave results, however, it was not clear if the benzoyl protecting groups were not suitable for this reaction or if the reaction did not work due to the microwave malfunctions.

2.2.1.2 Structure characterization

Compounds **2, 19**, **20** and **21** were fully characterized by NMR spectroscopy and HRMS. The anomeric configuration of all compounds was determined by considering the coupling constants in the ^{1}H NMR spectra. Purine's carbon 5 has a characteristic chemical shift that allows to distinguish between the regioisomers N^{7} and N^{9} [66], therefore this method was used to determine purine's position of its linkage to the sugar moiety.

The four compounds show chemical shifts between 125.4 and 122.1 ppm for purine's carbon 5, which is indicative that they are linked to the purine by a N^{9} ligation, as previously discovered by our group (unpublished results). Both **19** and **2** seem to present the a anomeric configuration, since both show $^{3}J_{1',2'}$ values of 7.99 Hz and of 7.60 Hz, respectively, which suggest a *trans*-diaxial position for these protons, in agreement with the $^{4}C_{1}$ configuration for **19** (Scheme 2.11) and with the $^{1}C_{4}$ configuration for **2** (Scheme 2.12).

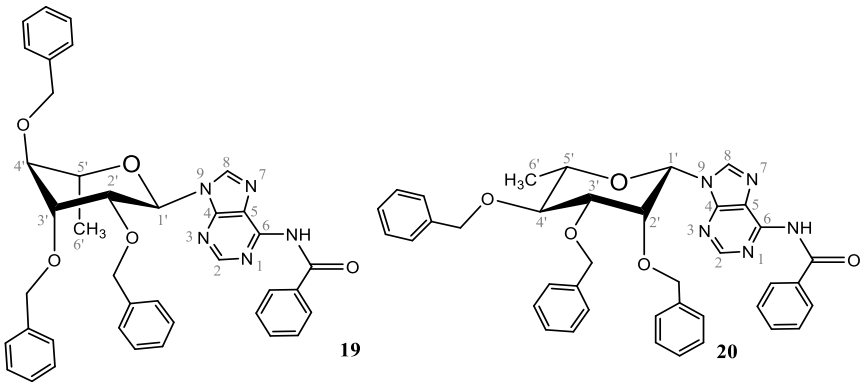

Scheme 2.11. Nucleosides **19** and **20** final conformations

Compound **21** has a $^{3}J_{1',2'}$ of 0.75 Hz, which suggests that it adopted the $^{4}C_{1}$ conformation (Scheme 2.12), indicating that it presents the β anomeric configuration.

For compound **20**, it was not possible to determine the coupling constants for protons 1' and 2', however, this nucleoside presents a $^{3}J_{3',2'}$=2.47 Hz and a $^{3}J_{3',4'}$=9.21 Hz, which is characteristic of a $^{1}C_{4}$ configuration. If the base is in equatorial position as indicated in previous findings (unpublished results), the $^{1}C_{4}$ conformation translates into a β anomeric configuration (Scheme 2.11).

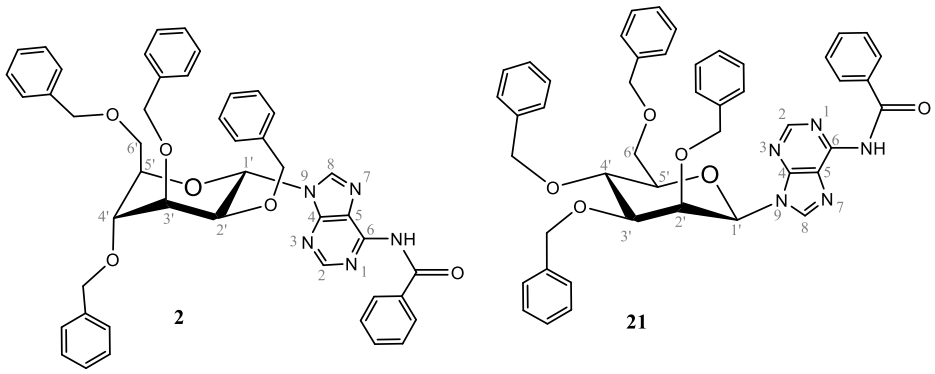

Scheme 2.12. Nucleosides **2** and **21** final conformations

2.2.2 Conventional stirring method for *N*-glycosylation (method 2)

2.2.2.1 Synthesis

Due to the inability to keep using the microwave reactor, another procedure, already reported by our group [69], was experimented, being similar to the method described for the microwave assisted synthesis.

The original procedure was described as follows: BSA (3.00 equiv.) was added to a solution of N^6-benzoyladenine (1.50 equiv.) in dry ACN and the reaction was carried out for 40 minutes until a clear solution was obtained. Then, a solution of the starting material (1 mmol) in the same solvent and TMSOTf (8.00 equiv.) were added to the mixture. The reaction was carried out at 65 ºC for 2 hours, until the complete reaction was achieved. However, these conditions were found not to be suitable for substrates **16** and **18**.

The reaction with compound **16** was attempted twice (Scheme 2.13). In the first attempt, the reaction was carried out with no modification of the original procedure, except for the amount of starting material (0.45 mmol). Some products were formed, in small quantities, however, by NMR spectra analysis, we found out that no nucleosides were formed, since the protons corresponding to the purine base were not found. Moreover, it was not possible to identify the formed compounds (Entry 1, Table 2.2). Aiming to obtain larger amounts of this reaction products, a scale up was attempted, from 0.45 to 2.00 mmol of the starting material. Instead of 2 hours, this reaction was carried out for 24 hours, however, the formation of a large quantity of products, which were not separable nor identifiable, was found, therefore the reaction was considered not successful (Entry 2, Table 2.2).

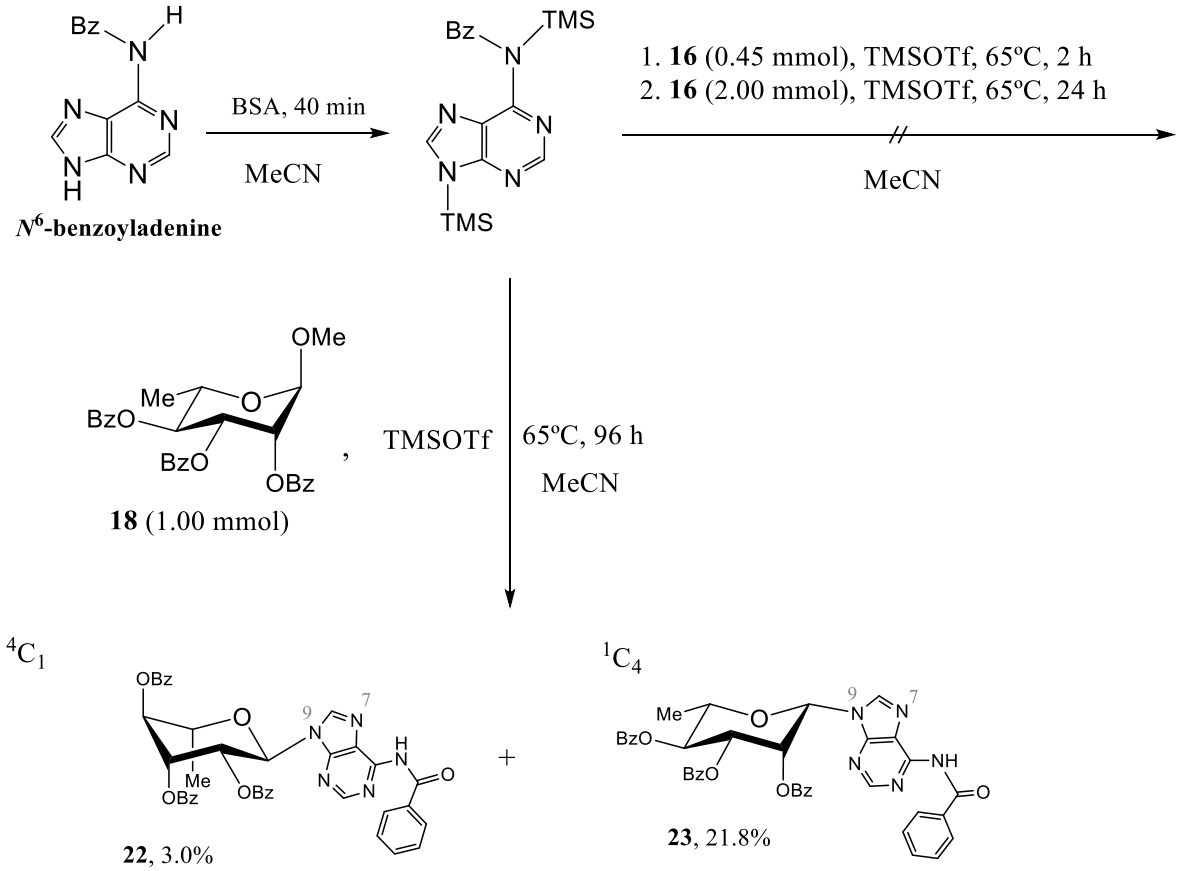

Scheme 2.13. Reaction between **16** or **18** and silylated N^6-benzoyladenine

For intermediate **18**, the reaction mechanism is similar to the one described in section 2.2.2.1. and represented in Scheme 2.13. Two hours after starting the reaction, only traces of one product were detected. The reaction mixture was then kept under stirring for 4 days (96 hours) and controlled by TLC. A mixture of inseparable regioisomers was found, composed by, presumably, the N^9-linked α-isomer (**22**) and by the N^9-linked β (**23**) one, in a ratio of 0.12:1.00 (**22**:**23**), as determined by ^{1}H NMR spectroscopy (Entry 3, Table 2.2).

Table 2.2. Conditions for *N*-glycosylation reaction with intermediates **16** and **18**

Entry	S.m., n (mmol)	Time (h)	Conversion (%)	Calculated yield (%)[a]
1	**16**, 0.45	2	90	-
2	**16**, 2.00	24	86	-
3	**18**, 1.00	96	100	**22**- 3.0 **23**- 21.8

[a]Yields calculated by the proportions determined by ^{1}H NMR for the two isomers in the mixture

2.2.2.2 Structure characterization

As aforementioned, compounds **22** and **23** were obtained as an inseparable mixture. Hence, although the major isomer could be characterized by NMR spectroscopy, it was not possible to clearly identify all the protons and carbons belonging to the minority compound **22**.

In Figure 2.1, the signals corresponding to H-2 protons of each compound are represented, being the 8.69 ppm signal corresponding to compound **22** and the 8.63 ppm signal corresponding to compound **23**. It is possible to verify that the integration suggests a ratio of 0.12:1.00 for the compounds. The aromatic region in the ^{1}H NMR spectrum presents multiple signals, corresponding to both compounds.

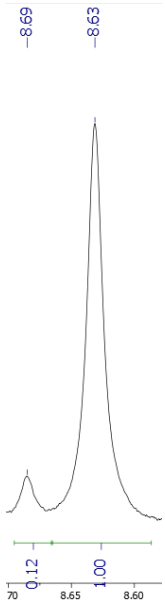

Figure 2.1. ^{1}H NMR signals corresponding to H-2 protons in both **22** and **23**

All proton and carbon signals from nucleoside **23** could be identified and the purine's carbon 5 signal at 122.3 ppm was indicative that the sugar moiety should be linked to the purine by a N^9 ligation. The coupling constants $^3J_{3',4'}$ and $^3J_{4',5'}$, in the ^1H NMR spectrum, with values above 8 Hz, suggested the $^1C_4$ conformation, in agreement with the anomeric β conformation, if the base is in equatorial orientation.

For nucleoside **22**, although no coupling constants could be analyzed, it was possible to observe signals due to the protons belonging to the sugar moiety and those of purine, protons H-2 and H-8, while the protons of the phenyl groups seem to be together with those of the **23** nucleoside. Unfortunately, it was not possible to identify any compound **22** carbons, so we could not identify the signal corresponding to the purine's carbon 5 and, therefore, know exactly how the purine was linked to the sugar moiety. Moreover, since there were no coupling constants to evaluate, it was not possible to know exactly the conformation adopted by this compound. Nevertheless, by comparing all the results and knowing that the N^9 isomers were always found to have similar polarities, it is presumable that this nucleoside is the N^9-linked α anomer (Scheme 2.14).

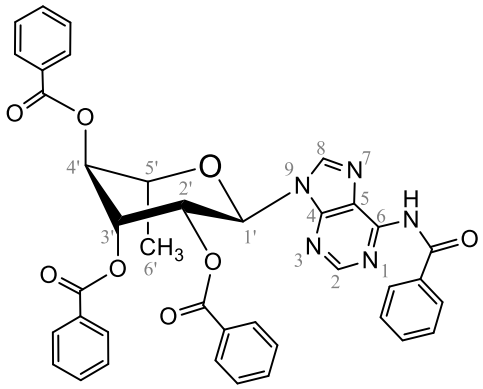

22

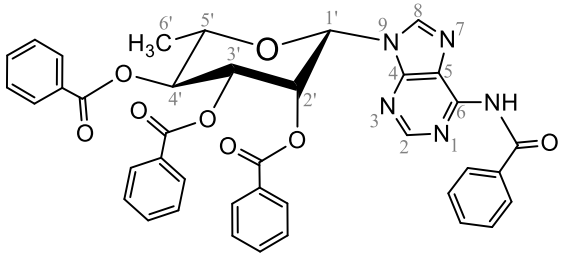

23

Scheme 2.14. Presumable structure of **22** and structure of **23**

2.2.3 New method for *N*-glycosylation (method 3)

Since the previous results obtained by our group showed that the microwave assisted *N*-glycosylation was not selective for mannopyranosides, leading to four isomers, a new method

was tested, aiming to find a regio- and stereoselective methodology for the synthesis of purine nucleosides.

This new method was inspired by a procedure found in the literature in which the reaction of an open chain dithioacetal with the non-silylated *N*^{6}-benzoyladenine led to the formation of the N^9-thioaminals, while the use of the silylated purine led to the generation of the N^7-thioaminals, due to the steric hindrance caused by the silylated amine in the C-6 position, as shown in Scheme 2.15 [67].

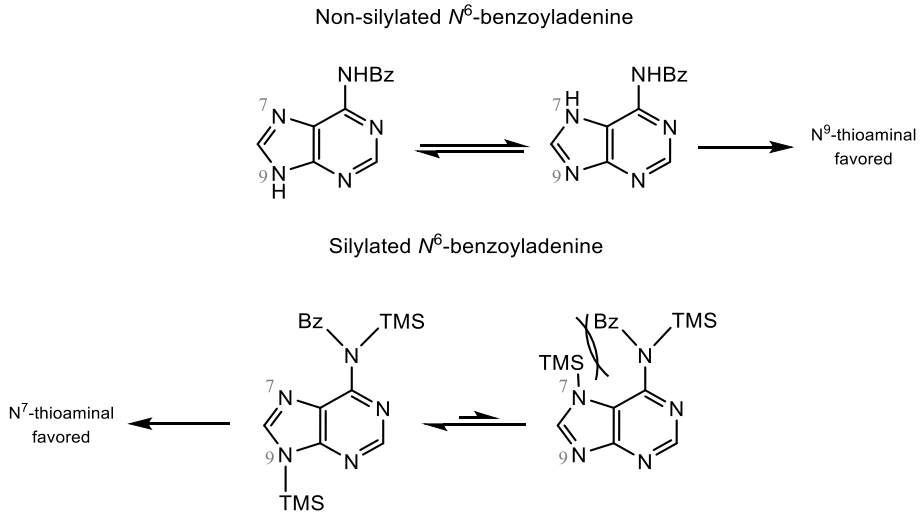

Scheme 2.15. Non-silylated and silylated purine base *N*^{6}-benzoyladenine [67]

2.2.3.1 Synthesis using *N* ^{6}-benzoyladenine and 2-acetamido-6-chloropurine

By the aforementioned methodology, the synthesis was reported as follows: *N*^{6}-benzoyladenine (3.50 equiv.) and I_2 (2.00 equiv.) were added to a solution (0.10M) of the starting material (1.00 equiv.) in anhydrous toluene containing 4 Å activated molecular sieves. The mixture was stirred for 30 minutes at room temperature, followed by the addition of a saturated aqueous solution of sodium thiosulfate ($Na_2S_2O_3$) to consume the excess iodine and by the extraction with ethyl acetate (EtOAc) [67].

The methodology was first tested for the same purine base. Following the reported method, with the intermediate **17** (0.68 mmol) as the starting material, no results were obtained in 30 minutes of stirring at room temperature. The mixture was then left under stirring for 24 hours and no results were obtained. The reaction mixture was then heated up to 65ºC and, after 2 hours at this temperature, some products were formed, therefore, the reaction was left under stirring for another 24 hours, with hourly TLC control during the day. After this period, the reaction was not complete, so the mixture was heated up to the reflux temperature (110 ºC). After 4 hours, no changes were observed and the work-up was done with no modification

of the original protocol. For this reaction, 0.44 mmol of the starting material was recovered. Moreover, two products were obtained, **2** and **21**, with yields of 17.6% and 11.8%, respectively (Scheme 2.16; Entry 1, Table 2.3).

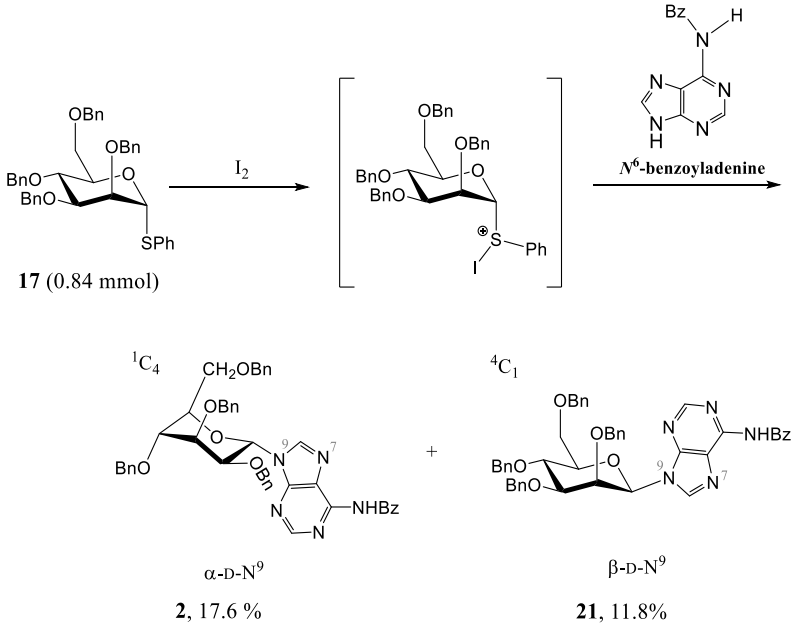

Scheme 2.16. First attempt of the synthesis of nucleosides **2** and **21**, by the new methodology

Trying to improve the conversion rate and the yields of the reaction, some modifications of the protocol were tested. A solution of **17** (0.84 mmol) in anhydrous toluene was added to a flask containing 4 Å activated powdered molecular sieves (0.74 g). Purine base (3.50 equiv.) and I_2 (4.00 equiv.) were added to the previous solution. The reaction was carried out at 65ºC for 6 hours until the complete reaction was achieved and the work-up was done with no modifications of the original method. Although a conversion rate of 100% was found for this method, products **2** and **21** were obtained with yields of 35.7% and 13.1%, respectively (Entry 2, Table 2.3). Nevertheless, this method seems to be more suitable for this reaction than the original one since it was able to improve the reaction yields.

Since the previous reaction seemed to be successful, a scale-up was attempted. The followed procedure was similar to the one previously described, with 1.13 g of 4 Å activated powdered molecular sieves and with 1.58 mmol of the starting material. The corresponding equivalents of the N^6-benzoyladenine and of I_2 were used, and the reaction was carried out at 65 ºC for 22 hours, until the complete reaction was achieved. For this reaction, compounds **2** and **21** were obtained with 31.0% and 10.1% isolated yields (Entry 3, Table 2.3).

The tested reaction conditions are summarized in Table 2.3.

Table 2.3. Tested reaction conditions for the new methodology

Entry	S.m. (mmol)	T / t	Purine (equiv.)	I_2 (equiv.)	Isolated yield (%)
1	0.68	R.t /24 h; 65ºC/24 h; 110ºC/4 h	3.50	2.00	**2**- 17.6 **21-** 11.8
2	0.84	65ºC/6 h		4.00	**2**- 35.7 **21**- 13.1
3	1.58	65ºC/22h		4.00	**2**- 31.0 **21**- 10.1

S. m.- Starting material; T-temperature; t-time

Finally, it is possible to verify that this new method is promising since it was shown to be an improvement of the known methodologies in terms of selectivity since, as expected for the reaction with the non-silylated N^6-benzoyladenine, it only led to the formation of the N^9 isomers. Furthermore, it is an improvement in terms of simplicity both of apparatus and of the number of needed reagents. Moreover, although it was not ideal, it improved the reaction yields, being still available for further optimization.

Since the reactions for the N^6-benzoyladenine were quite successful, this method was tested for a different purine base, the 2-acetamido-6-chloropurine (ACP).

For this purine, the method was attempted twice. At first, a solution of **17** (0.89 mmol, 1.00 equiv.) in anhydrous toluene (0.10 M) was added to a flask containing 0.53 g of 4 Å activated powdered molecular sieves. ACP (3.50 equiv.) and I_2 (4.00 equiv.) were added to the previous solution and the reaction was heated up to 65ºC and stirred for 5 hours. This reaction was not complete, having been recovered 0.44 mmol of the starting material and having 0.14 mmol of this been converted to the deprotected sugar (**11**). The remaining 0.31 mmol of **17** were converted to different products, which structures were not identifiable by NMR spectroscopy, however it was possible to verify that no nucleosides were formed in this reaction since the protons corresponding to the purine were not found in the ^{1}H NMR spectra.

Aiming to synthesize the nucleosides by this reaction, the same procedure was performed for 1.00 mmol of the starting material and with stirring at 110ºC for 5 hours, however no significant results were obtained and the reaction of the intermediate **17** with ACP was then considered not successful.

2.2.3.2 Synthesis with silylated N^6-benzoyladenine

In [67], a methodology for the silylation of N^6-benzoyladenine and a glycosylation method for the coupling reaction of a dithioacetal and the silylated base were reported. Under inert atmosphere (N_2 atmosphere), to a suspension of N^6-benzoyladenine (0.60 mmol, 1.00 equiv.) in hexamethyldisilazane (HMDS, 0.50 M), ammonium sulfate [$(NH_4)_2SO_4$, 0.10 equiv.] and trimethylsilyl chloride (TMSCl, 3.50 equiv.) were added. The solution was refluxed (T=125ºC) for about 50 minutes, until a clear solution was obtained. The reaction was cooled to room temperature and was then put under high vacuum (0 mbar) at 45ºC for an hour to remove the excess HMDS and a solution 0.60 M in DCM was then made. This reaction was attempted three times and all the attempts were successful (Scheme 2.17).

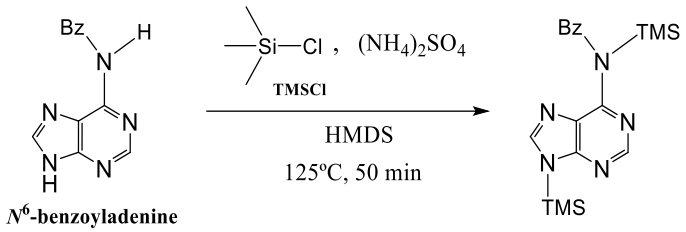

Scheme 2.17. Silylation of N^6-benzoyladenine by a reported method [67]

Aiming at the glycosylation reaction, the silylated base (0.89 mL of the 0.60M solution in DCM, 3.50 equiv) and I_2 (4.00 equiv.) should be added to a solution of the starting material **17** (100 mg, 0.16 mmol, 1.00 equiv) in anhydrous THF (0.10M). This reaction was attempted twice, however, in the first attempt, by a mistake, compound **11** (100 mg, 0.37 mmol) was used as the starting material instead of the intermediate **17**. This reaction was carried out for 4:30 hours, and some products were formed, yet the coupling reaction of the starting material with the purine did not occur. It is noteworthy that, by mistakenly adding the purine and the iodine to the unprotected compound **11**, the reaction proportions were modified: instead of adding 3.50 equivalents of the silylated purine and 4.00 equivalents of iodine, 1.44 and 1.70 equivalents were added, respectively.

Finally, the right reaction was tested. Following the procedure above described, the reaction was stirred for 24 hours at room temperature, followed by 4:30 hours at 65ºC, until the complete reaction was achieved. By this method, products **2** and **21** were again obtained but, this time, with 62.5% and 6.3% yields, respectively (Scheme 2.18).

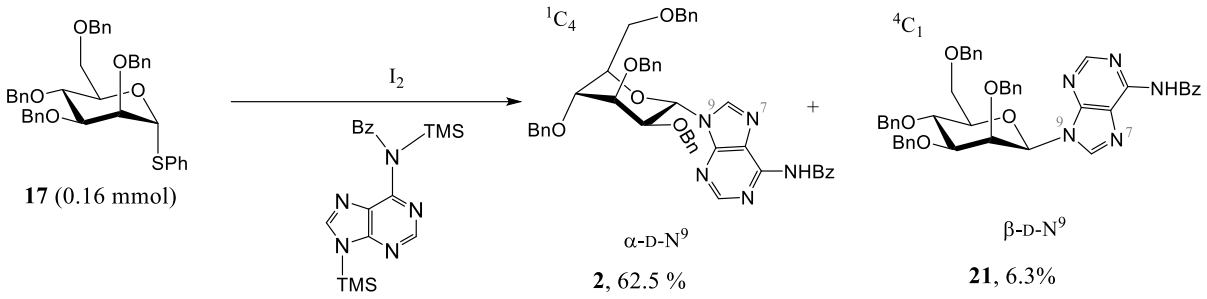

Scheme 2.18. *N*-glycosylation reaction of **17** with the silylated *N*^{6}-benzoyladenine

It is possible to verify that this reaction did not occur as expected by the literature with the selective formation of the N^7 isomers, having the N^9 isomers been again formed. Nevertheless, in comparison with the previous attempted reactions with the non-silylated purines, this stereoselective method gave the same products with a higher yield for the compound **2**, the α-anomer.

2.2.3.3 Synthesis with silylayed 2-acetamido-6-chloropurine

Since the reaction between the intermediate **17** and the silylated *N*^{6}-benzoyladenine was successful, the method was tested for ACP base.

By following the same protocol for the silylation reaction, no satisfying results were obtained, since the clear solution was never achieved and, therefore, the protection of the N-H positions of the purine with TMS groups did not occur. This procedure was tested twice and the same results were obtained for both attempts. This method was then considered not suitable for the ACP base (Scheme 2.19).

Due to the impossibility of using this method for the silylation of this purine, another procedure was tested, similar to the one already described in section 2.2.1.1, with a solvent modification from ACN to THF. BSA (3.00 equiv) was added to a suspension of ACP (1.50 equiv.) in anhydrous THF (10 mL) and the mixture was stirred for 40 minutes (Scheme 2.19). Upon obtaining a clear solution, a solution of **17** (0.33 mmol, 1.00 equiv.) in anhydrous THF (2 mL) and I_2 (4.00 equiv.) were added. The mixture was stirred for 20 hours at room temperature and no results were obtained. The reaction mixture was then heated up to 65ºC and stirred at this temperature for 3 days, 72 hours, however, no results were obtained and the reaction was considered not successful.

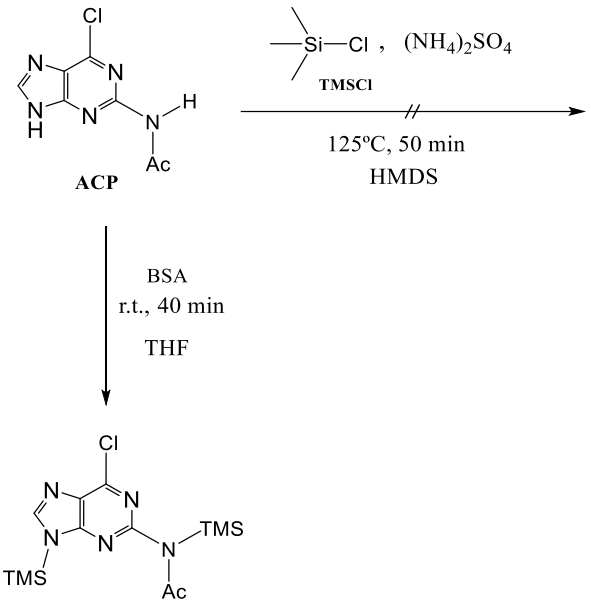

Scheme 2.19. Silylation of 2-acetamido-6-chloro-purine

Finally, since the previous reaction did not give any results, the order of addition was modified and the temperature was risen up to 65ºC at the beginning of the reaction. To a flask containing 4 Å activated powdered molecular sieves (0.30 g), a solution of compound **17** (0.33 mmol, 1.00 equiv.) in anhydrous THF (4 mL) and I_2 (4.00 equiv.) were added. The solution containing the silylated purine was then added to the previous mixture and the reaction was carried out for 23 hours at 65ºC until the reaction was complete. From this reaction, a large number of products, which structures could not be identified by NMR spectroscopy, with the exception of N^9-linked α nucleoside (**24**), isolated in 24.2% isolated yield (Scheme 2.20), was found.

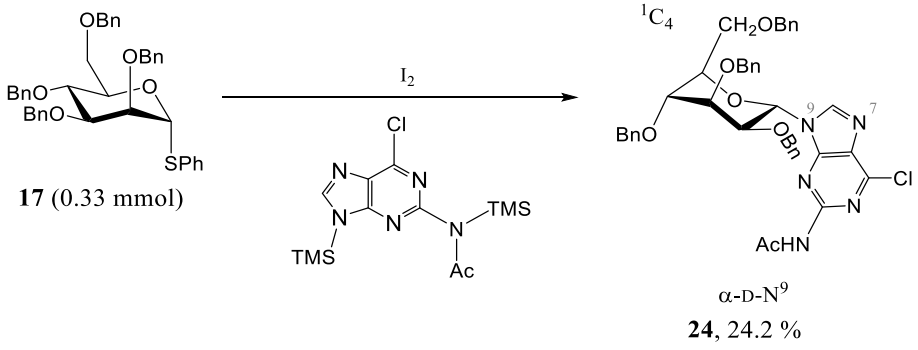

Scheme 2.20. Synthesis of nucleoside **24**

Even though this reaction yield was not ideal and the formed product was not expected as shown by the literature [67], this reaction was considered an improvement of the reaction

with the non-silylated purine since it was actually able to produce a nucleoside and selectively provided the N^9-linked a isomer.

2.2.3.4 Structure characterization

From the reaction described above for the development of the new method for the *N*-glycosylation, three products were obtained: **2**, **21** and **24**. Since the first two compounds were already prepared in reactions previously described, their characterization can be found in the section 2.2.1.2.

Nucleoside **24** was fully characterized by NMR spectroscopy and HRMS. Again, the anomeric configuration was determined by analysis of the value of the coupling constant of protons H-1' and H-2' and the position of the purine ligation was determined by the purine's carbon 5 characteristic chemical shift.

At first, all the protons corresponding to the sugar moiety and the protons corresponding to purine's H-8 and acetamido group were clearly identified. Furthermore, the signals corresponding to the carbonyl and the methyl groups from purine acetate group were possible to identify. Hence, it was proved that the coupling reaction of **17** with the silylated ACP occurred.

The coupling constant $^3J_{1',2'}$ with a value of 8.51 Hz suggests a *trans*-diaxial conformation, in agreement with the $^1C_4$ conformation for this compound. Purine's carbon 5 chemical shift had a value of 128.3 ppm, which suggests a N^9 purine ligation and, therefore, this compounds' final structure should be the one represented in Scheme 2.21.

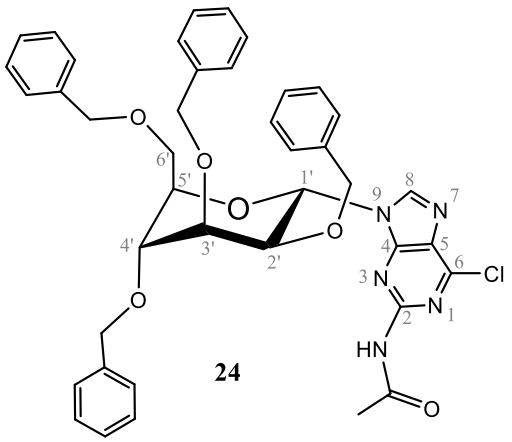

24

Scheme 2.21. Final structure of nucleoside **24**

2.3 Evaluation of nucleosides' biological properties

2.3.1 Metal chelation properties

All purine nucleosides' (**2**,**19-24**) chelating activities were evaluated by UV-Visible spectroscopy. This compounds' absorbance spectra were recorded both in the absence and in the presence of solutions of four different metal ions (Cu^{2+}, Zn^{2+}, Fe^{2+} and Al^{3+}). Amongst all synthesized compounds, nucleosides **19**, **20** and **21** showed the most interesting results. In Figure 2.2, spectra corresponding to the interaction of **19** with the four metal ions can be found and it is possible to verify that pure compound spectrum is characterized by a maximum at λ=284 nm.

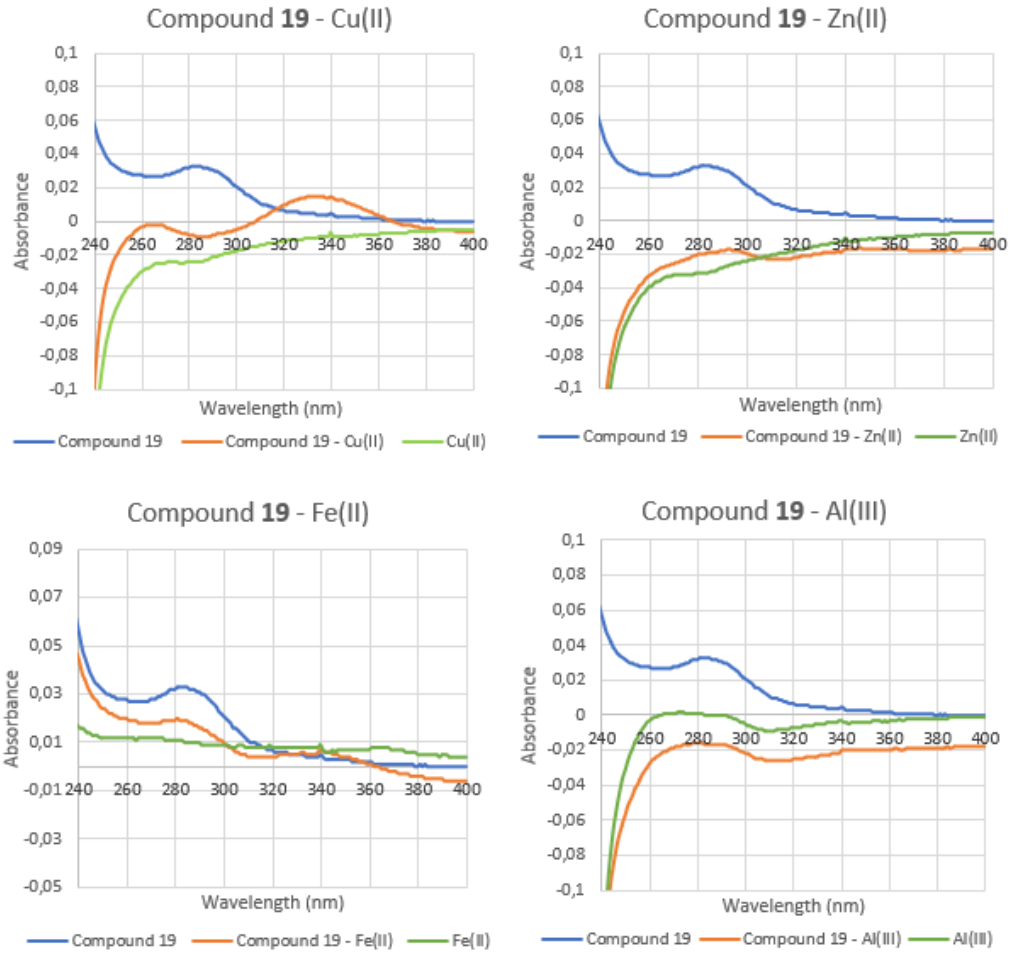

Figure 2.2. Absorbance spectra of **19** both in the absence and in the presence of metal ions

In the spectra corresponding to the interaction of the nucleoside with Zn(II) and with Al(III), it is possible to verify that no interaction can be considered since both show the same characteristic maximum as the pure compound and no other alteration can be found. In the **19**-Fe(II) interaction spectrum, a small interaction may be identified. Although no wavelength alteration in the λ=284 nm maximum occurs, there is the appearance of another maximum at 342 nm with very low intensity. Finally, in the spectrum corresponding to the interaction between the nucleoside and the copper ions, there is a perceptible wavelength shift from λ=284 nm to λ=334 nm, which is indicative of a conformational rearrangement. These results suggest a strong interaction of **19** with the copper ions, an almost neglectable interaction with iron (II) and no interaction with zinc or aluminum ions. Hence, this nucleoside seems to be a selective copper chelating agent.

In Figure 2.3, it is possible to verify that nucleoside **20** is characterized by a band at λ=290 nm.

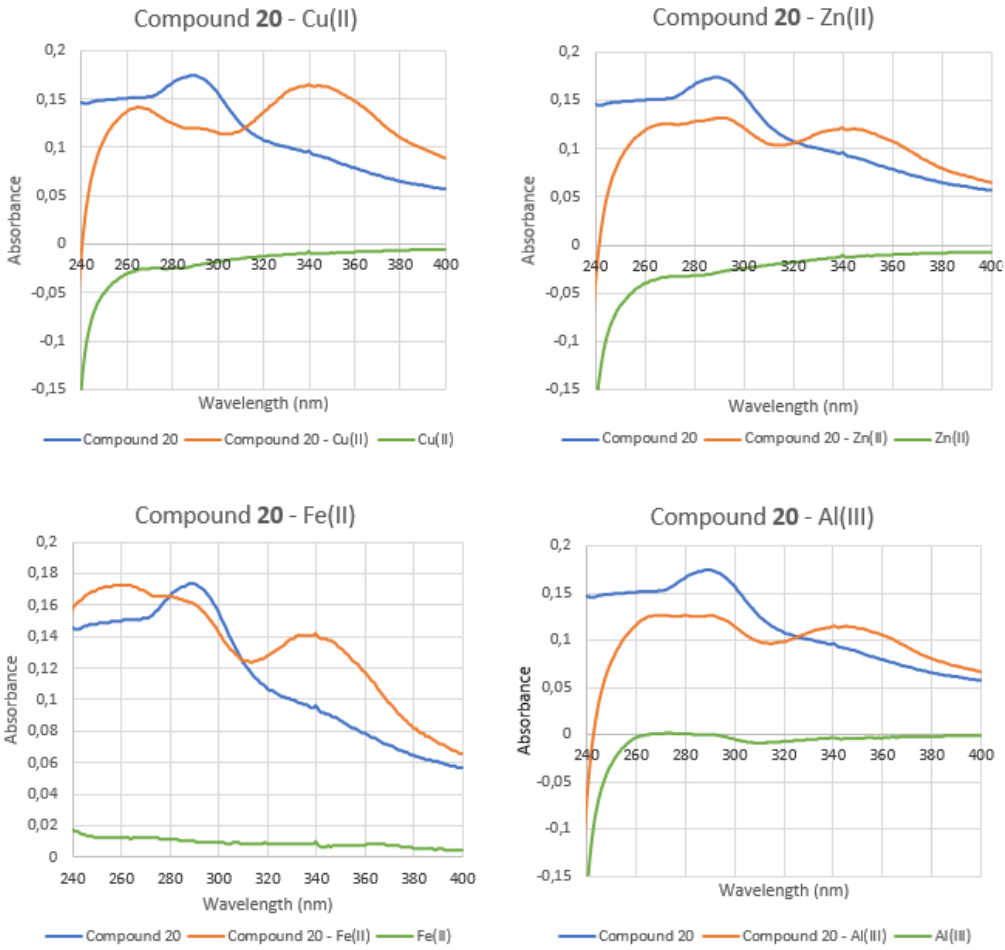

Figure 2.3. Absorbance spectra of **20** both in the absence and in the presence of metal ions

Moreover, this compound clearly shows interaction with each tested metal ion, being possible to observe wavelength shifts from 290 nm to 345, 346, 339 and 351 nm for copper, zinc, iron and aluminum ions, respectively. Hence, unlike **19**, this nucleoside seems to be a non-selective metal chelator for the tested ions.

Compound **21**'s spectra corresponding to its interaction with the four different ions is represented in Figure 2.4. This compound is characterized by a maximum at λ=301 nm and, by analyzing the absorbance spectra, it is possible to verify that **21** only presents interaction with copper ions, as demonstrated by the wavelength shift from 301 to 350 nm in the interaction spectrum. With zinc, iron and aluminum no chelating activity can be considered since in the spectra corresponding to interaction of the nucleoside with these metals there is no maximum wavelength alteration. Thus, this compound may be considered a selective copper chelator.

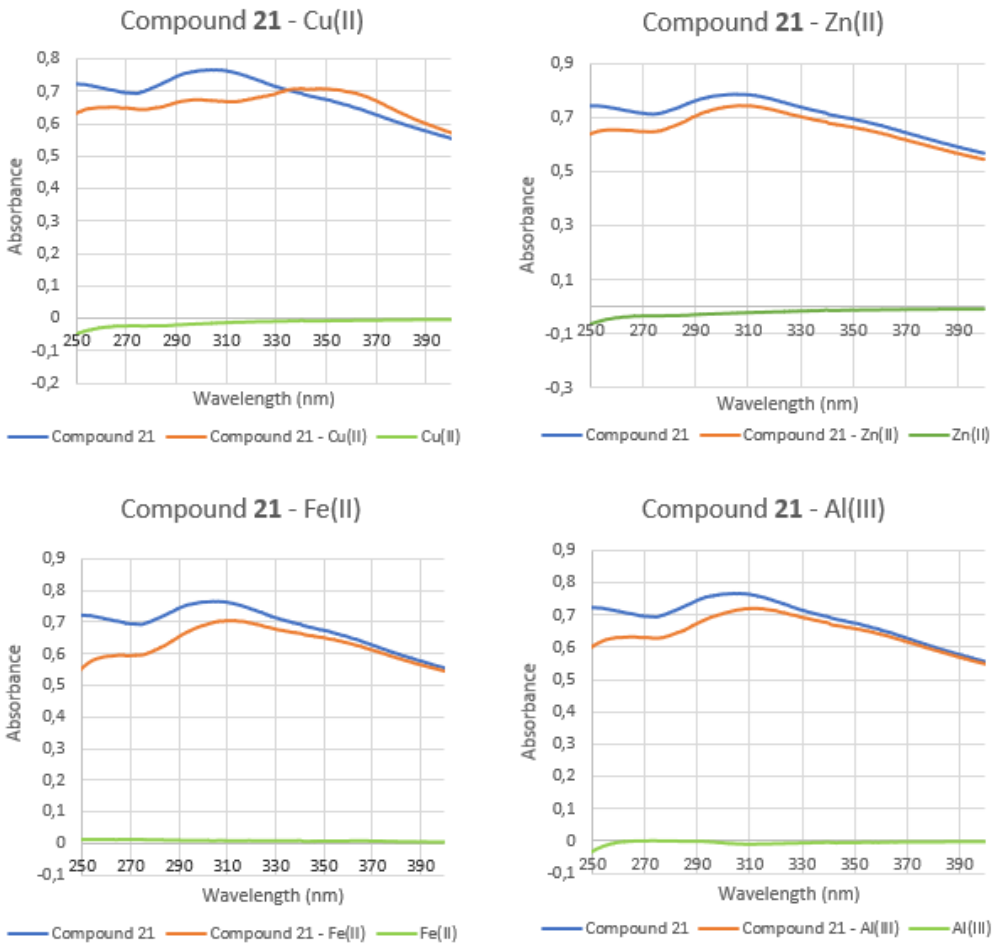

Figure 2.4. Absorbance spectra of **21** both in the absence and in the presence of metal ions

Nucleosides **2** and **22-24** did not display any properties as metal chelators, therefore, the corresponding UV-Vis spectra are not here represented, however they can be found in the Appendix A.5-A.10.

To conclude this section, compounds **19**, **20**, and the inseparable mixture **22/ 23** embody a sugar L configuration, while nucleosides **2**, **21** and **24** present a D configuration. Amongst all compounds, **19**, **20** and **21** were the only to show metal chelating properties. These results suggest that, contrary to our group's previous findings, the metal chelating properties might be related not only to the glycone L-configuration but also to the D-configuration, which increases the number of compounds that might be designed, synthesized and studied in order to achieve these properties. Moreover, this kind of activity may be related not only to the N^9 purine ligation, since the N^7 isomers synthesized did not show chelating activity (unpublished results), but also to sugar substitution pattern, conformation and anomeric configuration, suggesting that stereochemical issues may be relevant for chelation.

2.3.2 Anticholinesterase activity

The AChE and BChE inhibitory activities of the synthesized nucleosides were determined *in vitro* by using the Ellman's colorimetric assay [70] with some modifications [60, 61].

The original method was reported by Ellman *et. al* in 1960 and was described as a rapid and sensitive photometric method for the determination of cholinesterase activity and the determination of the hydrolysis of ACh by AChE and BChE. The activity of these enzymes was then measured by following the increase of the yellow color caused by the reaction of thiocholine with 5,5'-dithiobis(2-nitrobenzoic acid) (DTNB) that leads to the formation of the yellow 5-thio-2-nitrobenzoic acid (TNB), at pH 8.0 [59, 62]. The following equations summarize these reactions (Scheme 2.22, Scheme 2.23).

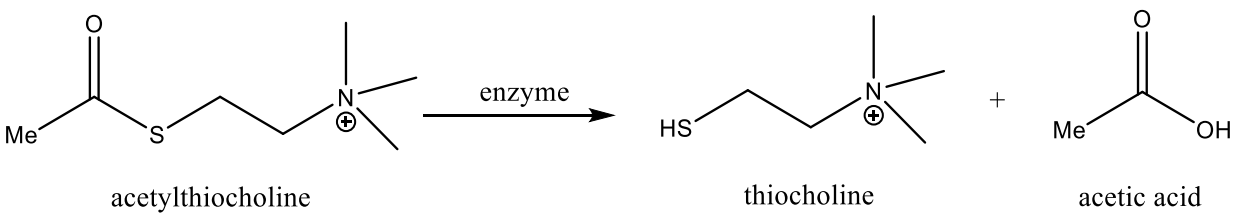

acetylthiocholine thiocholine acetic acid

Scheme 2.22. Hydrolysis of acetylthiocholine

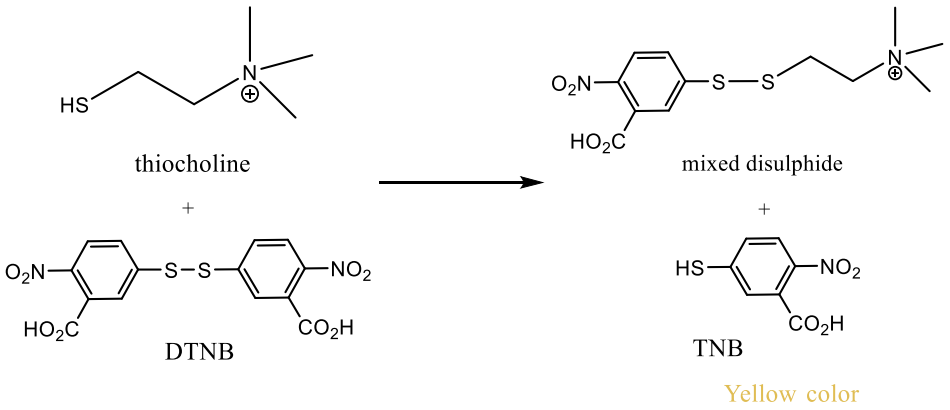

Scheme 2.23. Ellman's reaction

The maximum absorption coefficient was found at 412 nm for TNB and, for that reason, the increase of absorbance is recorded at this wavelength as the substrate is hydrolyzed. The activity of the enzyme is calculated as the reaction rate from the slope of the linear part of the graph resulting from the increase of absorbance with time [59, 62].

The modifications that were made to the original procedure are the ones that were previously carried out and disclosed by Prof. Dr. Modesto de Candia's research group, where this dissertation's anticholinesterase assays were made [60, 61].

The half maximal inhibitory concentration values (IC_{50}) found for nucleosides **2**, **19** and **20** against electric eel AChE (*ee*AChE) and horse serum BChE (*eq*BChE) are summarized in Table 2.4 and it is possible to verify that none of the tested compounds were efficient for the inhibition of 50% of these enzymes' activity at the tested concentrations.

Table 2.4. Inhibition of AChE and BChE by the synthesized nucleosides (IC_{50} values)

Compound	**IC_{50} (μM)**	
	*ee*AChE	*eq*BChE
19[a]	> 5	> 5
20[a]	> 5	> 5
2[b]	> 20	> 20
Donepezil[c]	0.021 ± 0.020	2.75 ± 0.20
Galantamine[c]	0.56 ± 0.12	12.0 ± 0.3

[a] results obtained for 5 μM final concentration due to poor water solubility

[b] result obtained for 20 μM final concentration

[c] Donepezil and galantamine were used as positive controls [60, 63]

Nucleosides inhibition assays were performed at different times, the **19** and **20** ones were performed during this dissertation period and the compound **2** one was previously performed by our group (unpublished results). In Table 2.5, the inhibition results, at 5 μM final concentration for compounds **19** and **20** against *ee*AChE, human AChE (*h*AChE), *eq*BChE and human BChE (*h*BChE) are disclosed. These results show, once again, that the tested concentration was not sufficient to produce 50% of inhibition for the tested enzymes, however both compounds show some inhibition which suggests that both could be cholinesterase inhibitors if there was a possibility of improving their water solubility. The latter results also show that **19** presents a slightly higher inhibition of AChE and, at the opposite side, **20** shows a higher inhibition of BChE, however, both of them seem to have potential to be non-selective cholinesterase inhibitors.

Table 2.5. Inhibition of AChE and BChE by nucleosides **19** and **20**

Nucleoside	**Inhibition (%) at 5 μM final concentration**			
	*ee*AChE	*h*AChE	*eq*BChE	*h*BChE
19	31±4	28±3	24±6	18±5
20	18±3	16±9	26±6	30±7

Nucleoside **24** was not possible to obtain in a sufficient amount to carry out all the structural and biological characterization assays, therefore, since data was already reported by our group for this compound's cholinesterase inhibition [66], this test was not performed for this dissertation. The work published by our group in 2014 reported the K_i values for a library of nucleosides, including **24**, whose results are summarized in Table 2.6, using galantamine hydrobromide as a positive control.

As aforementioned galantamine is a selective AChE inhibitor, which was proven by this publication's results, showing a selectivity factor of 0.06 given by the quotient of K_i (AChE) and K_i (BChE), being the K_i (AChE)= 0.5 ± 0.0 μM. **24** seems to have more impact in BChE inhibition, however, with a K_i (BChE) of 10.3 ± 2.6 μM, seems to be not as effective as it would be desired.

Table 2.6. K_i values for nucleoside **24** [66]

Compound	**K_i (μM)**	
	AChE	BChE
24	17.1 ± 2.5	10.3 ± 2.6
Galantamine hydrobromide	0.5 ± 0.0	9.4 ± 0.7

Finally, results for nucleoside **21** inhibitory activity were not possible to determine before the end of the delivery period of this dissertation, therefore, they are not shown here. Compounds **22** and **23**, since obtained as an inseparable mixture, were not considered for these assays.

3

CONCLUSIONS AND FUTURE WORK

This dissertation's work aimed at investigating purine nucleosides for which some questions were raised resulting from our group's previous findings (unpublished results): would it be possible to selectively synthesize compounds **2** and **3** (N^9 isomers) or **4** and **5** (N^7 isomers)? Would it be possible to synthesize compound **3**, the β nucleoside**,** exhibiting the usual $^4C_1$ conformation? May the chelating activity only be achieved through compounds with no aromatic ring in its structure and is this kind of activity really related to the glycone L-configuration? Could a nucleoside bearing a L-configurated sugar moiety with benzyl protecting groups be a dual target drug against cholinesterase and the biometal accumulation?

To answer these questions, in this dissertation, five new nucleosides (**19**, **20**, **21**, **22** and **23**) and two already known ones (**2** and **24**) were synthesized and studied. In order to answer the first two questions, the reaction with the per-benzylated methyl α-D-mannopyranoside was attempted by three different methods. By the microwave assisted methodology, it was actually possible to obtain N^9 selectivity and the nucleosides **2** and **21** (**3** with the $^4C_1$ conformation) were prepared. Another method without microwave irradiation was attempted but the required results were not obtained. A new methodology was then developed and experimented, reacting either silylated and non-silylated *N*^{6}-benzoyladenine with **17** to obtain N^7 or N^9 selectivity, respectively. In fact, this new method gave N^9 selectivity for the reaction of the per-benzylated phenyl α-D-thiomannopyranoside with *N*^{6}-benzoyladenine, however, by using the silylated base, also N^9 selectivity was achieved and the N^7 isomers were not found in the reaction mixtures. This method was also experimented for a different purine base, ACP, and the non-silylated base did not lead to the expected results. However, the reaction of the substrate and the silylated base allowed the selective formation of the N^9-linked α isomer (**24**). Nevertheless, although this method did not conduct to N^7 regioselectivity, actually N^9

selectivity was obtained for the reactions with two different purine bases and it turned out as an improvement of the previous methods in terms of simplicity of the apparatus and of the number of needed reagents.

In order to answer the remaining questions, nucleosides **19** and **20** were successfully synthesized by the microwave assisted method (leading to N^9 selectivity, as expected from the group previous findings). It is noteworthy that **22** and **23** were also synthesized (by the second methodology) in view of answering these questions, however since obtained as an inseparable mixture, it was not possible to consider them for the biological assays. **19** and **20**, being the only available L-glycone configuration compounds, showed metal chelating properties, **19** being a selective copper chelator and **20** being a non-selective one, showing interaction with Cu^{2+}, Zn^{2+}, Fe^{2+} and Al^{3+}. Compound **21** was synthesized to answer the question about the $^4C_1$ usual conformation for the β-isomer, however, this nucleoside revealed metal chelating activity, being a selective copper chelator. These results then contributed to enhance the previous findings, adding the concept that this activity may not only be achieved by sugar L-configurated compounds but also by D-configurated ones, increasing the number of compounds that might, in the future, be designed, synthesized and studied, in order to achieve this kind of activity. In addition, the results obtained revealed that compounds with aromatic rings in their structure also show this important chelating property.

The previous findings also suggested that the cholinesterase activity seemed to be related with the aromatic rings, the AChE selective inhibition seemed to be related with the N^9 purine ligation while the BChE selective inhibition was related with the N^7 one. Compounds **19** and **20** showed poor water solubility and the maximum concentration that was possible to test (5 μM) was not able to produce 50% inhibition of AChE and/or BChE activities. Nevertheless, **19** showed 31 and 28% inhibition against *ee*AChE and *h*AChE, respectively, and 24 and 18% inhibition against *eq*BChE and *h*BChE, respectively, while **20** produced 18 and 16% inhibition of both AChEs, respectively, and 26 and 30% inhibition of both tested BChEs. Although not being able to produce 50% inhibition at the tested concentration, these results seem promising towards the achievement of a dual-target drug against AD since these two nucleosides were the only ones that could present chelating and anticholinesterase activities, if there was the possibility to improve their water solubility. **2** was already known by previous findings (unpublished results) as not-active against any of the enzymes and, unfortunately, results for nucleoside **21**'s activity against cholinesterases were not obtained before the end of the delivery period of this work. Finally, nucleoside **24** properties as an anticholinesterase agent were

already reported, however the found K_i values for the inhibition of AChE and BChE did not seem relevant when compared with an already approved drug for AD by the FDA.

To conclude, in this dissertation it was possible to answer the questions that had arisen from the previous works and, in addition, a new method with improved simplicity was developed for the selective synthesis of nucleosides, however, this method is still available for further optimization. In this work, it was also showed that it could be interesting to study structural modifications that might lead to an improvement of compounds **19** and **20** water solubility and, therefore, lead to obtaining a dual-target drug against AD. Furthermore, the study of nucleoside's ability to cross the BBB and their toxicity could also be investigated. Finally, since mannosylpurine nucleosides previously synthesized by our group showed a potent antitumoral activity, the idea of studying the synthesized compounds properties as antitumor agents seemed interesting, therefore, the nucleosides are currently under evaluation.

Hence, this dissertation work opens the opportunity for further development and optimization of synthetic methodologies for the preparation of nucleosides and for the future research of nucleoside potential as dual- or multitarget compounds against AD. Finally, this work seems to be a step forward towards finding a disease-modifying therapy for this devastating neurogenerative disease.

4

MATERIALS AND METHODS

4.1 General information about nomenclature, reagents, solvents, spectroscopic measurements and chromatography

All compounds (intermediates and nucleosides) mentioned in this work were numbered according to the nomenclature defined by the IUPAC [75]. Reagents were purchased from commercial suppliers (Acros, Aldrich, Alfa Aesar, Sigma, Chemlab and RDH) and used without further purification. The starting materials **9**, **10** and **11** were available from Alfa Aesar, TCI and Aldrich, respectively. Purine base *N*^{6}-benzoyladenine was purchased from TCI and Thermo Scientific, and 2-acetamido-6-chloropurine was already available in the laboratory and synthesized by our group in 2013, having been used after recording the ^{1}H NMR spectrum to confirm that it was not degraded. Solvents were dried before use with 4 Å activated molecular sieves. Microwave assisted synthesis was performed with a CEM Discover and Explorer SP. NMR spectra were recorded on a Bruker Advance 400 spectrometer at 18 ºC, being the chemical shift values (δ) given in parts per million (ppm) and the coupling constants (J) values given in hertz (Hz). ^{1}H NMR spectra were recorded at 400 MHz and ^{13}C NMR spectra were recorded at 101 MHz, being the internal standard given by the solvent residual signal (MeOD, 3.31 ppm and $CDCl_3$, 7.26 ppm, for ^{1}H NMR; MeOD, 49.00 ppm; $CDCl_3$, 77.16 ppm, for ^{13}C NMR). Compounds optical rotations were determined on an Anton Paar MCP 100 polarimeter, with a 10 mm length cell, being the concentration (*c*) given in g/100 mL. HRMS analyses were performed on a QqTOF Impact II™ mass spectrometer (Bruker Daltonics), operating in the high-resolution mode, at Instituto Superior Técnico. TLC was performed on silica gel 60 F_{254} plates, 200 μM thick, from Sigma-Aldrich and visualized by UV light and by a $EtOH/H_2SO_4$ (9:1) stain followed by heating. Flash column chromatography, for compound isolation, was performed either by conventional methods or by Buchi Sepacore® automated system on silica gel 60 (PanReac).

4.2 Synthesis and characterization

4.2.1 Benzylation procedure and products

Compounds **9**, **10** and **11** hydroxy groups were protected with benzyl groups following a reported procedure [68], with some modifications already carried out by our group. The structures of the compounds synthesized by this method are represented in Scheme 4.1.

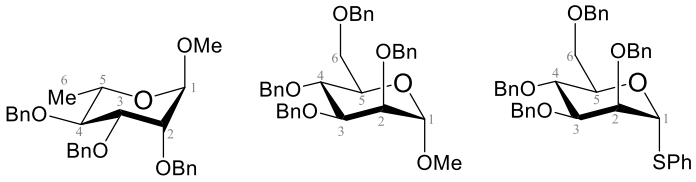

15 **16** **17**

Scheme 4.1. Structure of the benzylation products

NaH (2.00 equiv./-OH) was added to a solution of the starting material (**9**,**10** or **11**) (2 mmol) in THF (16 mL), left under stirring for 30 minutes at 0ºC, and then heated to room temperature. BnBr (2.00 equiv./-OH) was added dropwise to the solution and the mixture was stirred at room temperature for 24 hours. MeOH was then added to the mixture and the solution was concentrated at low pressure. Finally, the mixture was poured into DCM, washed with distilled water and extracted with DCM (3 x 20 mL). The combined organic layers were then washed with brine, dried over magnesium sulfate ($MgSO_4$) and concentrated. Compounds were isolated and purified by column chromatography (EtOAc/Hex 1:8 for compounds **15** and **16**; EtOAc/Hex 1:9 for compound **17**). Compounds **15** and **16** were isolated as colorless syrups and **17** as a yellow syrup.

Methyl 2,3,4-tri-*O*-benzyl-α-L-rhamnopyranoside (**15**, Scheme 4.1), methyl 2,3,4,6-tetra-*O*-benzyl-α-D-mannopyranoside (**16**, Scheme 4.1) and phenyl 2,3,4,6-tetra-*O*-benzyl-α-D-thiomannopyranoside (**17**, Scheme 4.1).

Data for compound **15**, using compound **9** as starting material: Syrup. Isolated yield=90.3%. Rf=0.38 (EtOAc/Hex 1:8). $[\alpha]_D^{20}$=-2.913º (*c* 1.0, MeOH). ^{1}H NMR (400 MHz, $CDCl_3$): δ 7.32-7.14 (m, 15H, Ph), 4.85, 4.83 (part A of AB system, 1H, OCH_2-2, J_{AB}=10.95 Hz), 4.67, 4.64, 4.63, 4.60 (AB system, 2H, OCH_2-3, J_{AB}=12.39 Hz), 4.58 -4.49 (m, 4H, part B of AB system, 1H, OCH_2-2, 2H, OCH_2-4, H-1), 3.73 (dd, 1H, H-3, $^3J_{3,2}$=3.04 Hz, $^3J_{3,4}$=8.83 Hz,), 3.68 (dd,

1H, H-2, $^{3}J_{2,1}$=1.81 Hz, $^{3}J_{2,3}$=3.04 Hz,), 3.62-3.47 (m, 2H, H-4, H-5), 3.19 (s, 3H, OCH_3), 1.24 (d, 3H, H-6, $^{3}J_{6,5}$=5.88 Hz). ^{13}C NMR (100 MHz, $CDCl_3$): δ 138.8, 138.7(5), 138.5 (CqPh), 128.5, 128.1, 128.0(5), 127.8, 127.7, 127.6(5), (Ph), 99.2 (C-1), 80.6 (C-4), 80.3 (C-2), 75.5 (OCH_2-2), 74.9 (C-3), 72.9 (OCH_2-3), 72.3 (OCH_2-4), 68.0 (C-5), 54.8 (OCH_3), 18.2 (H-6). HRMS (m/z) calculated for $[C_{28}H_{32}NaO_5]^+$: 471.2142, found: 471.2142. Data in accordance with previously reported data [76].

Data for compound **16**, using compound **10** as starting material: Syrup. Isolated yield= 87.0%. Rf=0.41(EtOAc/Hex 1:8). $[\alpha]_D^{20}$=20.192º (*c* 1.0, MeOH). ^{1}H NMR (400 MHz, $CDCl_3$): δ 7.42-7.09 (m, 20H, Ph), 4.87, 4.85 (part A of AB system, 1H, OCH_2-W, J_{AB}=10.65 Hz), 4.75 (br s, 1H, H-1), 4.71 (br s, 2H, OCH_2-X), 4.66, 4.63 (part A of AB system, 1H, OCH_2-Y, J_{AB}=12.09 Hz), 4.58 (br s, 2H, OCH_2-Z), 4.55, 4.52 (part B of AB system, 1H, OCH_2-Y, J_{AB}=12.09 Hz), 4.50, 4.47 (part B of AB system, 1H, OCH_2-W, J_{AB}=10.65 Hz), 3.95 (t, 1H, H-4, $^{3}J_{4,3}$=$^{3}J_{4,5}$=9.18 Hz), 3.86 (dd, 1H, H-5, $^{3}J_{5,6b}$= 2.67 Hz), 3.80-3.67 (m, 4H, H-2, H-3, H-6_a, H-6_b), 3.30 (s, 3H, OCH_3). ^{13}C NMR (100 MHz, $CDCl_3$): δ 138.7, 138.6, 138.5, 138.4(5) (CqPh), 128.5, 128.4(5), 128.4, 128.1, 128.0, 127.9, 127.7, 127.6(8), 127.6(6), 127.6 (Ph), 99.1 (C-1), 80.3 (C-5), 75.2 (OCH_2), 75.0 (C-4), 74.6 (C-3), 73.5 (OCH_2), 72.7 (OCH_2), 72.2 (OCH_2), 71.8 (C-2), 69.4 (C-6), 54.9 (OCH_3). HRMS (m/z) calculated for $[C_{35}H_{38}NaO_6]^+$: 577.2561, found: 577.2562. Data in accordance with previously reported data [77].

Data for compound **17**, using compound **11** as starting material: Syrup. Isolated yield=96.8%. Rf=0.47 (EtOAc/Hex 1:8). $[\alpha]_D^{20}$=79.612º (*c* 1.0, MeOH). ^{1}H NMR (400 MHz, $CDCl_3$): δ 7.46-7.39 (m, 2H, Ph), 7.37-7.17 (m, 23H, Ph), 5.60 (s, 1H, H-1), 4.91, 4.88 (part A of AB system, 1H, OCH_2-W, J_{AB}=10.71 Hz), 4.73, 4.70 (part A of AB system, 1H, OCH_2-X, J_{AB}=12.34 Hz), 4.67-4.55 (m, 4H, part B of AB system, 1H, OCH_2-X, 2H, OCH_2-Y, part A of AB system, 1H, OCH_2-Z), 4.53, 4.50 (part B of AB system, 1H, OCH_2-W, J_{AB}=10.71 Hz), 4.48, 4.45 (part B of AB system, OCH_2-Z, J_{AB}=11.96 Hz), 4.27 (dd, 1H, H-3, $^{3}J_{3,2}$=3.95 Hz, $^{3}J_{3,4}$=9.57 Hz), 4.06 (t, 1H, H-4, $^{3}J_{4,3}$=$^{3}J_{4,5}$=9.57 Hz), 3.98 (br t, 1H, H-2), 3.88-3.80 (m, 2H, H-5, H-6a), 3.73 (d, 1H, part BX of ABX system, H-6b, $J_{6b,6a}$=10.73 Hz). ^{13}C NMR (100 MHz, $CDCl_3$): δ 138.5, 138.4(6), 138.3, 138.0 (CqOBn), 134.5 (CqSPh), 131.7, 129.1, 128.6, 128.5, 128.4(8), 128.4, 128.1, 128.0(6), 128.0, 127.9, 127.8, 127.7(7), 127.6, 127.5 (Ph), 85.8 (C-1), 80.3 (C-5), 76.3 (C-2), 75.3 (OCH_2), 75.1 (C-4), 73.4 (OCH_2), 72.8 (OCH_2), 72.2 (C-3), 72.0 (OCH_2), 69.3 (C-6). HRMS (m/z) calculated for $[C_{40}H_{40}NaO_5S]^+$: 655.2489, found: 655.2487. Data in accordance with previously reported data [68].

4.2.2 Benzoylation procedure and product

Compound **9** was the only compound that was protected with benzoyl groups. The benzoylation reaction was performed following an optimization of a reported procedure [68] with some modifications and the structure of the synthesized product is represented in Scheme 4.2.

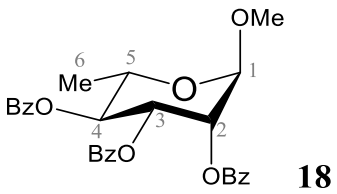

18

Scheme 4.2. Structure of the benzoylation product

NEt_3 (3.00 equiv./-OH) and BzCl (3.00 equiv./-OH) were added dropwise and DMAP was added in a catalytic amount to solution of **9** (2 mmol) in THF (10 mL) and stirred at room temperature for 20 hours. The resulting reaction mixture was concentrated and then poured into DCM. The solution was washed with a saturated aqueous solution of sodium bicarbonate ($NaHCO_3$) and extracted with DCM (3 x 15 mL). The combined organic layers were dried over $MgSO_4$, filtered and concentrated. Compound **18** was isolated, as a colorless syrup, and purified by column chromatography (EtOAc/DCM 1:1).

Methyl 2,3,4-tri-*O*-benzoyl-α-L-rhamnopyranoside (**18**, Scheme 4.2).

Data for compound **18**, using compound **9** as starting material: Syrup. Isolated yield=99.8%. Rf=0.31 (EtOAc/Hex 1:8). $[\alpha]_D^{20}$=-63.107º (*c* 1.0, MeOH). ^{1}H NMR (400 MHz, $CDCl_3$): δ 8.01 (d, 2H, Ph, J=7.12 Hz), 7.87 (d, 2H, Ph, J=7.12 Hz), 7.72 (d, 2H, Ph, J=7.12 Hz), 7.51 (t, 1H, Ph, J=7.45 Hz), 7.40 (m, 3H, Ph), 7.34-7.24 (m, 3H, Ph), 7.15 (m, 2H, Ph), 5.73 (dd, 1H, H-3, $^3J_{3,2}$=3.41 Hz, $^3J_{3,4}$=10.14 Hz), 5.60-5.54 (m, 2H, H-2, H-4), 4.82 (d, 1H, H-1, $^3J_{1,2}$=1.38 Hz), 4.09 (qd, 1H, H-5), 3.41 (s, 3H, OCH_3), 1.28 (d, 3H, H-6, $^3J_{5,6}$=6.30 Hz). ^{13}C NMR (100 MHz, $CDCl_3$): δ 165.9, 165.8, 165.6 (CqPh), 133.6, 133.4, 133.2, 130.1, 129.9, 129.8, 129.5, 129.4, 128.7, 128.6, 128.4 (Ph), 98.7 (C-1), 72.0 (C-4), 71.0 (C-2), 70.1 (C-3), 66.7 (C-5), 55.5 (OCH_3), 17.8 (CH_3). HRMS (m/z) calculated for $[C_{28}H_{26}NaO_8]^+$: 513.1520, found: 513.1514.

4.2.3 *N*-glycosylation procedures and products (methods 1 and 2)

4.2.3.1 Microwave-assisted method (method 1)

Microwave-assisted reactions were performed following a reported procedure [66] and the products obtained are represented in Scheme 4.3.

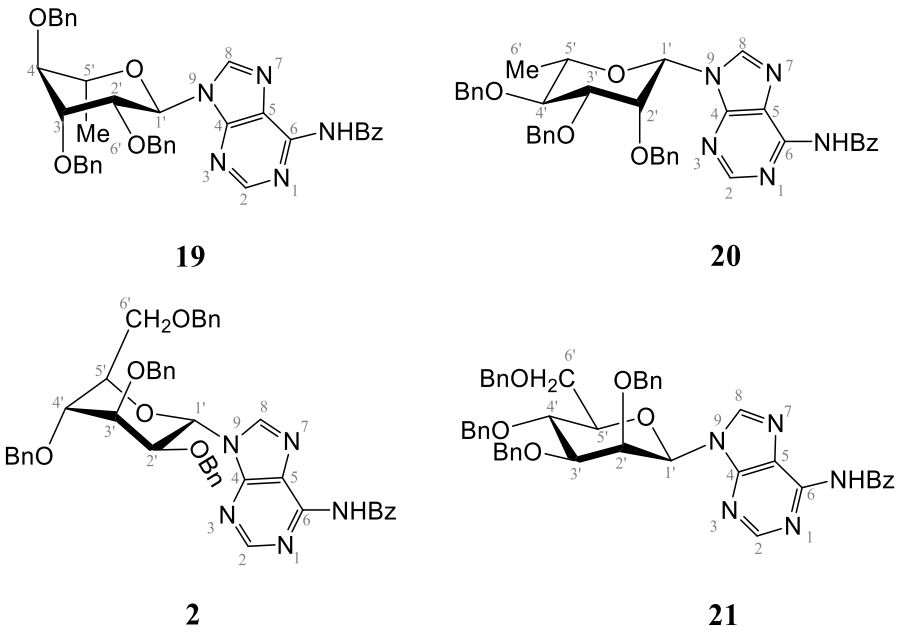

Scheme 4.3. Microwave assisted *N*-glycosylation products

In a 10 mL microwave vial, BSA (3.00 equiv.) was added to a solution of N^6-benzoyladenine (1.50 equiv.) in dry ACN (3 mL) and the mixture was stirred for 50 minutes at room temperature, until a clear solution was obtained. A solution of the fully protected glycoside [**15**, **16** (Scheme 4.1) or **18** (Scheme 4.2)] (1 mmol) in dry ACN (3 mL) and TMSOTf (8.00 equiv.) were added to the reaction mixture. The reaction was carried out under microwave irradiation (150 W, 65ºC, 15 PSI) for 60 minutes. The mixture was then poured into DCM, washed with a saturated aqueous solution of $NaHCO_3$ and extracted with DCM (3 x 20 mL). The combined organic layers were washed with brine, dried over $MgSO_4$ and concentrated. The compounds obtained were isolated and purified by column chromatography (EtOAc/Hex from 1:9 to 7:3 for all compounds). **19** and **20** were isolated as colorless syrups, while compounds **2** and **21** were isolated as yellow and yellowish-brown syrups, respectively.

N-6-benzamido-9-(2,3,4-tri-*O*-benzyl-α-L-rhamnopyranosyl)purine (**19**, Scheme 4.3), *N*-6-benzamido-9-(2,3,4-tri-*O*-benzyl-β-L-rhamnopyranosyl)purine (**20**, Scheme 4.3).

Data for compound **19**, using **15** as starting material: Syrup. Isolated yield=8.1%. Rf=0.9 (EtOAc/DCM 1:1). $[\alpha]_D^{20}$=-75.000º (*c* 0.2, MeOH). ^{1}H NMR (400 MHz, MeOD): δ 8.59 (s, 1H, H-2), 8.41 (s, 1H, H-8), 8.09 (d, 2H, *ortho* PhCO, J=7.38 Hz), 7.63 (t, 1H, *para* PhCO, J=6.98 Hz), 7.54 (t, 2H, *meta* PhCO, J=7.86 Hz), 7.41-7.24 (m, 11H, Ph, NH), 7.15-7.04 (m, 3H, Ph), 6.93 (dd, 2H, Ph, J=1.46 Hz, J=7.61 Hz), 6.17 (d, 1H, H-1', $^3J_{1',2'}$=7.99 Hz), 4.82 (dd, 1H, H-2', $^3J_{2',3'}$=2.49 Hz), 4.75, 4.72, 4.70, 4.67 (AB system, 2H, OCH_2-3', J_{AB}=12.02 Hz), 4.60, 4.57, 4.56, 4.53 (AB system, 2H, OCH_2-4', J_{AB}=11.91 Hz), 4.45, 4.42 (part A of AB system, 1H, OCH_2-2', J_{AB}=12.00 Hz), 4.37 (qd, 1H, H-5'), 4.26, 4.23 (part B of AB system, 1H, OCH_2-2', J_{AB}=12.00 Hz), 4.10 (t, 1H, H-3', $^3J_{3',4'}$=3.00 Hz), 3.64 (dd, 1H, H-4', $^3J_{4',5'}$= 5.11 Hz), 1.35 (d, 3H, H-6, $^3J_{6',5'}$=6.70 Hz). ^{13}C NMR (100 MHz, MeOD): δ 168.1 (CO), 153.4 (CqPh), 153.0 (C-2, C-4), 151.0 (C-6), 145.1 (C-8, CqPh), 139.5, 139.4, 138.5 (CqPh), 138.5, 135.0, 133.9, 129.8, 129.5, 129.4, 129.3(5), 129.3, 129.2(5), 129.2, 129.1, 129.0, 128.9, 128.8(6), 128.7 (Ph), 125.1 (C-5), 81.3 (C-1'). 81.1 (C-4'), 76.0 (C-3'), 74.6 (C-2'), 74.1 (C-5'), 73.8 (OCH_2-3'), 73.3 (OCH_2-4'), 72.4 (OCH_2-2'), 18.3 (C-6'). HRMS (m/z) calculated for $[C_{39}H_{37}N_5NaO_5]^+$: 678.2687, found: 678.2695.

Data for compound **20**, using **15** as starting material: Syrup. Isolated Yield=36.2%. Rf=0.7 (EtOAc/DCM 1:1). $[\alpha]_D^{20}$=-29.000º (*c* 1.0, MeOH). ^{1}H NMR (400 MHz, MeOD): δ 8.55 (s, 1H, H-2), 8.32 (s, 1H, H-8), 8.10 (d, 2H, *ortho* PhCO, J=6.91 Hz), 7.63 (t, 1H, *para* PhCO, J=7.30 Hz), 7.54 (t, 2H, *meta* PhCO, J=7.50 Hz), 7.41 (d, 2H, Ph, J=7.49 Hz), 7.35-7.23 (m, 9H, Ph, NH), 7.01 (dd, 3H, Ph, J=2.00 Hz, J=5.11 Hz), 6.88-6.83 (m, 2H, Ph), 5.92 (d, 1H, H-1', $^3J_{1',2'}$= 0.72 Hz), 4.94, 4.91 (part A of AB system, 1H, OCH_2-4', J_{AB}=11.05 Hz), 4.83, 4.80 (part A of AB system, 1H, OCH_2-3', J_{AB}=12.05 Hz), 4.76, 4.73 (part B of AB system, 1H, OCH_2-3'), 4.72, 4.69 (part B of AB system, 1H, OCH_2-4'), 4.69, 4.66 (part A of AB system, 1H, OCH_2-2', J_{AB}=11.79 Hz), 4.29, 4.27 (part B of AB system, 1H, OCH_2-2', J_{AB}=11.59 Hz), 4.23 (br s, 1H, H-2'), 3.95 (dd, 1H, H-3', $^3J_{3',2'}$=2.47 Hz, $^3J_{3',4'}$=9.21 Hz), 3.77-3.59 (m, 2H, H-4', H-5'), 1.36 (d, 3H, H-6', $J_{6',5'}$=5.87 Hz). ^{13}C NMR (100 MHz, MeOD): δ 167.9 (CO), 153.8 (C-2), 151.7 (C-4), 150.8 (C-6), 144.0 (C-8), 139.7, 139.5, 138.1, 135.0 (CqPh), 129.8, 129.6, 129.5, 129.4, 129.3, 129.2, 129.1, 128.9, 128.8(7), 128.8(5), 128.8 (Ph), 124.2 (C-5), 84.0 (C-3'), 83.2 (C-1'), 80.6 (C-4'), 76.3 (C-5'), 76.2 (OCH_2-4'), 75.5 (OCH_2-2'), 74.5 (C-2'), 73.8 (OCH_2-3'), 18.5 (C-6'). HRMS (m/z) calculated for $[C_{39}H_{37}N_5NaO_5]^+$: 678.2687, found: 678.2683.

N-6-benzamido-9-(2,3,4,6-tetra-*O*-benzyl-α-D-mannopyranosyl)purine (**2**, Scheme 4.3), *N*-6-benzamido-9-(2,3,4,6-tetra-*O*-benzyl-β-D-mannopyranosyl)purine (**21**, Scheme 4.3).

Data for **2**, using **16** as starting material: Syrup. Isolated yield=16.4%. Rf=0.9 (EtOAc/DCM 1:1). $[\alpha]_D^{20}$= 37.864º (*c* 1.0, MeOH). ^{1}H NMR (400 MHz, $CDCl_3$): δ 8.67 (s, 1H, H-2), 8.00-7.93 (m, 3H, H-8, 2H *ortho* PhCO), 7.55 (t, 1H, *para* PhCO, J=7.34 Hz), 7.46 (t, 2H, *meta* PhCO, J=7.75 Hz), 7.31-7.04 (m, 19H, Ph, NH), 6.95-6.90 (m, 2H, Ph) 5.99 (d, 1H, H-1', $^3J_{1',2'}$=7.60 Hz), 4.88 (dd, 1H, H-2', $^3J_{2',3'}$=2.72 Hz), 4.66, 4.63, 4.58, 4.55 (AB system, 2H, OCH_2, J_{AB}=12.10 Hz), 4.50-4.33 (m, 6H, H-5', 2 x OCH_2, 4H, OCH_2, 1H), 4.21, 4.18 (part B of AB system, 1H, OCH_2, J_{AB}=12.12 Hz), 3.89 (br t, 1H, H-3', $^3J_{3',4'}$=3.15 Hz), 3.81 (dd, 1H, H-4', $^3J_{4',5'}$=5.90 Hz), 3.70 (dd, part AX of ABX system, 1H, H-6'$_a$, $^3J_{6'a,5'}$=6.09 Hz, $J_{6'a,6'b}$=10.80 Hz), 3.61 (dd, part BX of ABX system, 1H, H-6'$_b$, $^3J_{6'b,5'}$=3.79 Hz). ^{13}C NMR (100 MHz, $CDCl_3$): δ 164.6 (CO), 152.8 (C-2), 151.7 (C-4), 149.5 (C-6), 142.9 (C-8), 138.0, 137.9, 137.7, 137.0, 133.9 (CqPh), 129.0, 128.6, 128.5, 128.4, 128.2, 128.1(5), 128.1, 128.0(9), 128.0(6), 127.9(6), 127.9, 127.8 (Ph), 123.3 (C-5), 81.2 (C-1'), 75.8 (CH_2Ph), 75.0 (C-3', C-4'), 73.3, 73.2(8), 72.7, 72.5 (3 x OCH_2, C-5'), 68.5 (C-6'). HRMS (m/z) calculated for $[C_{46}H_{43}N_5NaO_6]^+$: 784.3106, found: 784.3114. Data in accordance with previously obtained data (unpublished results).

Data for **21**, using **16** as starting material: Syrup. Isolated yield=10.4%. Rf=0.78 (EtOAc/DCM 1:1). $[\alpha]_D^{20}$= 41.000º (*c* 1.0, MeOH). ^{1}H NMR (400 MHz, $CDCl_3$): δ 8.64 (s, 1H, H-2), 8.27 (s, 1H, H-8), 8.02 (d, 2H, *ortho* PhCO, J=7.66 Hz), 7.57 (t, 1H, *para* PhCO, J=7.33 Hz), 7.49 (t, 2H, *meta* PhCO, J=7.55 Hz), 7.36-7.12 (m, 16H, Ph, NH), 7.07-6.97 (m, 3H, Ph), 6.89 (d, 2H, Ph, J=7.07 Hz), 5.83 (br d, 1H, H-1', $^3J_{1'2'}$=0.75 Hz), 4.90, 4.87 (part A of AB system, 1H, OCH_2-4', J_{AB}=10.75 Hz), 4.76 (s, 2H, OCH_2-3'), 4.73, 4.70 (part A of AB system, 1H, OCH_2-2', J_{AB}=11.42 Hz), 4.62-4.54 (m, 2H, part B of AB system, 1H, OCH_2-4', part A of AB system, 1H, OCH_2-6'), 4.52, 4.49 (part B of AB system, 1H, OCH_2-6', J_{AB}=12.04 Hz), 4.28, 4.25 (part B of AB system, 1H, OCH_2-2', J_{AB}=11.42 Hz), 4.11-4.01 (m, 2H, H-2', H-4'), 3.87 (dd, 1H, H-3', $^3J_{3',2'}$=2.06 Hz, $^3J_{3',4'}$=9.40 Hz), 3.79-3.64 (m, 3H, H-5', H-6'a, H-6'b). ^{13}C NMR (100 MHz, $CDCl_3$): δ 164.7 (CO), 152.4 (C-2), 150.3 (C-4), 149.3 (C-6), 142.6 (C-8), 138.1, 138.0, 137.8, 136.6, 133.9 (CqPh), 133.0 (*para* PhCO), 129.2, 129.0, 128.8, 128.6, 128.5(7), 128.5, 128.4, 128.3(6), 128.3, 128.1, 128.0(7), 128.0, 127.9, 127.7, (Ph), 125.4 (C-5), 83.3 (C-3'), 81.9 (C-1'), 78.9 (C-5'), 75.6 (OCH_2-4'), 74.8 (OCH_2-2'), 74.2 (C-4), 73.7 (OCH_2-6'), 73.6 (C-2), 73.2 (OCH_2-3'), 69.0 (C-6'). HRMS (m/z) calculated for $[C_{46}H_{44}N_5O_6]^+$: 762.3286, found: 762.3282.

Using **18** as starting material, no results were obtained for this method.

4.2.3.2 Conventional stirring method (method 2)

The method without microwave irradiation was tested and performed following a reported procedure [69] and the two products obtained are represented in Scheme 4.4. BSA (3.00 equiv.) was added to a solution of *N*^{6}-benzoyladenine (1.50 equiv.) in dry ACN (10 mL) and the mixture was stirred for 40 minutes at room temperature. Then, a solution of the fully protected glycosyl donor (**16** or **18**) (2.00 mmol for **16** and 1.00 mmol for **18**) in dry ACN (2 mL) and TMSOTf (8.00 equiv.) were added to the mixture. The reaction mixture was stirred at room temperature, for 24 hours for **16**, and for 4 days for **18**. The solution was then poured into DCM (10 mL), washed with a saturated aqueous solution of Na_2CO_3 and extracted with DCM (3 x 15 mL). The combined organic layers were washed with brine, dried over $MgSO_4$, filtered and concentrated. For the reaction with **16** as starting material, no results were obtained. For the reaction with **18**, products **22** and **23** were obtained as a colorless syrup and an inseparable mixture, after isolation by column chromatography (EtOAc/Hex from 1:9 to 7:3). The ratio of the regioisomers was determined by ^{1}H NMR integration of the H-2 signals in $CDCl_3$ (8.69 ppm for **22** and 8.63 ppm for **23**). The ratio was found to be 0.12:1 (**22**: **23**).

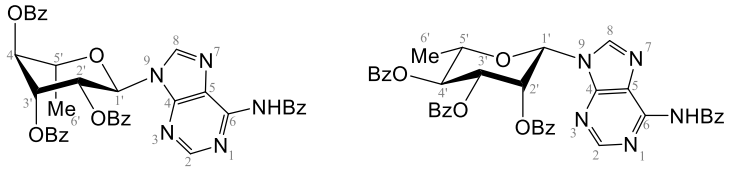

22 **23**

Scheme 4.4. Structure of compounds **22** and **23**

N-6-benzamido-9-(2,3,4-tri-*O*-benzoyl-α-L-rhamnopyranosyl)purine (**22**, Scheme 4.4), *N*-6-benzamido-9-(2,3,4-tri-*O*-benzoyl-β-L-rhamnopyranosyl)purine (**23**, Scheme 4.4).

Data for compound **22**, using **18** as starting material. Syrup. Calculated yield=3.0%. Rf=0.64 (EtOAc/DCM 1:1). As **22** is the minor isomer, it was not possible to identify all the NMR signals.

Data for compound **23**, using **18** as starting material. Syrup. Calculated yield=21.8%. Rf=0.64 (EtOAc/DCM 1:1). ^{1}H NMR (400 MHz, $CDCl_3$): δ 8.63 (s, 1H, H-2), 8.09 (s, 1H, H-8), 7.91-6.99 [m, 20 H, Ph(**23**), 1H, NH (**23**), 20H, Ph(**22**), 1H, NH (**22**), $CHCl_3$], 6.34 (br s, 1H, H-1'), 5.94 (br s, 1H, H-2'), 5.70 (dd, 1H, H-3', $^3J_{3',2'}$=2.34 Hz, $^3J_{3',4'}$=9.95 Hz), 5.62 (t, 1H, H-4', $^3J_{4',5'}$=9.64 Hz), 4.03 (qd, 1H, H-5'), 1.35 (d, 3H, H-6', $^3J_{6',5'}$=5.82 Hz). ^{13}C NMR (100 MHz, $CDCl_3$): δ 165.7,

165.5, 164.9 (CO), 151.2 (C-2), 151.1 (C-4), 149.6 (C-6), 141.1 (C-8), 134.2, 133.8, 133.6, 133.0 (CqPh), 130.0, 129.9, 129.8(7), 129.1, 129.0, 128.9, 128.8, 128.7, 128.6(6), 128.5, 128.4, 128.1 (Ph), 122.3 (C-5), 80.4 (C-1'), 74.8 (C-5'), 71.7 (C-3'), 70.8 (C-4'), 70.0 (C-2'), 18.0 (C-6'). HRMS calculated for $[C_{39}H_{32}N_5O_8]^+$: 698.2245, found: 698.2251.

4.2.4 New *N*-glycosylation method (method 3)

Having tried two different already reported methods, a new methodology was experimented inspired by a reported procedure [67].

4.2.4.1 Procedure for *N*-glycosylation using a non-silylated base

After optimization, the best conditions found are here described. To a solution of the fully protected methyl glycoside (**17**) (0.86 mmol) in anhydrous toluene (0.10 M), N^6-benzoyladenine (3.50 equiv.) and iodine (I_2) (4.00 equiv.) were added. The mixture was then stirred, at 65ºC, for 4 hours. The resultant solution was washed with a saturated aqueous solution of $Na_2S_2O_3$ and extracted with EtOAc (3 x 20 mL). The organic layers were combined, washed with brine, dried over $MgSO_4$, filtered and concentrated. The final compounds (**2** and **21**) were isolated by column chromatography (EtOAc/Hex from 1:9 to 7:3).

Compounds **2** and **21** were obtained using **17** as starting material, having 35.4% and 10.4% isolated yields, respectively. The data for both compounds was already reported in the section 4.2.3.1.

For the reaction between **17** and the non-silylated ACP, no results were obtained.

4.2.4.2 Procedure for *N*-glycosylation using a silylated base

4.2.4.2.1 Methodology followed for N^6-benzoyladenine

Inspired by the reported methodology [67], N^6-benzoyladenine was silylated by adding $(NH_4)_2SO_4$ (0.10 equiv.) and TMSCl (3.50 equiv.) to a solution of the purine (0.60 mmol, 1.00 equiv.) in HMDS (0.50 M). The mixture was stirred at 125ºC, for 50 minutes, until a clear solution was obtained. The solution was then cooled to room temperature and placed under high vacuum to remove excess HMDS. A solution in DCM (0.60 M) was made. The silylated N^6-benzoyladenine (3.50 equiv.) and I_2 (4.00 equiv.) were added to a solution of the fully protected phenyl α-D-thiomannoside (**17**, 0.16 mmol) and stirred at room temperature, for 24 hours, followed by heating to 65ºC for 4,5 hours. The final solution was washed with $Na_2S_2O_3$ and extracted with EtOAc (3 x 20 mL). The combined organic layers were washed with brine, dried

over $MgSO_4$, filtered and concentrated. The products were isolated and purified by column chromatography (EtOAc/Hex from 1:9 to 7:3).

Compounds **2** and **21** were obtained using **17** as the starting material for this method, with 64.3% and 7.1% isolated yields, respectively.

4.2.4.2.2 Methodology followed for 2-acetamido-6-chloropurine

Inspired by the methodology reported by [69], with a solvent modification from ACN to THF, compound **24**, which structure is represented in Scheme 4.5, was synthesized. 2-acetamido-6-chloropurine was silylated by adding BSA (3.0 equiv.) to a solution of the purine (0.1058 g, 0.50 mmol, 1.50 equiv.) in anhydrous THF (10 mL). The mixture was stirred for 40 minutes at room temperature. The mixture was added to a solution of **17** (0.2109 g, 0.33 mmol, 1.00 equiv.) in anhydrous THF (2 mL). The reaction mixture was stirred, at 65ºC, for 23 hours. The solution was washed with a saturated aqueous solution of $Na_2S_2O_3$ and extracted with EtOAc (3 x 20 mL). The organic layers were then combined, dried over $MgSO_4$, filtered and concentrated. Product was isolated, as a yellow syrup, and purified by column chromatography (EtOAc/Hex from 1:9 to 7:3).

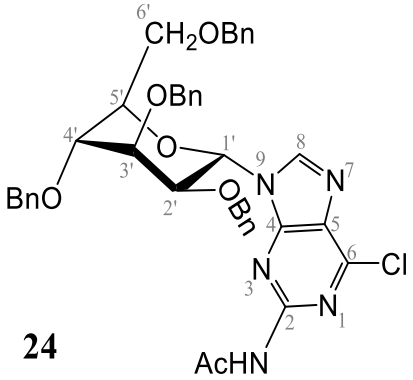

24

Scheme 4.5. Structure of compound **24**

2-acetamido-6-chloro-9-(2,3,4,6-tetra-*O*-benzyl-α-D-mannopyranosyl)purine (**24**, Scheme 4.5).

Data for **24** using **17** as starting material: Syrup. Isolated yield=24.2%. Rf=0.56 (EtOAc/Hex 1:1). $[\alpha]_D^{20}$=140.000º (*c* 0.1, MeOH). ^{1}H NMR (400 MHz, $CDCl_3$): δ 7.87 (s, 1H, H-8), 7.87 (s, 1H, NH) 7.32-7.09 (m, 16H, Ph), 7.04 (t, 1H, Ph, J=7.36 Hz), 6.97 (t, 1H, Ph, J=7.32 Hz), 6.75 (d, 2H, Ph, J=7.32 Hz), 5.78 (d, 1H, H-1', $^3J_{1',2'}$=8.51 Hz), 4.65-4.52 (m, 3H, OCH_2-3', H-2'), 4.46-4.29 (m, 6H, OCH_2-4', 2H, OCH_2-6', 2H, part A of AB system, 1H, OCH_2-2', H-5'), 4.05, 4.02 (part B of AB system, 1H, OCH_2-2', J_{AB}=12.19 Hz), 3.90 (br t, 1 H, H-3'), 3.74 (dd, 1H, H-4',

$^{3}J_{4',3'}$=2.89 Hz, $^{3}J_{4',5'}$=4.90 Hz), 3.64, 3.61 (part AX of ABX system, 1H, H-6'$_a$, $^{3}J_{6'a,5''}$=6.44 Hz, $^{3}J_{6'a,6'b}$=10.60 Hz), 3.53, 3.50 (part BX of ABX system, 1H, H-6'$_b$, $^{3}J_{6'b,5'}$=4.28 Hz, $^{3}J_{6'b,6'a}$=10.60 Hz), 2.27 (s, 3H, CH_3). ^{13}C NMR (100 MHz, $CDCl_3$): δ 171.0 (CO), 152.2 (C-4), 151.7, 151.3 (C-2, C-6), 144.6 (C-8), 137.9, 137.7, 137.5, 136.6 (CqPh), 128.7(0), 128.6(9), 128.5 (Ph), 128.3 (C-5), 128.3(2), 128.2, 128.1(3), 128.1, 127.9, 127.8 (Ph), 80.8 (C-1'), 76.1 (C-5'), 74.8 (C-4'), 73.7 (C-3'), 73.3, 72.9, 72.2 (OCH_2-3', OCH_2-4', OCH_2-6'), 72.0 (C-2'), 71.3 (OCH_2-2'), 68.2 (C-6'), 25.3 (CH_3). HRMS (m/z) calculated for $[C_{41}H_{40}ClN_5NaO_6]^+$: 756.2559, found: 756.2546. Data in accordance with previously reported data [66].

4.3 UV-Visible metal chelating assays

UV-visible studies were performed at Faculdade de Ciências, Universidade de Lisboa, following a procedure already reported by our group (unpublished procedure), with alteration of the chosen solvent from distilled water/dimethyl sulfoxide (H_2O/DMSO) 95:5 to 90:10, due to compounds **19** and **20** poor water solubility.

4.3.1 Probe and ion solutions preparation

Probe solutions were made by dissolving each of the synthesized compounds (**2**, **19-21** and **24**) (1 x 10^5 mol) in H_2O/DMSO 90:10, in order to obtain 100 mL of a 1 x 10^{-4} M final solution.

Ion solutions were made by dissolving the ion chloride salts [copper chloride ($CuCl_2$), zinc chloride ($ZnCl_2$), iron chloride ($FeCl_2$) and aluminum chloride ($AlCl_3$)] (5 x 10^{-4} mol) in the already mentioned solvent in order to obtain 50 mL of a 1 x 10^{-2} M solution. From this solution, five other solutions were made with 20, 10, 6, 4 and 2 μM final concentrations, by diluting, 50, 25, 15, 10 and 5 μL, respectively, in 25 mL volumetric flasks.

4.3.2 Chelating assays

To perform the metal chelating studies, 1.5 mL of each probe solution was added to 1.5 mL of each of the 20 μM ion salt's solutions and the spectra were recorded after 30 minutes in a wavelength range of 400 to 200 nm.

4.4 Anticholinesterase assays

Compounds **19** and **20** were assayed for their inhibitory activity towards *ee*AChE, *eq*BChE, *h*AChE and *h*BChE, following Ellman's colorimetric method [70] with some modifications [60, 61] carried out by Dr. Modesto de Candia's research group.

The results for compound **21** as an AChE and BChE inhibitor were not possible to obtain before the end of this dissertation delivery period. **2** properties were previously determined (unpublished results). For compounds **22** and **23**, these properties were not possible to determine due to being obtained in an inseparable mixture. Finally, nucleoside **24** was not obtained in an enough amount to determine its properties as AChE/BChE inhibitor, however its inhibitory constante (K_i) was previously determined and disclosed by our group [66].

4.4.1 General procedure

The inhibitory activity of AChE is usually determined in a reaction mixture containing 20 μL of a solution of *ee*AChE or *h*AChE [0.9 U/mL in 0.1 M pH 8.0 phosphate buffer (PB)], 20 μL of a DTNB solution (3.3 mM in 0.1 M pH 7.0 PB, containing 0.1 nM $NaHCO_3$), 20 μL of a solution of test compound (five to seven concentrations, ranging from 1×10^{-5} to 1×10^{-9} M, in 0.1 M pH 8.0 PB) and 120 μL of 0.1 M pH 8.0 PB. After 20 minutes of incubation at 25ºC, 20 μL of acetylthiocholine iodide (0.05 mM in 0.1 M pH 8.0 PB) are added as the substrate and the hydrolysis rate of the substrate was monitored at 412 nm for 5 minutes at 25ºC. The concentration of compounds which produced 50% inhibition of AChE activity (IC_{50}) is calculated by a nonlinear regression of response/concentration (log) curve, by using GraphPad Prism software (version 5.01). For the determination of BChE inhibitory activity, a similar method is used with a solution of *eq*BChE or *h*BChE (0.9 U/mL in 0.1 M, pH 8.0 PB) and butyrylthiocholine iodide (0.05 mM in 0.1 M, pH 8.0 PB) as the substrate. The inhibition data is then reported as means of IC_{50}'s determined at least in three independent measurements.

BIBLIOGRAPHY

[1] Balázs, N., Bereczki, D., Kovács, T., Cholinesterase inhibitors and memantine for the treatment of Alzheimer and non-Alzheimer dementias. Ideggyogy. Sz., **2021**, 74, 379–387. doi: 10.18071/isz.74.0379.

[2] Sharma, K., Cholinesterase inhibitors as Alzheimer's therapeutics (Review). Mol. Med. Rep., **2019**, 20, 1479–1487. doi: 10.3892/mmr.2019.10374.

[3] Karasova, J. Z., Hrabinova, M., Krejciova, M., Jun, D., Kuca, K., Donepezil and rivastigmine: Pharmacokinetic profile and brain-targeting after intramuscular administration in rats. Iran. J. Pharm. Res., **2020**, 19, 95–102. doi: 10.22037/ijpr.2019.1100723.

[4] Association, A., 2019 Alzheimer's disease facts and figures. Alzheimer's Dement., **2019**,15 (3), 321–387. doi: 10.1016/j.jalz.2019.01.010.

[5] Patrick, G. L., An Introduction to Medicinal Chemistry (5th ed.) **2013**, Oxford University Press.

[6] Chen, Z. R., Huang, J. B. , Yang, S. L., Hong, F. F., Role of Cholinergic Signaling in Alzheimer's Disease. Mol,. **2022**, 27, 1816. doi: 10.3390/molecules27061816.

[7] Li, Q., He, S., Chen, Y., Feng, F., Qu, W., Sun, H., Donepezil-based multi-functional cholinesterase inhibitors for treatment of Alzheimer's disease. Eur. J. Med. Chem., **2018**, 158, 463–477. doi: 10.1016/j.ejmech.2018.09.031.

[8] Moreira, N. C. D. S., Lima, J. E. B. F., Marchiori, M. F., Carvalho, I., Sakamoto-Hojo, E. T., Neuroprotective Effects of Cholinesterase Inhibitors: Current Scenario in Therapies for Alzheimer's Disease and Future Perspectives. J. Alz. Dis. Rep., **2022**, 6, 177–193. doi: 10.3233/ADR-210061.

[9] Bekdash, R. A., The cholinergic system, the adrenergic system and the neuropathology of alzheimer's disease. Int. J. Mol. Sci., **2021**, 22, 1–18. doi: 10.3390/ijms22031273.

[10] Johnson, G., Moore, S. W., Why has butyrylcholinesterase been retained? Structural and functional diversification in a duplicated gene. Neurochem. Int., **2012**, 61, 783–797. doi: 10.1016/j.neuint.2012.06.016.

[11] Xu, Y., Cheng, S., Sussman, J. L., Silman, I., Jiang, H., Computational studies on acetylcholinesterases. Mol., **2017**, 22, 1324. doi: 10.3390/molecules22081324.

[12] Alawode, D. O. T., Fox, N. C., Zetterberg, H., Heslegrave, A. J., Alzheimer's Disease Biomarkers Revisited From the Amyloid Cascade Hypothesis Standpoint. Front. Neurosci., **2022**, 16, 1-14. doi: 10.3389/fnins.2022.837390.

[13] Wu, T., Lin, D., Chen, Y., Jiang, S., Riaz, M. W., Fu, N., Mou, C., Ye, M., Zheng, Y., Amyloid Cascade Hypothesis for the Treatment of Alzheimer's Disease: Progress and Challenges. Agi. Dis., **2022**, 1-14 doi: 10.14336/AD.2022.0412.

[14] Roda, A., Serra-Mir, G., Montoliu-Gaya, L., Tiessler, L., Villegas, S., Amyloid-beta peptide and tau protein crosstalk in Alzheimer's disease. Neur. Regen. Res., **2022**, 17, 1666–1674,. doi: 10.4103/1673-5374.332127.

[15] Vijayan, D., Chandra, R., Amyloid Beta Hypothesis in Alzheimer's Disease: Major Culprits and Recent Therapeutic Strategies. Curr. Drug Targ., **2019**, 21, 148–166. doi: 10.2174/1389450120666190806153206.

[16] Wu, M., Zhang, M., Yin, X., Chen, K., Hu, Z., Zhou, Q., Cao, X., Chen, Z., Liu, D., The role of pathological tau in synaptic dysfunction in Alzheimer's diseases. Trans. Neurodeg., **2021**, 10, 1-11 doi: 10.1186/s40035-021-00270-1.

[17] Al Mamun, A., Uddin, M. S., Mathew, B., Ashraf, G. M., Toxic tau: Structural origins of tau aggregation in Alzheimer's disease. Neur. Regen, Res,. **2020**, 15, 1417–1420. doi: 10.4103/1673-5374.274329.

[18] Kametani, F., Hasegawa, M., Reconsideration of Amyloid Hypothesis and Tau Hypothesis in AD. Front. Neurosci., **2018**, 12, 1-11. doi: 10.3389/fnins.2018.00025.

[19] Yu, H., Wu, J., Amyloid-β: A double agent in Alzheimer's disease?. Biomed Pharmacother., **2021**, 139, 1-9.doi: 10.1016/j.biopha.2021.111575.

[20] Majdi, A., Sadigh-Eteghad, S., Aghsan, S. R., Farajdokht, F., Vatandoust, S. M., Namvaran, A., Mahmoudi, J., Amyloid-β, tau, and the cholinergic system in Alzheimer's disease: Seeking direction in a tangle of clues. Rev. Neurosci., **2020**, 31, 391–413. doi: 10.1515/revneuro-2019-0089.

[21] Nygaard, H. B., van Dyck, C. H., Strittmatter, S. M., Fyn kinase inhibition as a novel therapy for Alzheimer's disease. Alzh. Res. Ther., **2014**, 6, 1-8. doi: 10.1186/alzrt238.

[22] Nygaard, H. B., Targeting Fyn Kinase in Alzheimer's Disease. Biol. Psych., **2018**, 83, 369–376. doi: 10.1016/j.biopsych.2017.06.004.

[23] de Matos, A. M., Blásquez-Sánchez, M. T., Bento-Oliveira, A., de Almeida, R., Nunes, R. S., Lopes, P., Machuqueiro, M., Cristovão, J., Gomes, C. M., Souza, C. S., El Idrissi, I. G., Colabufo, N. C., Diniz, A., Marcelo, F., Oliveira, M. C., López, O., Fernández-Bolaños, J. G., Dätwyler, P., Ernst, B., Ning, K., Garwood, C., Chen, B., Rauter, A. P., Glucosylpolyphenols as Inhibitors of Aβ-Induced Fyn Kinase Activation and Tau Phosphorylation: Synthesis, Membrane Permeability, and Exploratory Target Assessment within the Scope of Type 2 Diabetes and Alzheimer's Disease. J. Med. Chem., **2020**, 63, 11663–11690. doi: 10.1021/acs.jmedchem.0c00841.

[24] de Matos, A. M., Man, T., El Idrissi, I., Souza, C. C., Mead, E., Dunbar, C., Wolak, J., Oliveira, M. C., Evans, D., Grayson, E., Partridge, B., Garwood, C., Ning, K., Sharman, G., Chen, B., Rauter, A. P., Discovery of *N*-methylpiperazinyl flavones as a novel class of compounds with therapeutic potential against Alzheimer's disease: Synthesis, binding affinity towards amyloid β oligomers (Aβo) and ability to disrupt Aβo-PrPC interactions. Pure Appl. Chem., **2019**, 91, 1107–1136. doi: 10.1515/pac-2019-0114.

[25] Grayson, J. D., Baumgartner, M. P., Souza, C. C., Dawes, S. J., El Idrissi, I., Louth, J. C., Stimpson, S., Mead, E., Dunbar, C., Wolak, J., Sharman, G., Evans, D., Zhuravleva, A., Roldan, M. S., Colabufo, N. A., Ning, K., Garwood, C., Thomas, J. A., Partridgr, B. M., de Leon, A. V., Gillet, V. J., Rauter, A. P., Chen, B., Amyloid binding and beyond: A new approach for Alzheimer's disease drug discovery targeting Aβo-PrP^C binding and downstream pathways. Chem. Sci., **2021**, 12, 3768–3785. doi: 10.1039/d0sc04769d.

[26] Kerchev, P. I., Van Breusegem, F., Improving oxidative stress resilience in plants. Plant J., **2022**, 109, 359–372. doi: 10.1111/tpj.15493.

[27] Cioffi, F., Adam, R. H. I., Broersen, K.,mMolecular Mechanisms and Genetics of Oxidative Stress in Alzheimer's Disease. J. Alzh. Dis., **2019**, 72, 981–1017. doi: 10.3233/JAD-190863.

[28] Tamagno, E., Guglielmotto, M., Vasciaveo, V., Tabaton, M., Oxidative stress and beta amyloid in alzheimer's disease. Which comes first: The chicken or the egg? Antiox., **2021**, 10, 1-15. doi: 10.3390/antiox10091479.

[29] Zubčić, K., Hof, P. R., Šimić, G., Jazvinšćak Jembrek, M., The Role of Copper in Tau-Related Pathology in Alzheimer's Disease. Front. Mol. Neurosci., **2020**, 13, 1-19. doi: 10.3389/fnmol.2020.572308.

[30] Lavado, L. K., Zhang, M., Patel, K., Khan, S., Patel, U. K., Biometals as Potential Predictors of the Neurodegenerative Decline in Alzheimer's Disease. Cureus, **2019**, 1, 1-11. doi: 10.7759/cureus.5573.

[31] Squitti, R., Faller, P., Hureau, C., Granzotto, A., White, A. R., Kepp, K. P., Copper Imbalance in Alzheimer's Disease and Its Link with the Amyloid Hypothesis: Towards a Combined Clinical, Chemical, and Genetic Etiology. J. Alzh. Dis., **2021**, 83, 23–41. doi: 10.3233/JAD-201556.

[32] Patel, R., Aschner, M., Commonalities between copper neurotoxicity and Alzheimer's disease. Toxi., **2021**, 9, 1–11. doi: 10.3390/toxics9010004.

[33] Kabir, M. T., Uddin, M. S., Zaman, S., Begum, Y., Ashraf, G. M., Bin-Jumah, M. N., Bungau, S. G., Mousa, S. A., Abdel-Daim, M. M., Molecular Mechanisms of Metal Toxicity in the Pathogenesis of Alzheimer's Disease. Mol. Neurobio., **2021**, 58, 1-20. doi: 10.1007/s12035-020-02096-w.

[34] Kim, A. C., Lim, S., Kim, Y. K., Metal ion effects on Aβ and tau aggregation. Int. J. Mol. Sci., **2018**, 19, 1-15. doi: 10.3390/ijms19010128.

[35] Cummings, J., Lee, G., Nahed, P., Kambar, M. E. Z. N., Zhong, K., Fonseca, J., Taghva, K., Alzheimer's disease drug development pipeline: 2022. Alzh. Dement. Transl. Res. Clin. Interv., **2022**, 8, 1-24. doi: 10.1002/trc2.12295.

[36] Du, X., Wang, X., Geng, M., Alzheimer's disease hypothesis and related therapies. Trans. Neurodeg., **2018**, 7, 1-7. doi: 10.1186/s40035-018-0107-y.

[37] Zhao, J., Shi, Q., Tian, H., Li, Y., Liu, Y., Xu, Z., Robert, A., TDMQ20, a Specific Copper Chelator, Reduces Memory Impairments in Alzheimer's Disease Mouse Models. ACS Chem. Neurosci., **2021**, 12, 140–149. doi: 10.1021/acschemneuro.0c00621.

[38] Adlimoghaddam, A., Neuendorff, M., Roy, B., Albensi, B. C., A review of clinical treatment considerations of donepezil in severe Alzheimer's disease. CNS Neurosci. Therap., **2018**, 24, 876–888. doi: 10.1111/cns.13035.

[39] Yiannopoulou, K. G., Anastasiou, A. I., Kyrozis, A., Anastasiou, I. P., Donepezil Treatment for Alzheimer's Disease in Chronic Dialysis Patients. Case Rep. Nephrol. Dial., **2019**, 9, 126–136. doi: 10.1159/000502682.

[40] Mohsin, N. U. A., Ahmad, M., Donepezil: A review of the recent structural modifications and their impact on anti-alzheimer activity. Braz. J. Pharma. Sci., **2020**, 56, 1–16. doi: 10.1590/S2175-97902019000418325.

[41] Kaur, A., Nigam, K., Bhatnagar, I., Sukhpal, H., Awasthy, S., Shankar, S., Dang, S., Treatment of Alzheimer's diseases using donepezil nanoemulsion: an intranasal approach. Drug Deliv. Transl. Res., **2020**, 10, 1862–1875. doi: 10.1007/s13346-020-00754-z.

[42] Nguyen, K., Hoffman, H., Chakkamparambil, B., Grossberg, G. T., Evaluation of rivastigmine in Alzheimer's disease. Neurodegener. Dis. Manag., **2021**, 11, 35–48. doi: 10.2217/nmt-2020-0052.

[43] Chou, P. S., Jhang, K. M., Huang, L. C., Wang, W. F., Yang, Y. H., Skinfold thickness for rivastigmine patch application in Alzheimer's disease. Psychopharma., **2019**, 236, 1255–1260. doi: 10.1007/s00213-018-5135-x.

[44] Mora-Navarro, M. A., Rincón-Sánchez, A. R., Pacheco-Moisés, F. P., Mireles-Ramírez,

M. A., Delgado-Lara, D. L. C., Torres-Mendonza, B. M., Velásquez-Brizuela, I. E., Ortiz, G. G., Nutritional status in patients with probable Alzheimer's disease. J. Nutr. Health Agi., **2020**, 25, 340-346. doi: 10.1007/s12603-020-1519-9.

[45] Metz, C. N., Pavlov, V. A., Treating disorders across the lifespan by modulating cholinergic signaling with galantamine. J. Neurochem., **2021**, 158, 1359–1380. doi: 10.1111/jnc.15243.

[46] Ghosh, S., Jana, K., Wakchaure, P. D., Ganguly, B., Revealing the cholinergic inhibition mechanism of Alzheimer's by galantamine: a metadynamics simulation study. J. Biomol. Struct. Dyn., **2020**, 40, 5100-5111. doi: 10.1080/07391102.2020.1867644.

[47] Santos, G. S., Sinoti, S. B. P., de Almeida, F. T. C., Silveira, D., Simeoni, L. A., Gomes-Copeland, K. K. P., Use of galantamine in the treatment of Alzheimer's disease and strategies to optimize its biosynthesis using the in vitro culture technique. Plant Cell, Tissue Organ Cult., **2020**, 143, 13–29. doi: 10.1007/s11240-020-01911-5.

[48] Baakman, A. C., Gavan, C., van Doeslaar, L., de Kam, M., Broekhuizen, K., Bajenaru, O., Camps, L., Swart, E. L., Kalosvaart, K., Schoonenboom, N., Lemstra, E., Scheltens, P., Cohen, A., van Gerven, J., Groeneveld, G. J., Acute response to cholinergic challenge predicts long-term response to galantamine treatment in patients with Alzheimer's disease. Br. J. Clin. Pharmacol., **2022**, 88, 2814–2829. doi: 10.1111/bcp.15206.

[49] Koola, M. M., Galantamine-Memantine combination in the treatment of Alzheimer's disease and beyond. Psych. Res., **2020**, 293, 1-8. doi: 10.1016/j.psychres.2020.113409.

[50] Hampel, H., Mesulam, M. -M., Cuello, A. C., Khachaturian, A. S., Vergallo, A., Farlow, M. R., Snyder, P. J., Giacobini, E., Khachaturian, Z. S., Revisiting the Cholinergic Hypothesis in Alzheimer's Disease: Emerging Evidence from Translational and Clinical Research. J. Prev. of Alzh. Dis., **2019**, 6, 2–15. doi: 10.14283/jpad.2018.43.

[51] García-Ayllón, M. S., Silveyra, M. X., Sáez-Valero, J., Association between acetylcholinesterase and β-amyloid peptide in Alzheimer's cerebrospinal fluid. Chem. Biol. Interact., **2008**, 175, 209–215. doi: 10.1016/j.cbi.2008.04.047.

[52] Inestrosa, N. C., Sagal, J. P., Colombres, M., Acetylcholinesterase interaction with Alzheimer amyloid beta. Subcell. Biochem., **2005**, 38, 299–317. doi: 10.1007/0-387-23226-5_15.

[53] Inestrosa, N. C., Alvarez, A., Pérez, C. A., Moreno, R. D., Vicente, M., Linker, C., Casanueva, O. I., Soto, C., Garrido, J., Acetylcholinesterase accelerates assembly of amyloid-β-peptides into Alzheimer's fibrils: Possible role of the peripheral site of the enzyme. Neur., **1996**, 16, 881–891. doi: 10.1016/S0896-6273(00)80108-7.

[54] Macdonald, I. R., Maxwell, S. P., Reid, G. A., Cash, M. K., Debay, D. R., Quantification of Butyrylcholinesterase Activity as a Sensitive and Specific Biomarker of Alzheimer ' s Disease., **2017**, 58, 491–505. doi: 10.3233/JAD-170164.

[55] Fortuna, A., Costa, P. J., Piedade, M. F. M., Oliveira, M. C., Xavier, N. M., Synthesis of Triazole-Containing Furanosyl Nucleoside Analogues and Their Phosphate, Phosphoramidate or Phoshonate Derivatives as Potential Sugar Diphosphate or Nucleotide Mimetics. Chempluschem., **2020**, 85, 1676–1691. doi: 10.1002/cplu.202000424.

[56] Kaspar, F., Stone, M. R. L., Neubauer, P., Kurreck, A., Route efficiency assessment and review of the synthesis of β-nucleosides: Via N -glycosylation of nucleobases. Green Chem., **2021**, 23, 37–50. doi: 10.1039/d0gc02665d.

[57] Tranová, L., Stýskala, J., Study of the N7Regioselective Glycosylation of 6-Chloropurine

and 2,6-Dichloropurine with Tin and Titanium Tetrachloride. J. Org. Chem., **2021**, 86, 13265–13275. doi: 10.1021/acs.joc.1c01186.

[58] Kataev, V. E., Garifullin, B. F., Antiviral nucleoside analogs. Chem. Heterocycl. Compd., **2021**, 57, 326–341. doi: 10.1007/s10593-021-02912-8.

[59] Garner, A. L., Nucleosides, Nucleotides and Nucleic Acids as Therapeutics: A Virtual Special Issue. ACS Pharmacol. Transl. Sci., **2021**, 4, 1714–1715. doi: 10.1021/acsptsci.1c00231.

[60] Roy, V., Agrofoglio, L. A., Nucleosides and emerging viruses: A new story. Drug Discov. Tod., **2022**, 27, 1945–1953. doi: 10.1016/j.drudis.2022.02.013.

[61] Leoni, S., Casabianca, A., Biagioni, B., Serio, I., Viral hepatitis: Innovations and expectations. World J. Gastroenterol., **2022**, 28, 517–531. doi: 10.3748/wjg.v28.i5.517.

[62] Ami, E. I., Ohrui, H., Intriguing Antiviral Modified Nucleosides: A Retrospective View into the Future Treatment of COVID-19. ACS Med. Chem. Lett., **2021**, 12, 510–517. doi: 10.1021/acsmedchemlett.1c00070.

[63] Wallace, K. B., Bjork, J. A., Molupiravir; molecular and functional descriptors of mithocondrial safety. Toxic. App. Pharma., **2022**, 442, 1-6. doi: 10.1016/j.taap.2022.116003

[64] Niu, G., Li, Z., Huang, P., Tan, H., Engineering nucleoside antibiotics toward the development of novel antimicrobial agents. J. Antibiot., **2019**, 72, 906–912. doi: 10.1038/s41429-019-0230-8.

[65] Mirza, A. Z., Advancement in the development of heterocyclic nucleosides for the treatment of cancer - A review. Nucleos. Nucleot. Nuc. A., **2019**, 38, 836–857. doi: 10.1080/15257770.2019.1615623.

[66] Schwarz, S., Csuk, R., Rauter, A. P., Microwave-assisted synthesis of novel purine nucleosides as selective cholinesterase inhibitors. Org. Biomol. Chem., **2014**, 12, 2446–2456. doi: 10.1039/C4OB00142G.

[67] Cardinal-David, B., Labbé, M.-O., Prévost, M., Dostie, S., Guindon, Y., Diastereoselective and Regioselective Synthesis of Adenosine Thionucleoside Analogues Using an Acyclic Approach. Can. J. Chem., **2020**, 1-16. doi: 10.1139/cjc-2020-0049

[68] Heuckendorff, M., Poulsen, L. T., Hedberg, C., Jensen, H. H., Dissection of the effects that govern thioglucoside and thiomannoside reactivity. Org. Biomol. Chem., **2018**, 16, 2277–2288. doi: 10.1039/c7ob02968c.

[69] Schwarz, S., Siewert, B., Csuk, R., Rauter, A. P., New antitumor 6-chloropurine nucleosides inducing apoptosis and G2/M cell cycle arrest. Eur. J. Med. Chem., **2015**, 90, 595–602. doi: 10.1016/j.ejmech.2014.11.019.

[70] Ellman, G. L., Courtney, K. D., Andres, V., Featherstone, R. M. A new and rapid colorimetric determination of acetylcholinesterase activity. Biochem. Pharmacol., **1961**, 7, 88–95. doi: 10.1016/0006-2952(61)90145-9.

[71] Purgatorio, R., de Candia, M., Catto, M., Carrieri, A., Pisani, L., De Palma, A., toma, M., Ivanova, O. A., Voskressensky, L. G., Altomare, C. D., Investigating 1,2,3,4,5,6-hexahydroazepino[4,3-b]indole as scaffold of butyrylcholinesterase-selective inhibitors with additional neuroprotective activities for Alzheimer's disease. Eur. J. Chem., **2019**, 177, 414-424. doi: 10.1016/j.ejmech.2019.05.062.

[72] de Candia, M., Zaetta, G., Denora, N., Tricarico, D., Majellaro, M., Cellamare, S., Altomare, C. D., New azepino[4,3-b]indole derivatives as nanomolar selective

inhibitors of human butyrylcholinesterase showing protective effects against NMDA-induced neurotoxicity. Eur. J. Chem., **2017**, 125, 288-298. doi: 10.1016/j.ejmech.2016.09.037.

[73] Komersová, A., Komers, K., Cegan, A., New Findings about Ellman's Method to Determine Cholinesterase Activity. Zeit. Natur., **2007**, 62, 150–154. doi: 10.1515/znc-2007-1-225.

[74] Purgatorio, R., de Candia, Modesto, Catto, M., Rullo, M., Pisani, L., Denora, N., Carrieri, A., Nevskaya, A. A., Voskressensky, L. G., Altomare, C. D., Evaluation of Water-Soluble Mannich Base Prodrugs of 2,3,4,5-Tetrahydroazepino[4,3-b]indol-1(6H)-one as Multitarget-Directed Agents for Alzheimer's Disease. ChemMedChem., **2021**, 16, 589–598. doi: 10.1002/cmdc.202000583.

[75] Moss, G. P., International union of pure and applied chemistry and international union of biochemistry: Joint commission on biochemical nomenclature: Nomenclature of steroids. Pure Appl. Chem., **1989**, 61, 1783–1822. doi: 10.1351/pac198961101783.

[76] Yin, Q., Chen, Q., Lu, L. C., Han, B. H., Sugar-based micro/mesoporous hypercross-linked polymers with in situ embedded silver nanoparticles for catalytic reduction. Beilstein J. Org. Chem., **2017**, 13, 1212–1221. doi: 10.3762/bjoc.13.120.

[77] Zhang, G. T., Guo, Z. W., Hui, Y. Z., A facile regioselective 1,6-O-diacetylation method of methyl- glycopyranosides and their dimethyl phosphonates. Synth. Commun., **1997**, 27, 1907–1917. doi: 10.1080/00397919708006792.

A

APPENDIX

A.1 NMR spectra for compound 15 (methyl 2,3,4-tri-*O*-benzyl-α-L-rhamnopyranoside)

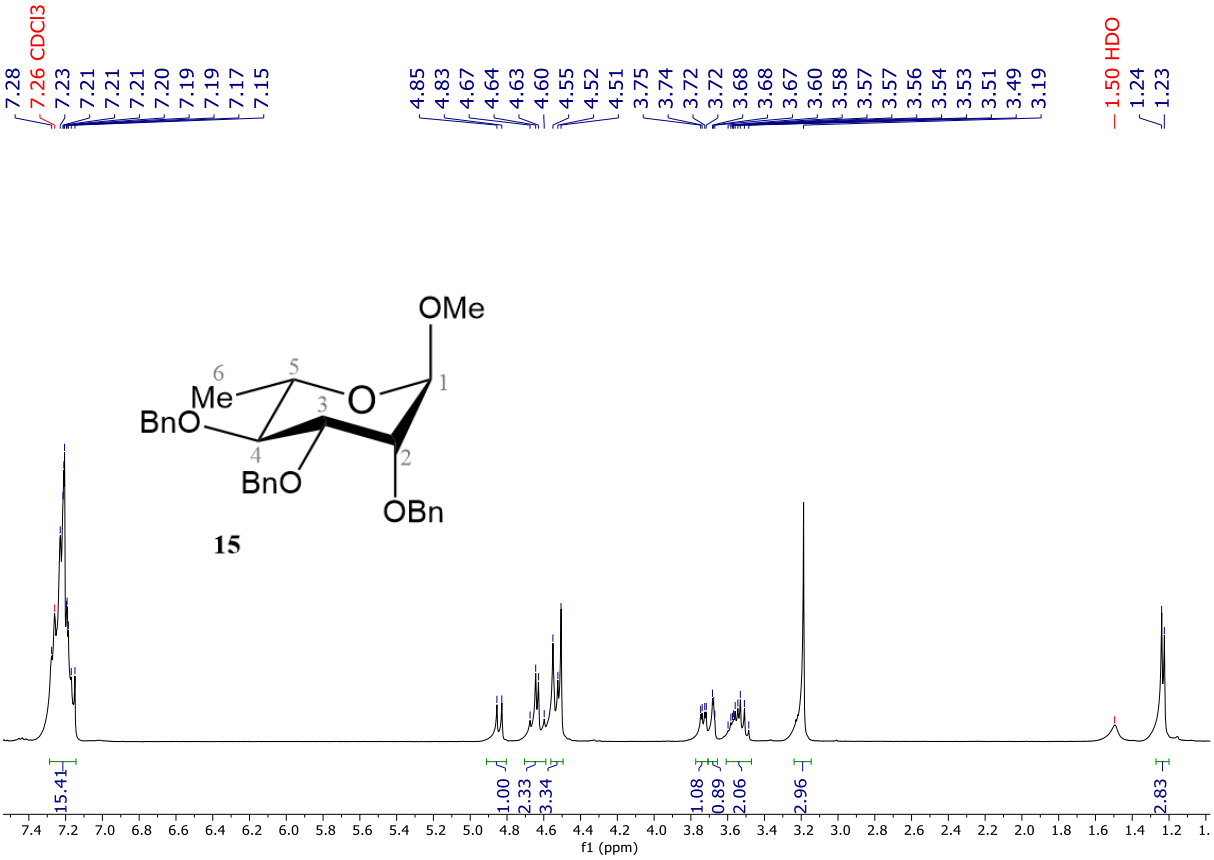

Figure 4.1. ^{1}H NMR spectrum for compound **15** (400 MHz, $CDCl_3$)

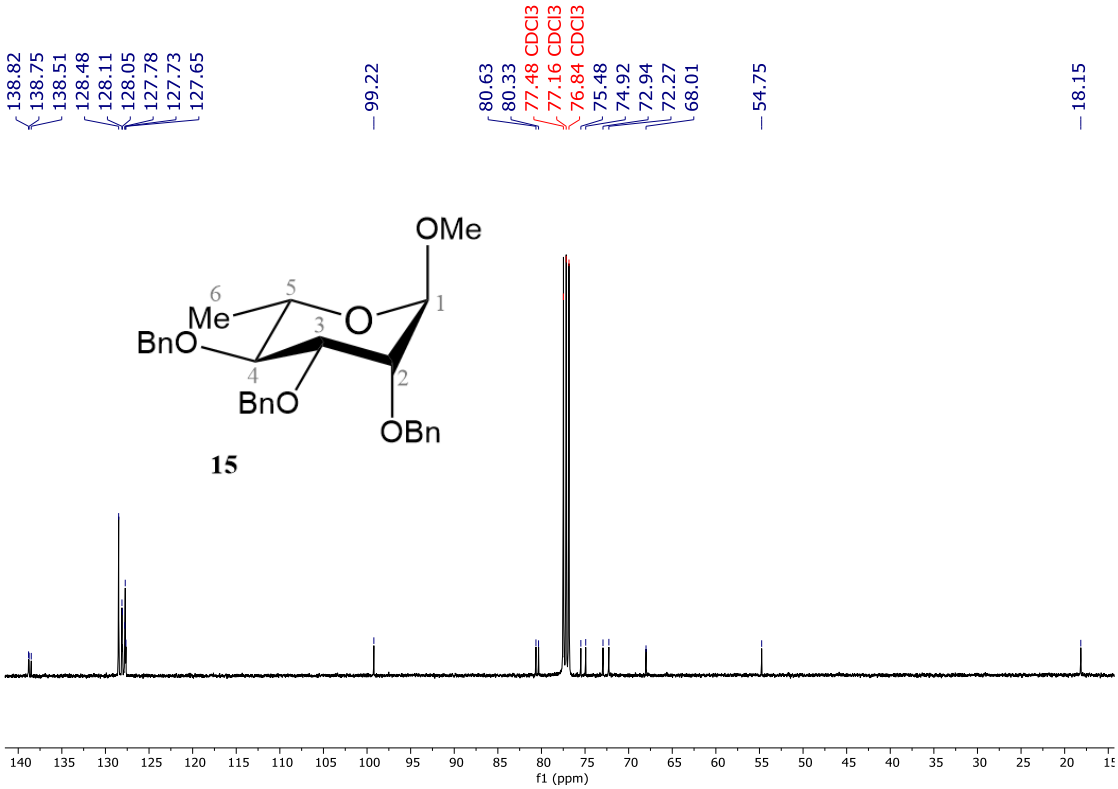

Figure 4.2. ^{13}C NMR spectrum for compound **15** (101 MHz, $CDCl_3$)

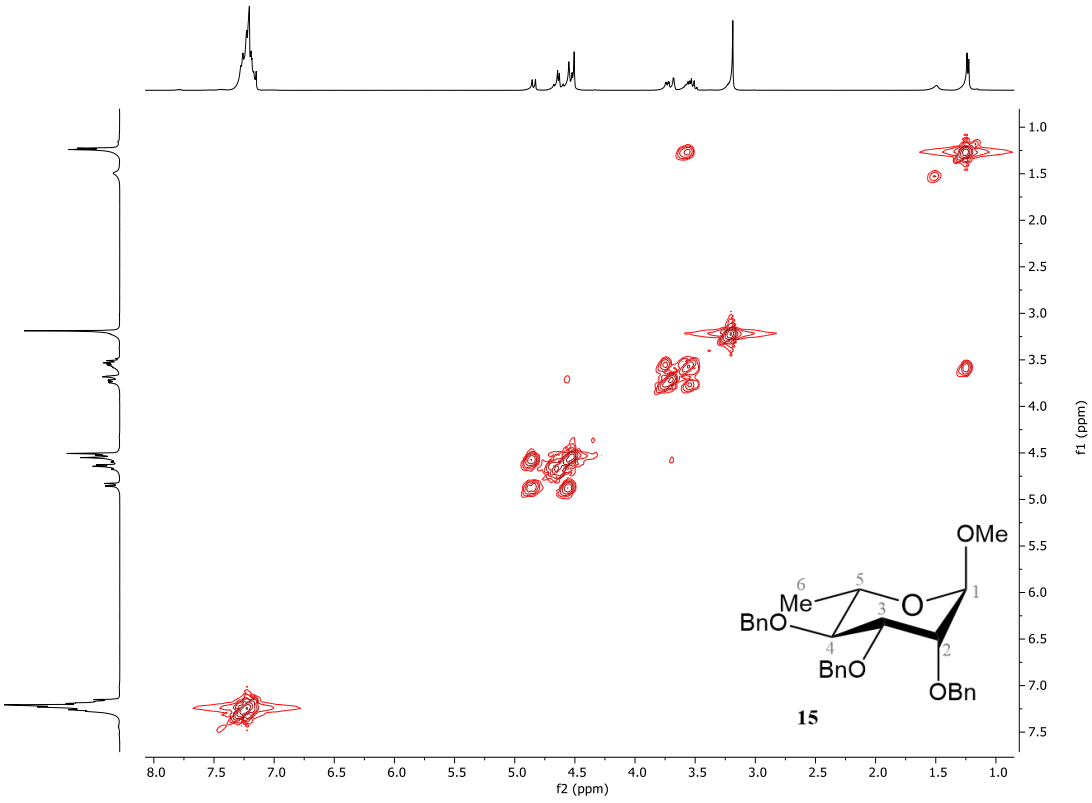

Figure 4.3. COSY spectrum for compound **15**

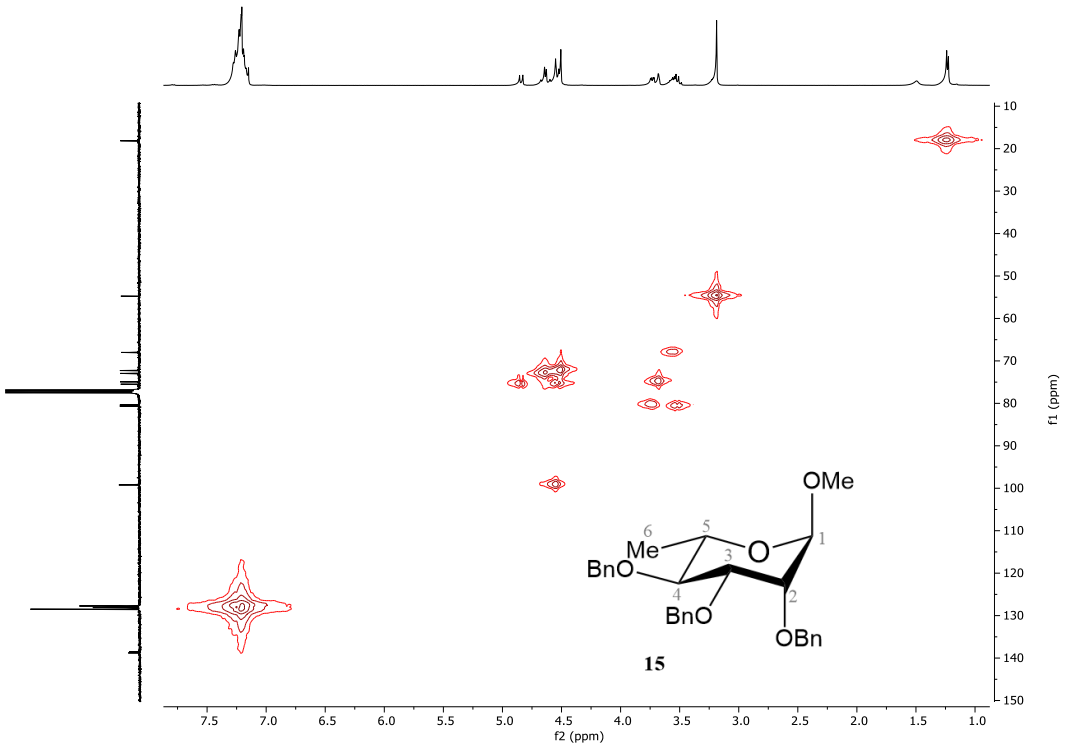

Figure 4.4. HSQC spectrum for compound **15**

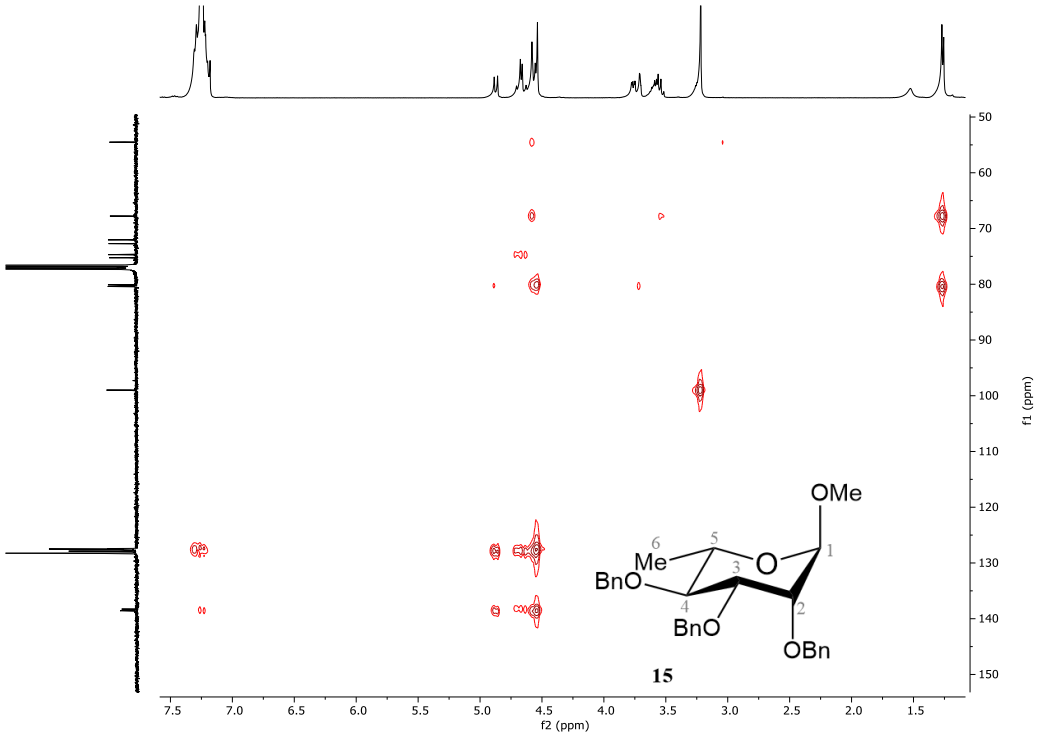

Figure 4.5. HMBC spectrum for compound **15**

A.2 NMR spectra for compound 16 (methyl 2,3,4,6-tetra-*O*-benzyl-α-D-mannopyranoside)

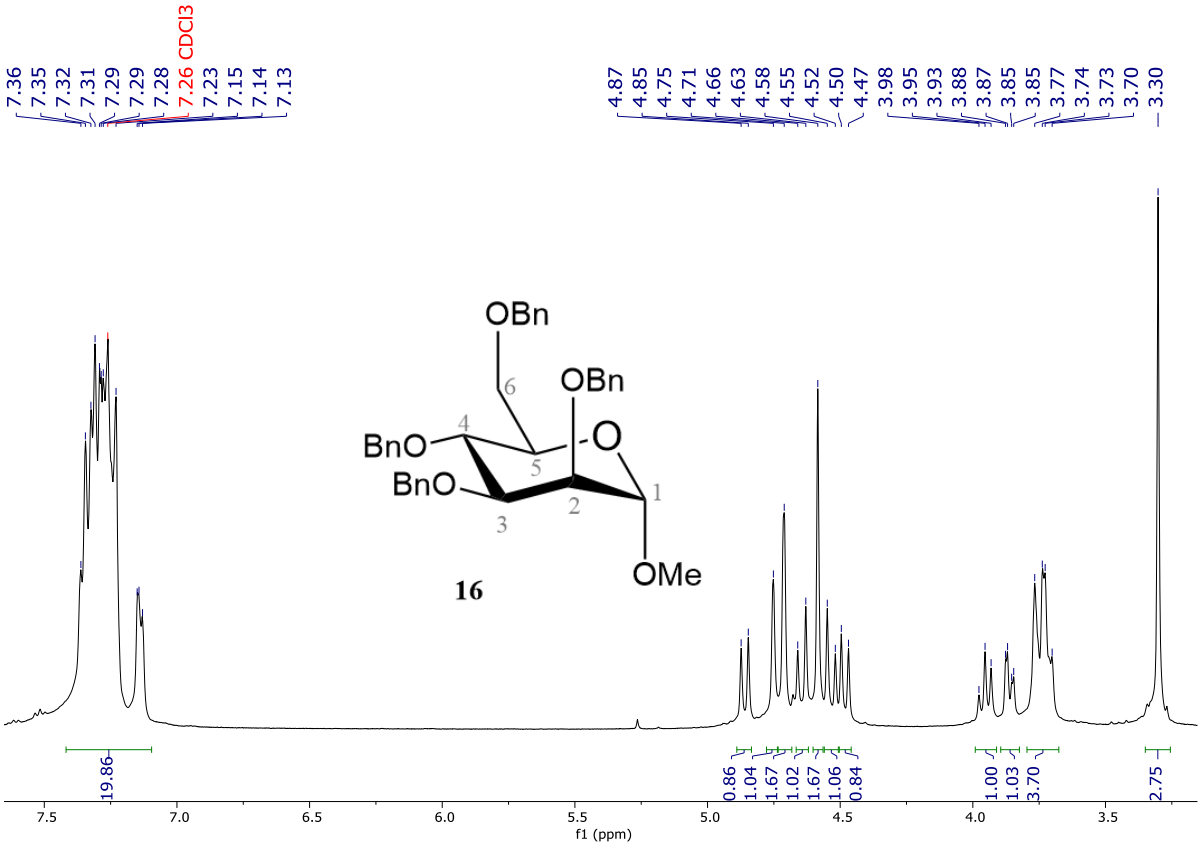

Figure 4.6. ^{1}H NMR spectrum for compound **16** (400 MHz, $CDCl_3$)

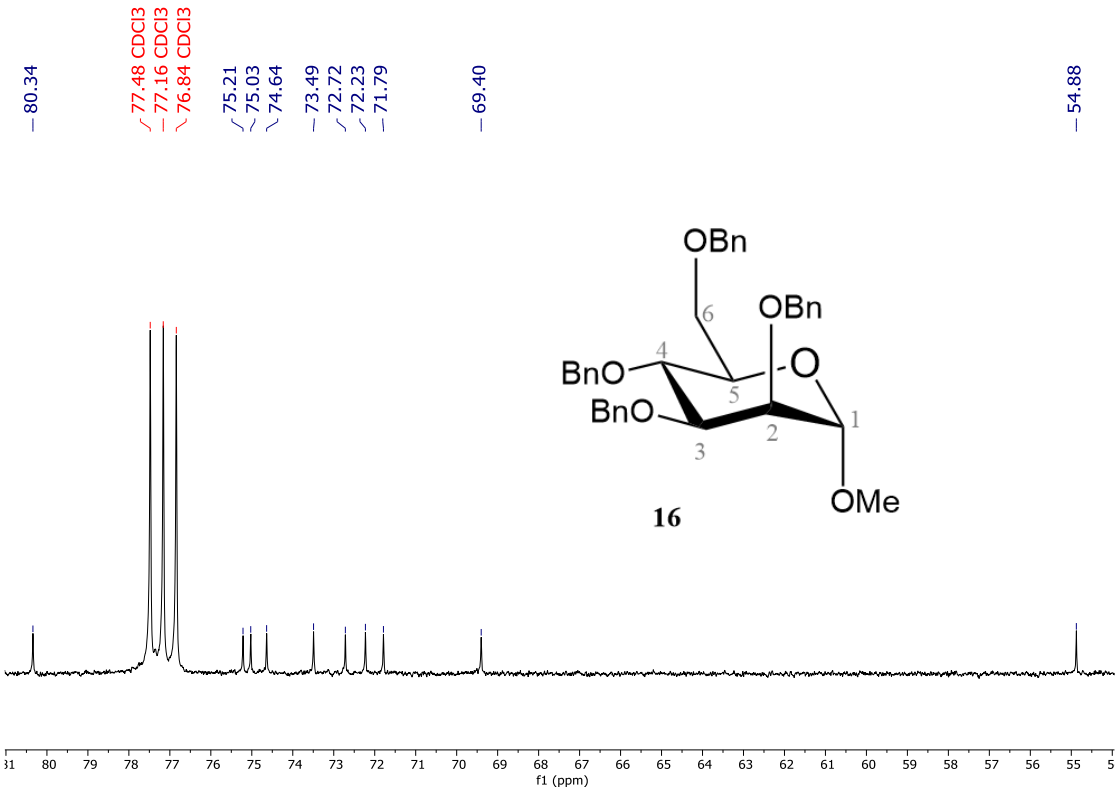

Figure 4.7. ^{13}C NMR spectrum for compound **16** (400 MHz, $CDCl_3$)

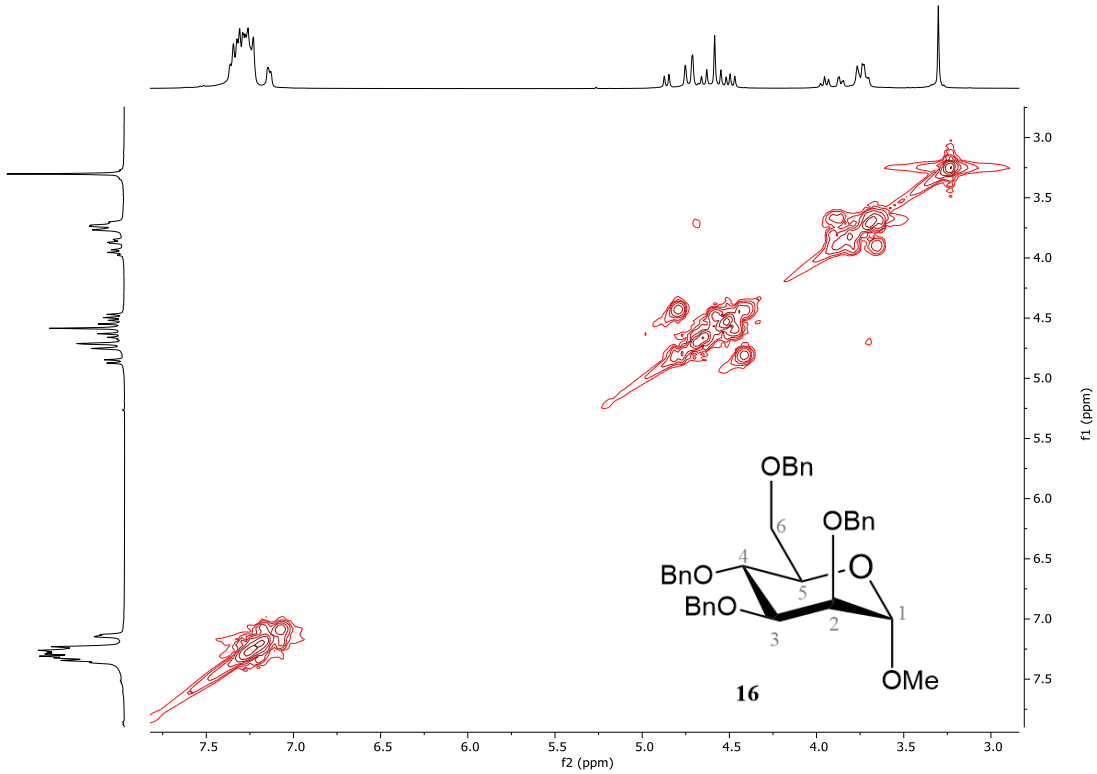

Figure 4.8. COSY spectrum for compound **16**

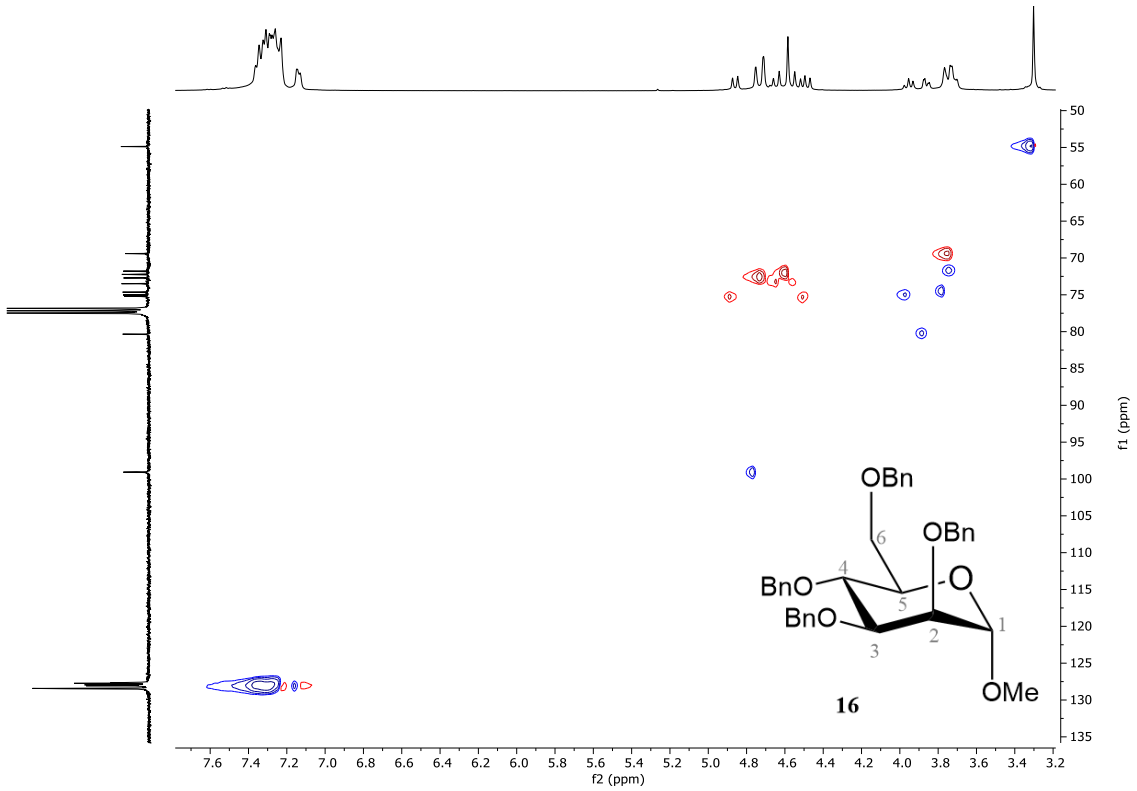

Figure 4.9. HSQC spectrum for compound **16**

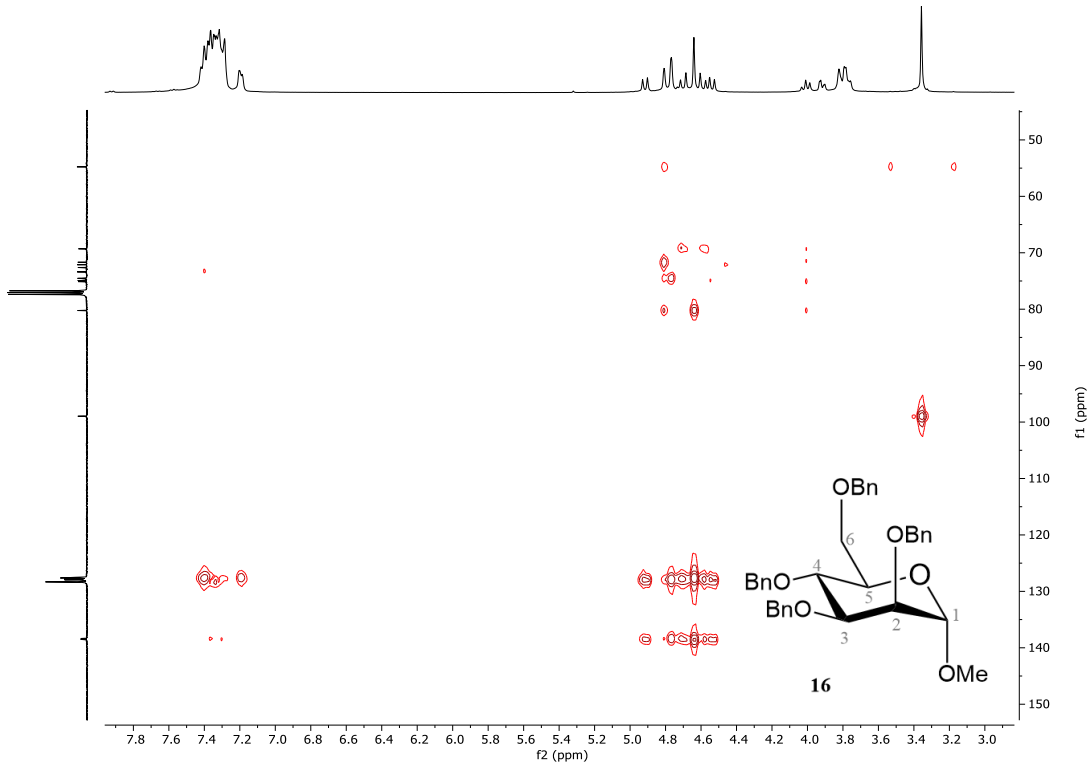

Figure 4.10. HMBC spectrum for compound **16**

A.3 NMR spectra for compound 17 (phenyl 2,3,4,6-tetra-*O*-benzyl-α-D-thiomannopyranoside)

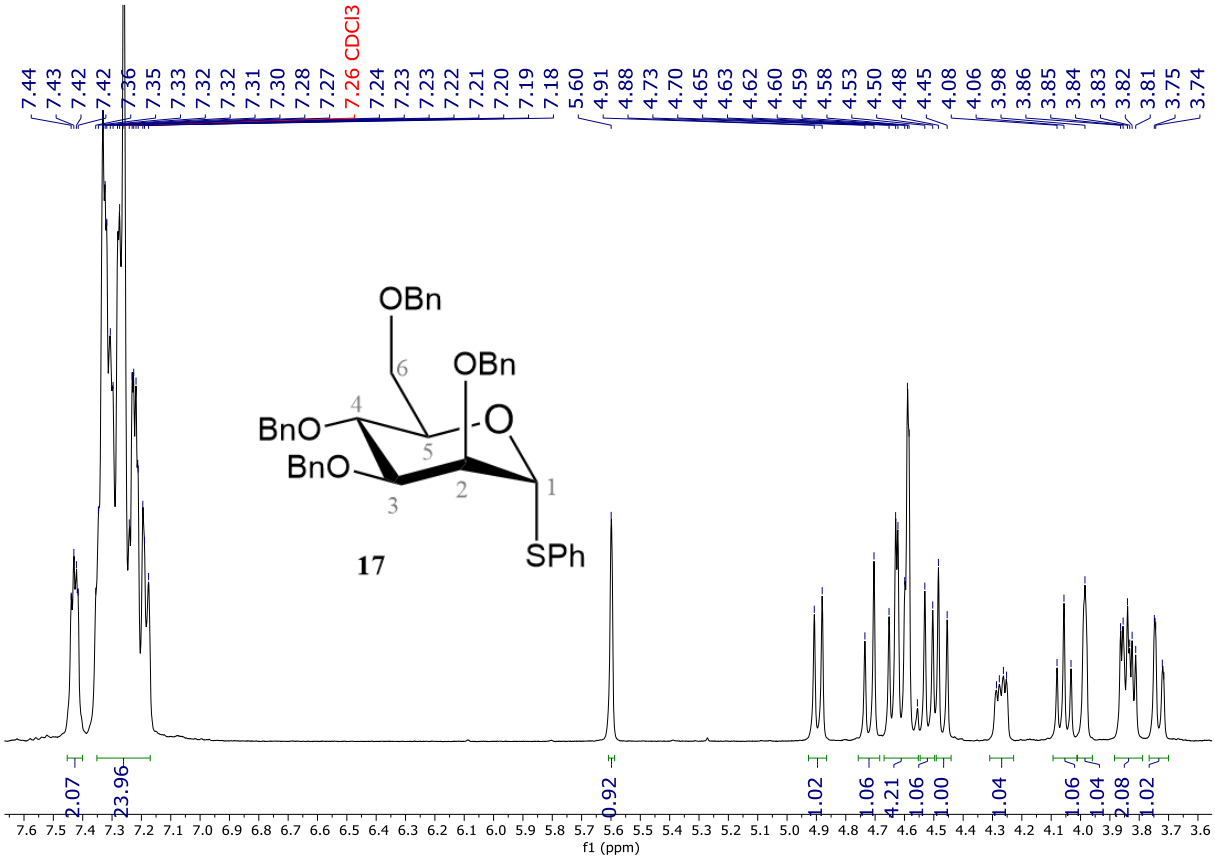

Figure 4.11. ^{1}H NMR spectrum for compound **17** (400 MHz, $CDCl_3$)

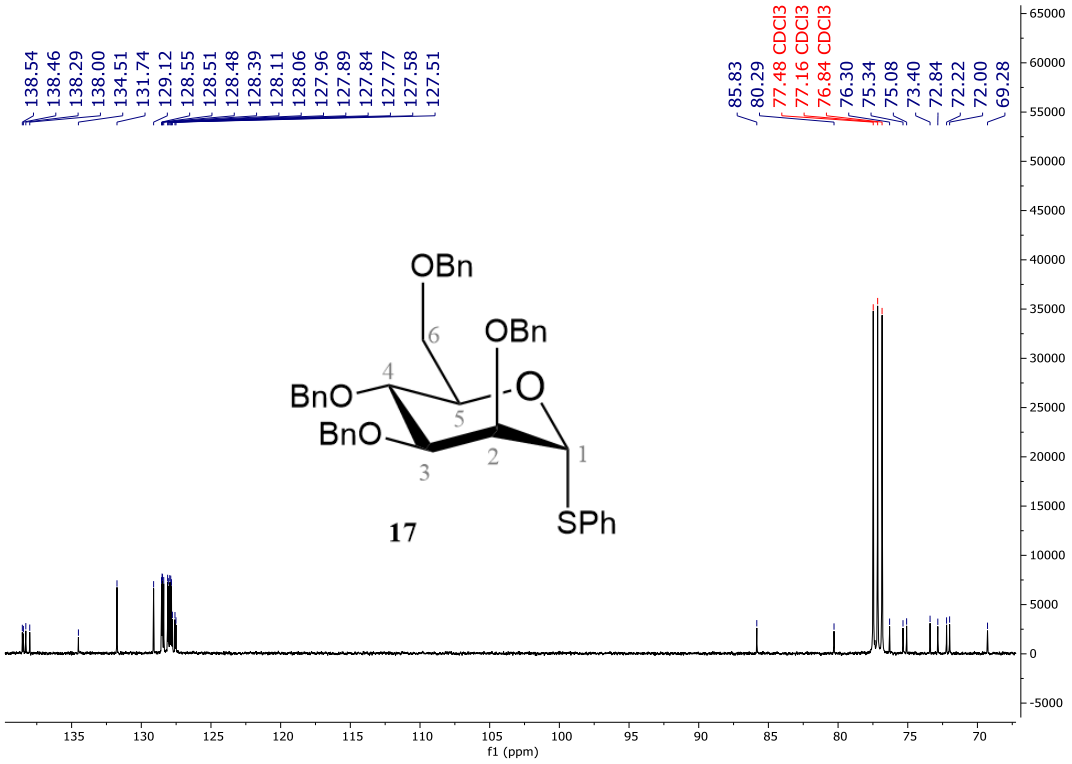

Figure 4.12. ^{13}C NMR spectrum for compound **17** (400 MHz, $CDCl_3$)

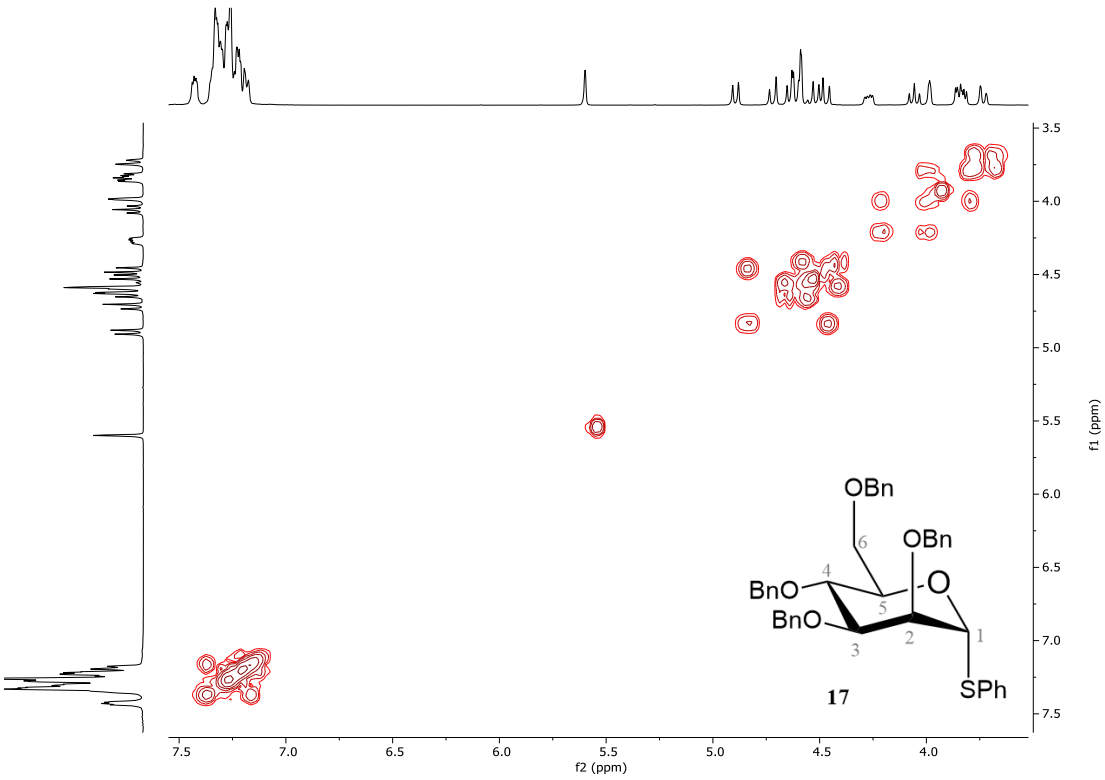

Figure 4.13. COSY spectrum for compound **17**

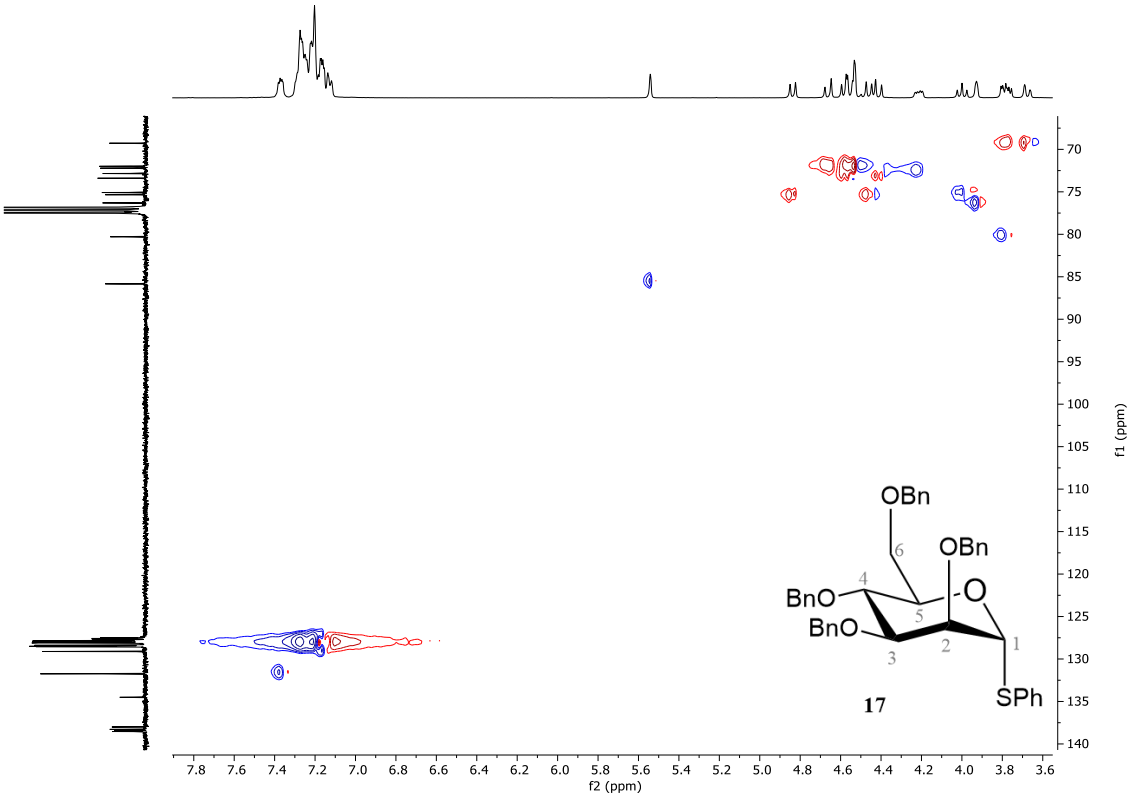

Figure 4.14. HSQC spectrum for compound **17**

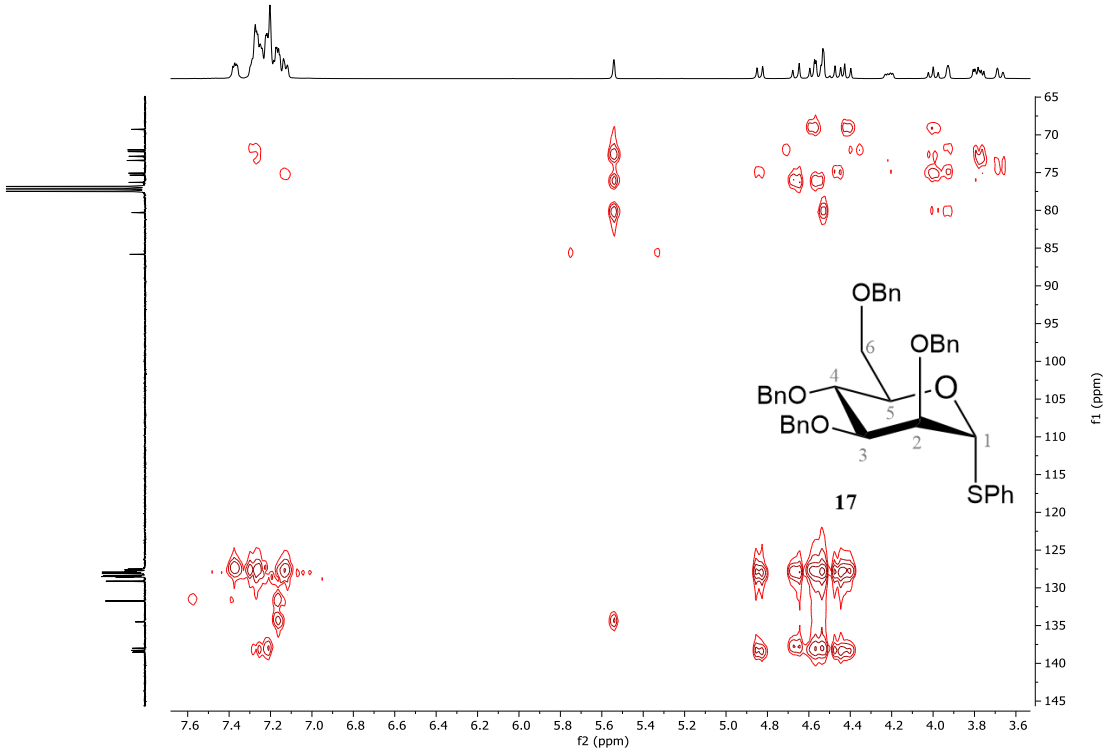

Figure 4.15. HMBC spectrum for compound **17**

A.4 NMR and UV-Vis spectra for compound 18 (methyl 2,3,4-tri-*O*-benzoyl-α-L-rhamnopyranoside)

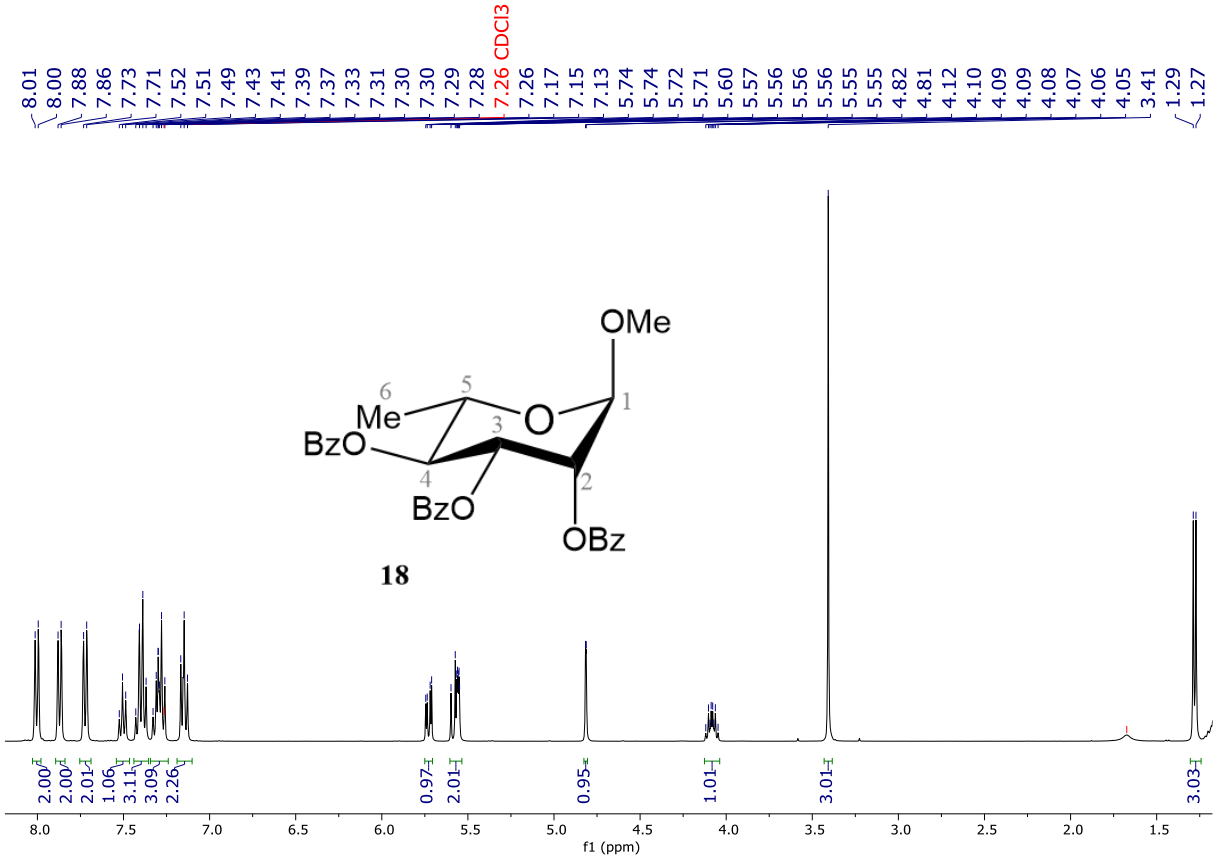

Figure 4.16. ^{1}H NMR spectrum for compound **18** (400 MHz, $CDCl_3$)

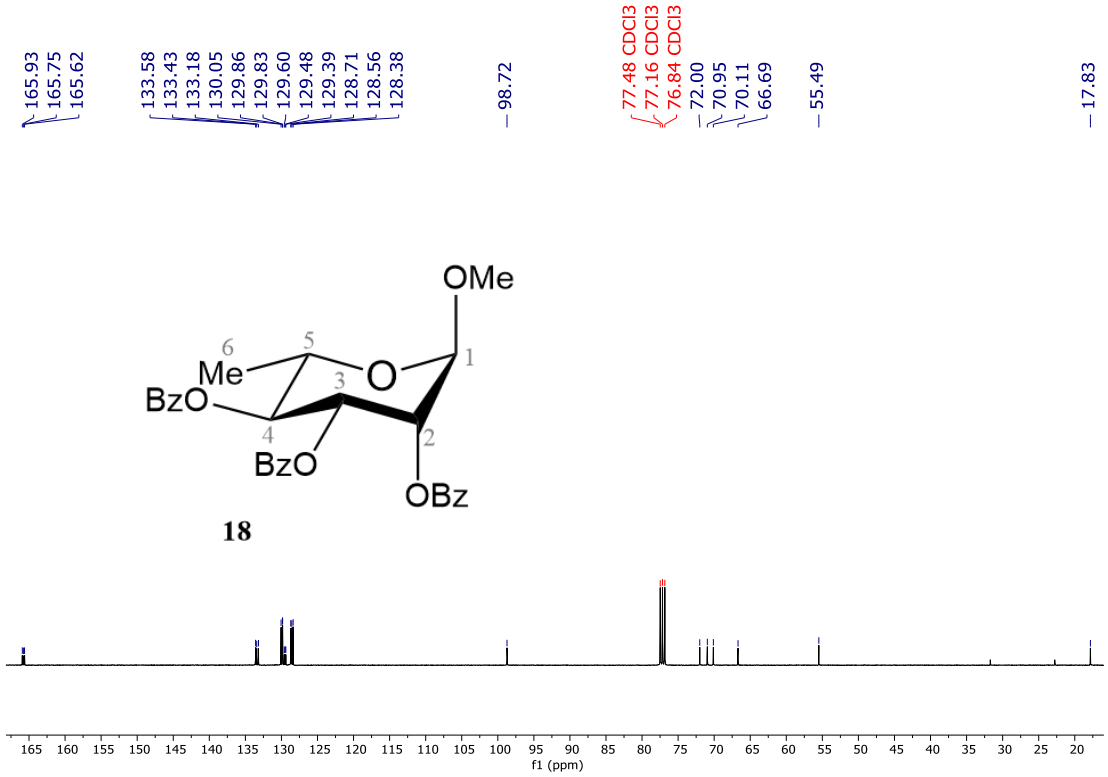

Figure 4.17. ^{13}C NMR spectrum for compound **18** (101 MHz, $CDCl_3$)

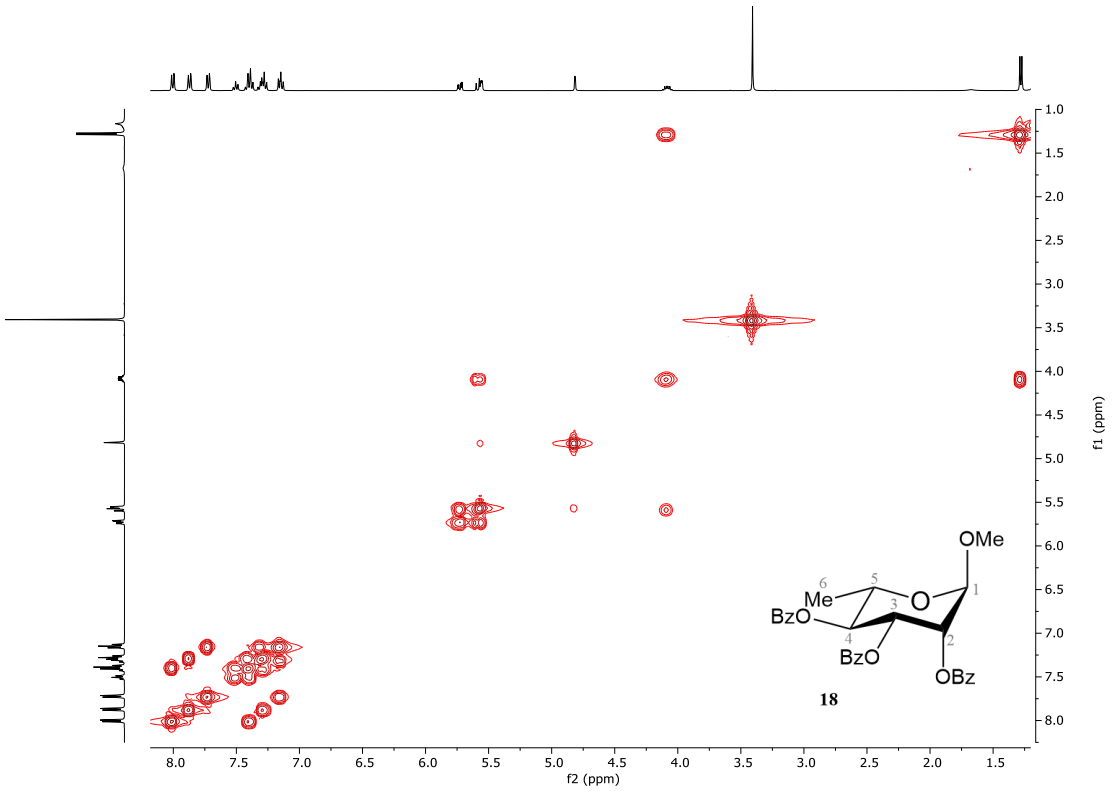

Figure 4.18. COSY spectrum for compound **18**

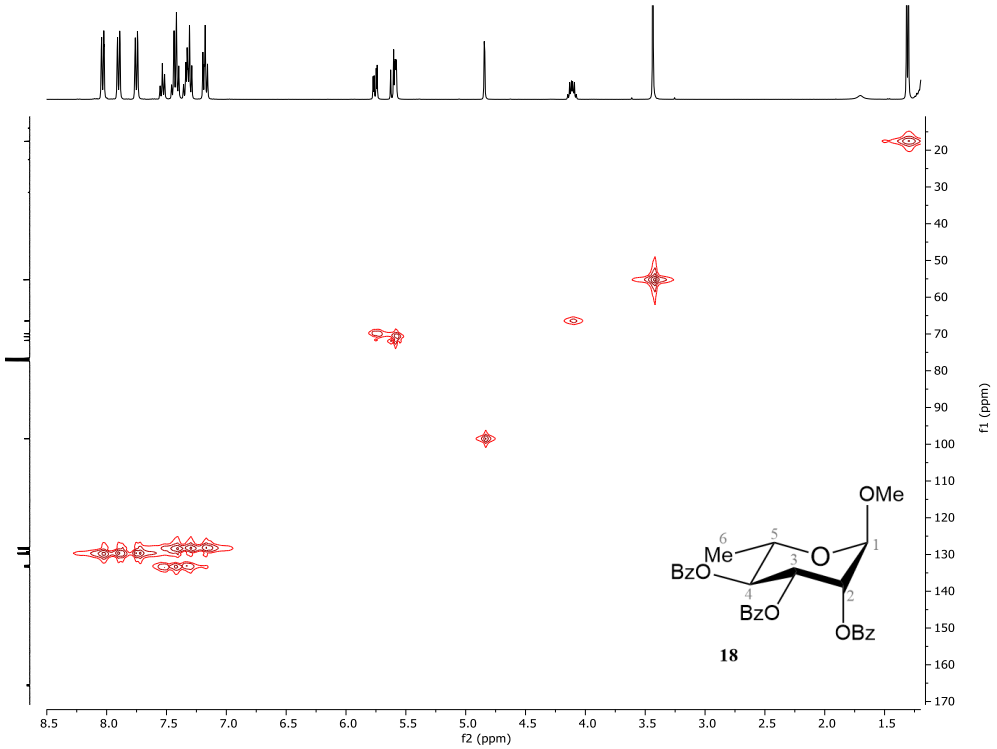

Figure 4.19. HSQC spectrum for compound **18**

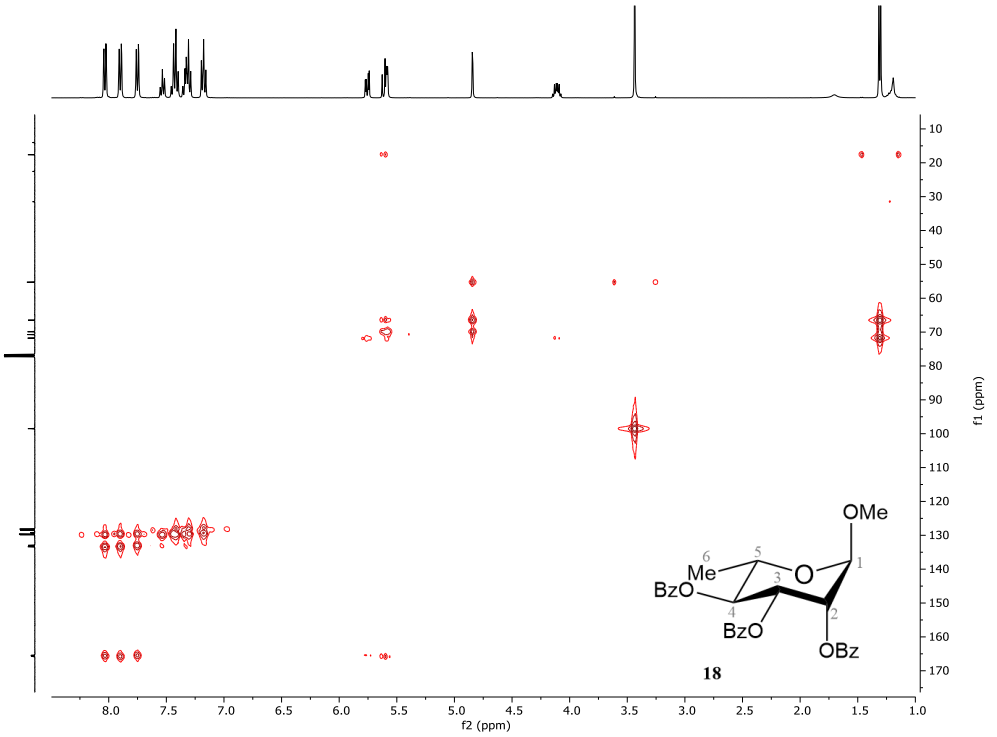

Figure 4.20. HMBC spectrum for compound **18**

A.5 NMR and UV-Vis spectra for compound 19 [*N*-6-benzamido-9-(2,3,4-tri-*O*-benzyl-α-L-rhamnopyranosyl)purine]

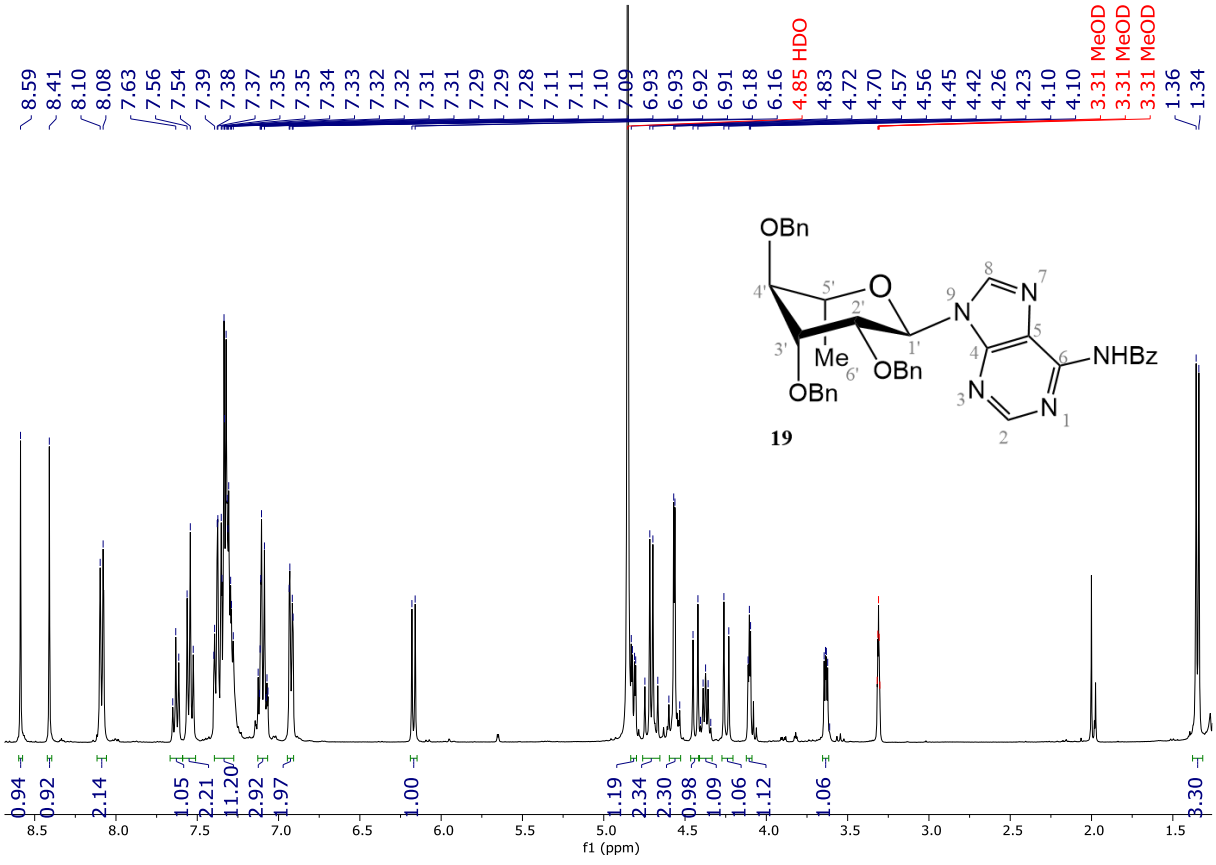

Figure 4.21. ^{1}H NMR spectrum for compound **19** (400 MHz, MeOD)

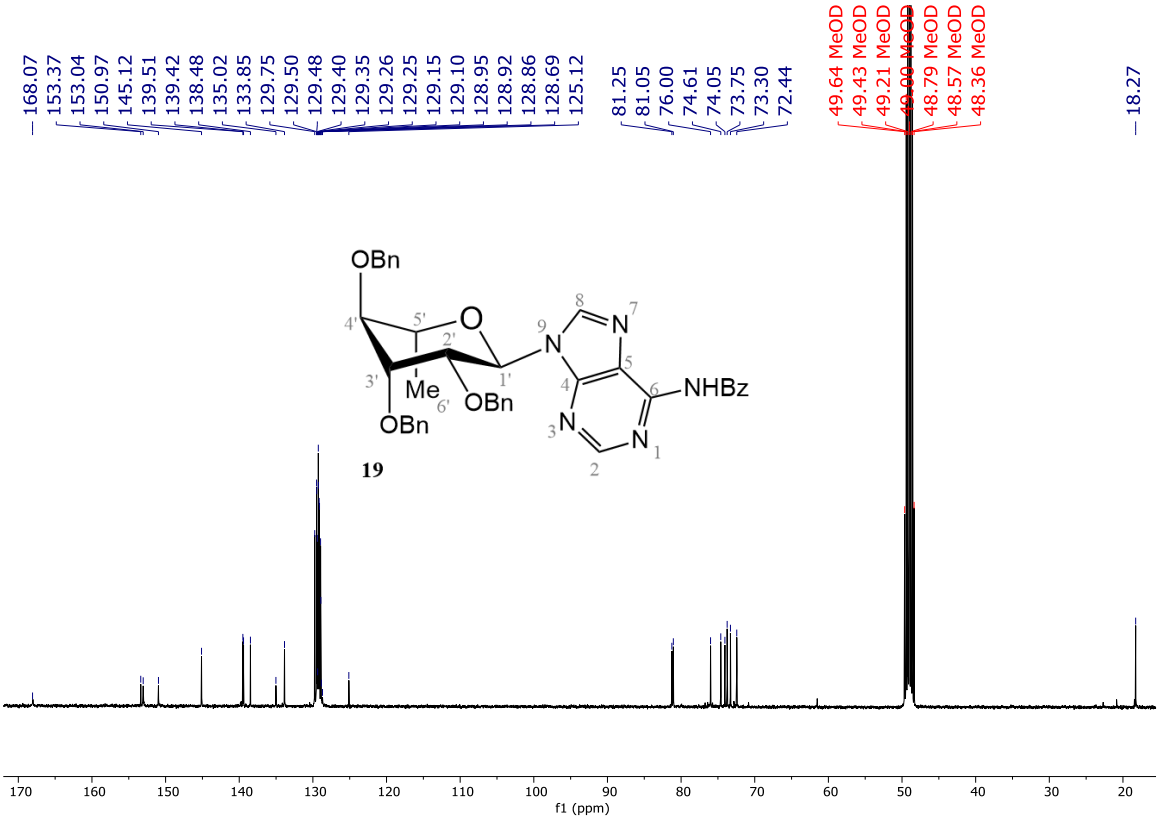

Figure 4.22. ^{13}C NMR for compound **19** (101 MHz, MeOD)

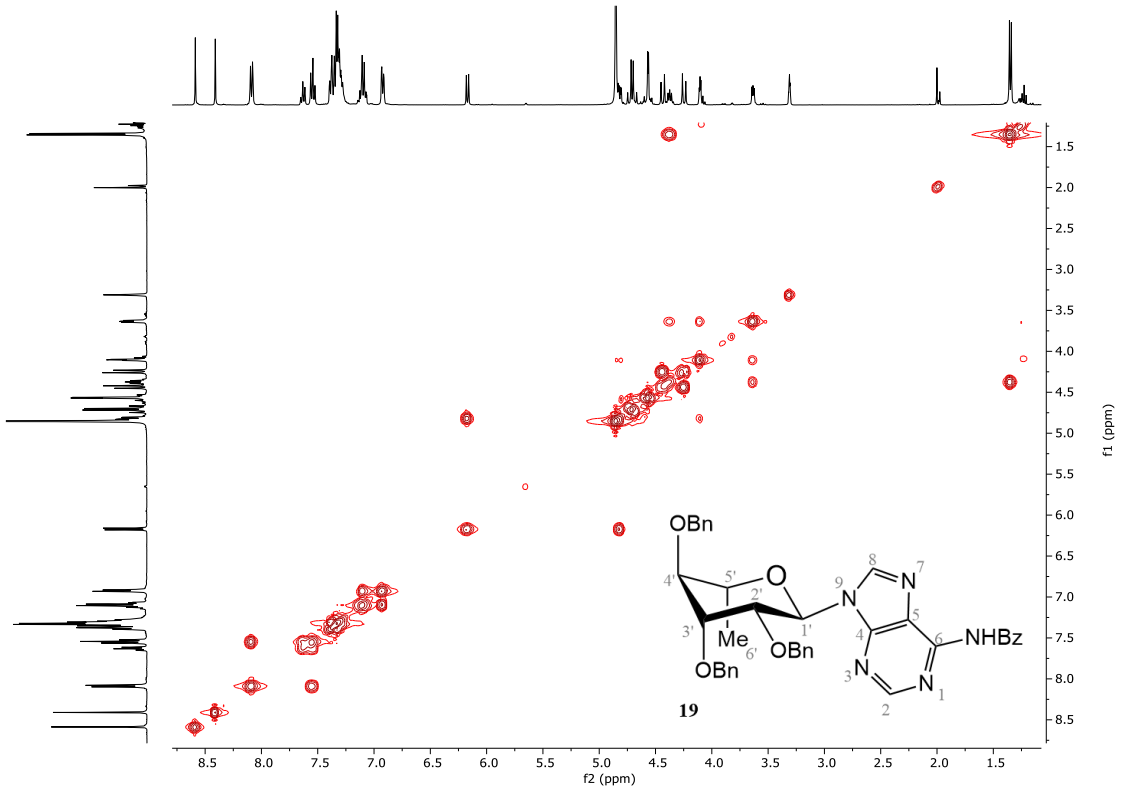

Figure 4.23. COSY spectrum for compound **19**

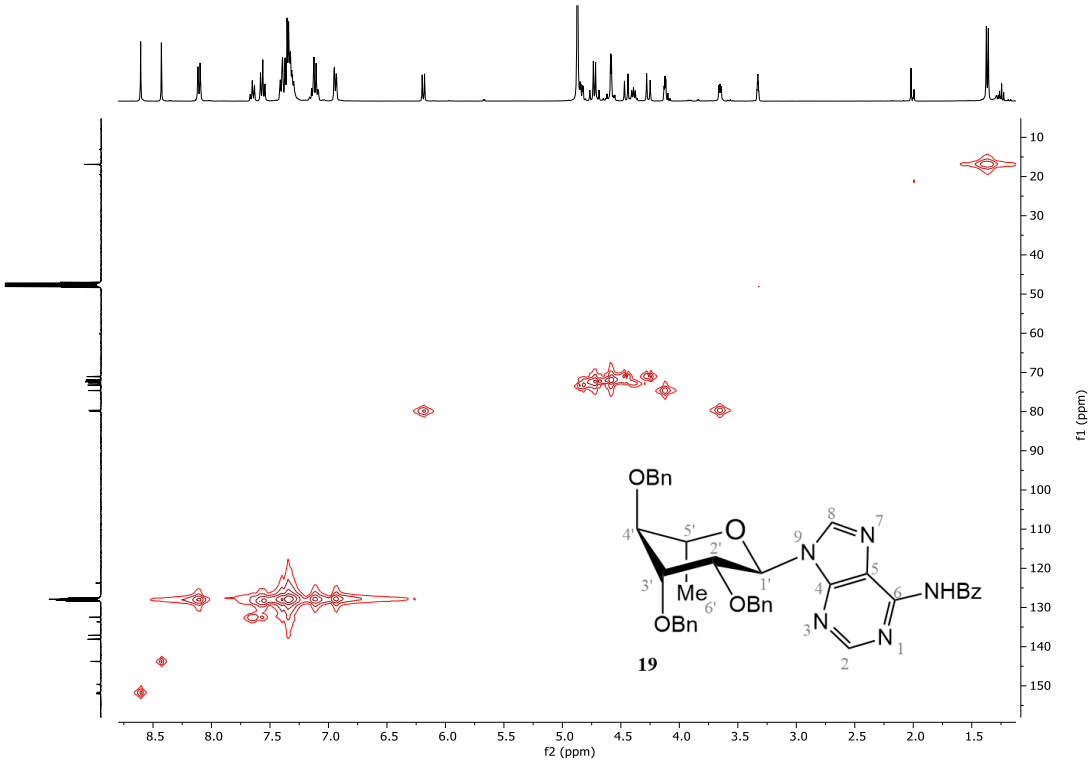

Figure 4.24. HSQC spectrum for compound **19**

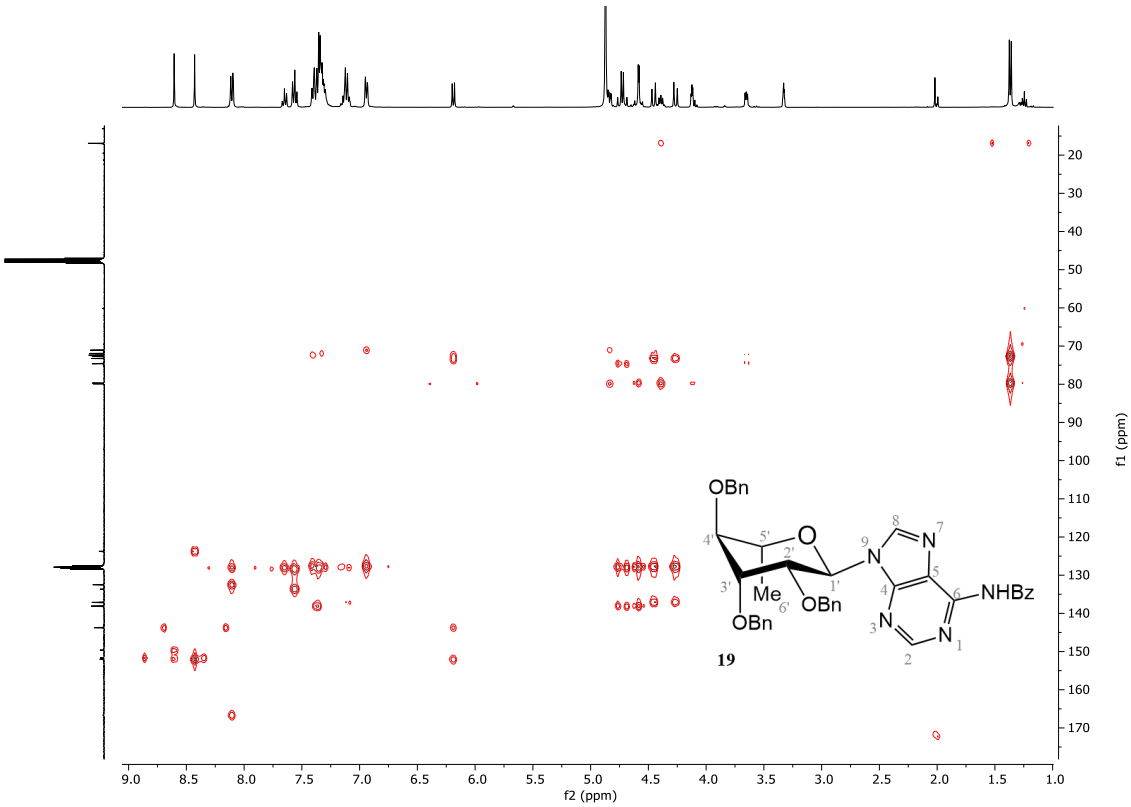

Figure 4.25. HMBC spectrum for compound **19**

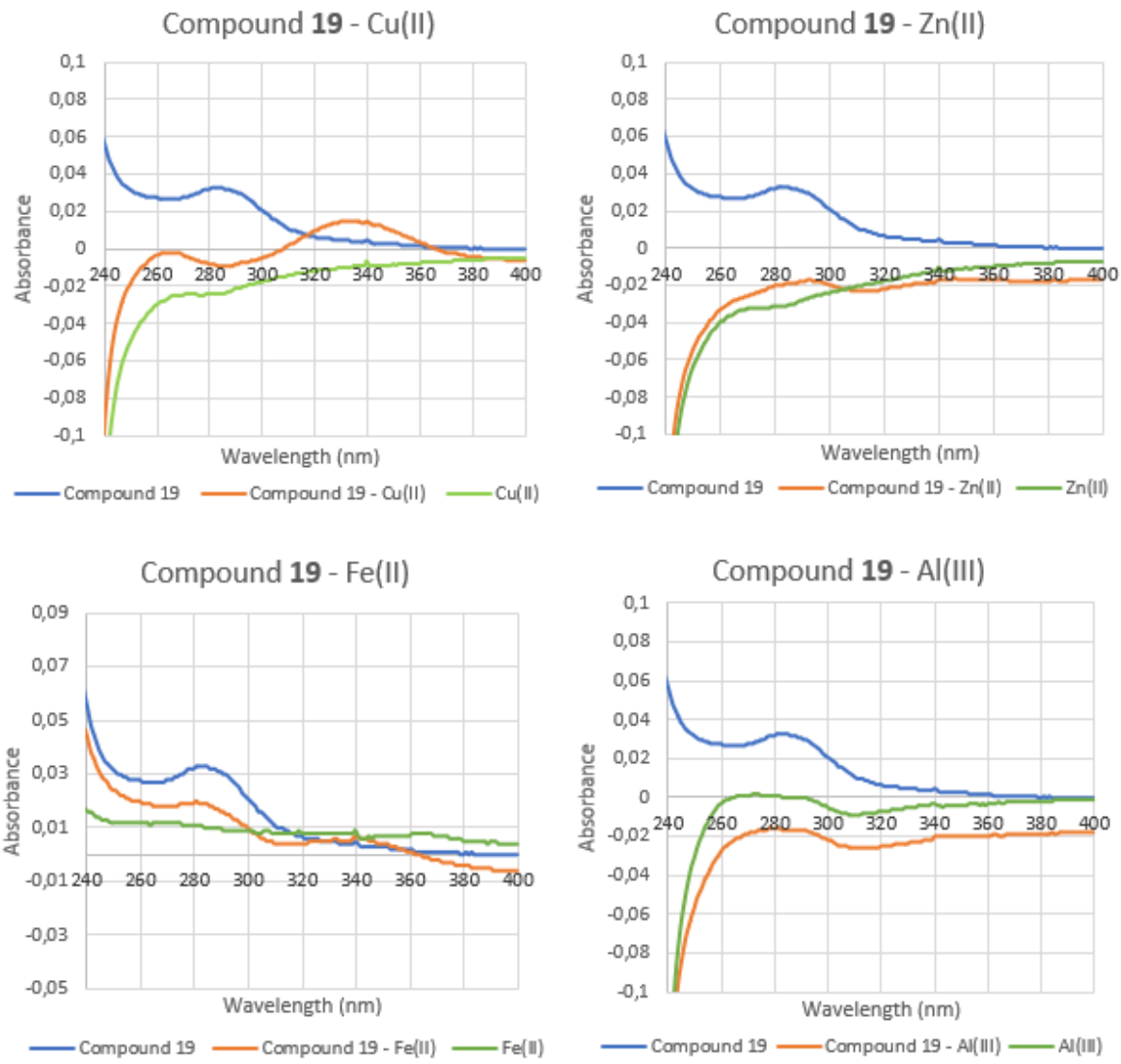

Figure 4.26. Interaction between compound **19** and metal ions

A.6 NMR and UV-Vis spectra for compound 20 [*N*-6-benzamido-9-(2,3,4-tri-*O*-benzyl-β-L-rhamnopyranosyl)purine]

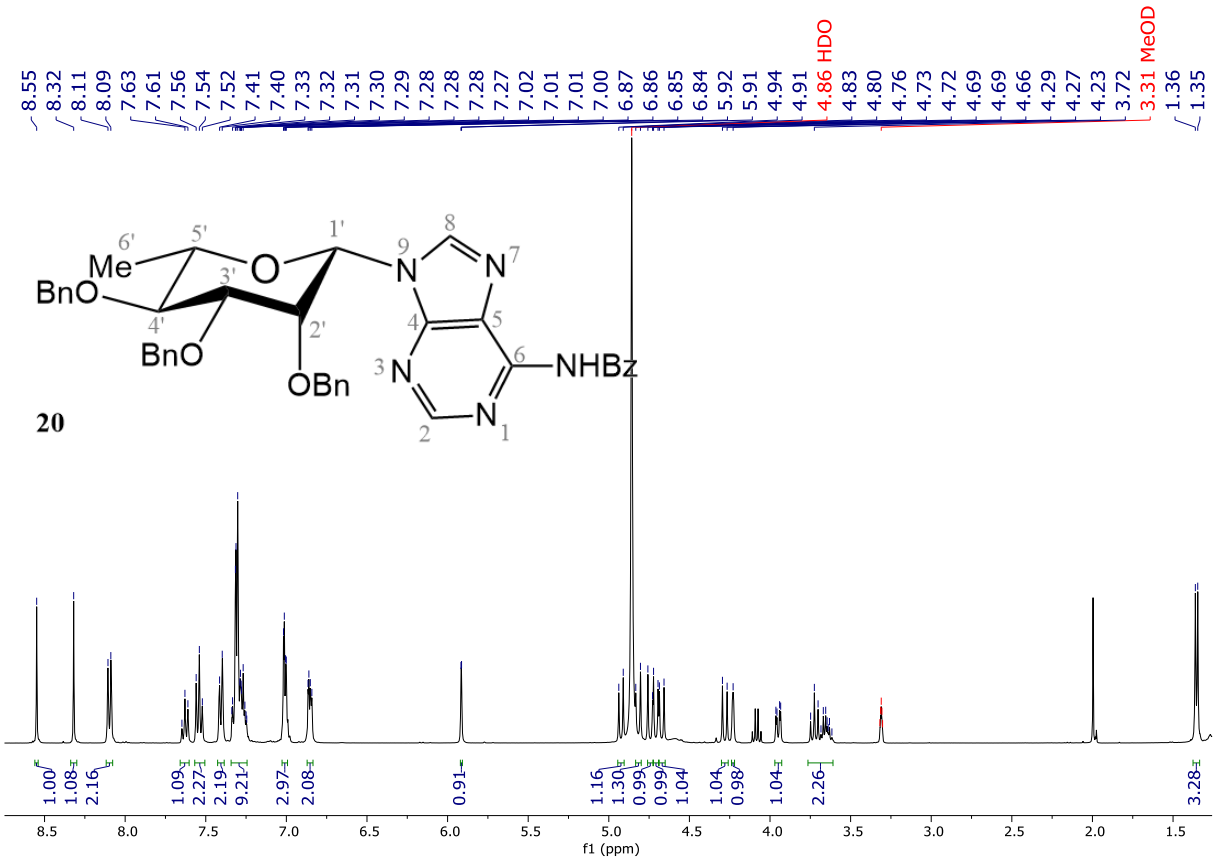

Figure 4.27. ^{1}H NMR spectrum for compound **20** (400 MHz, MeOD)

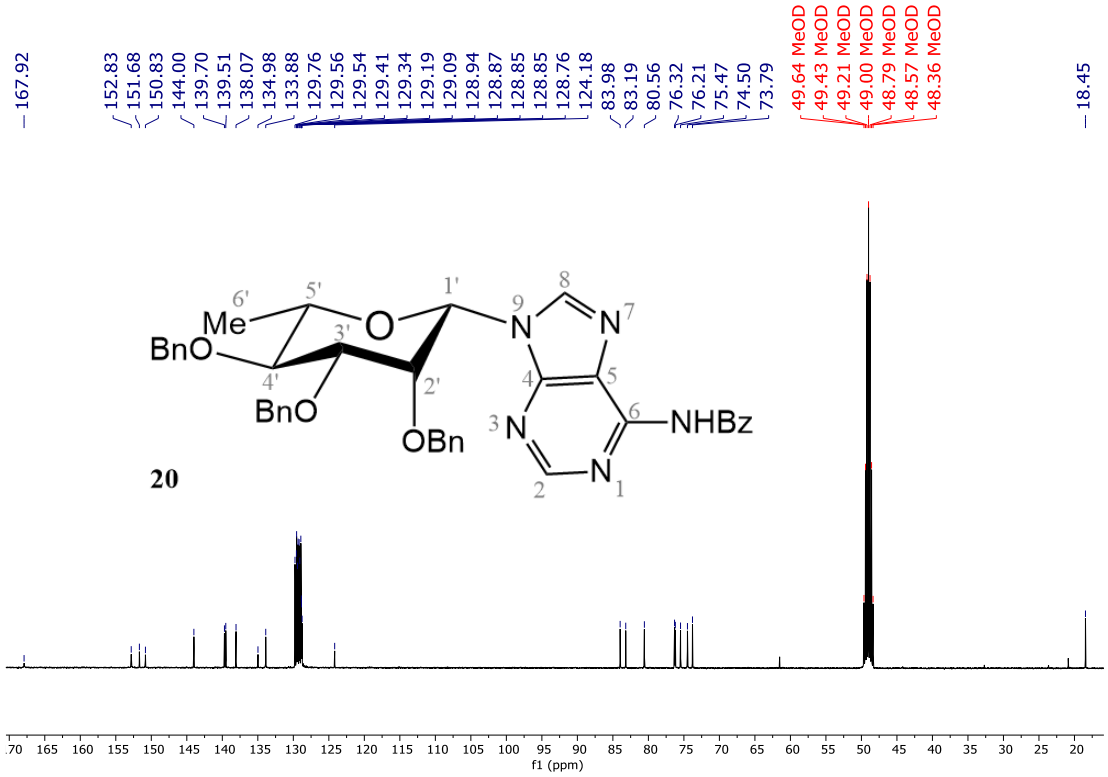

Figure 4.28. ^{13}C NMR spectrum for compound **20** (101 MHz, MeOD)

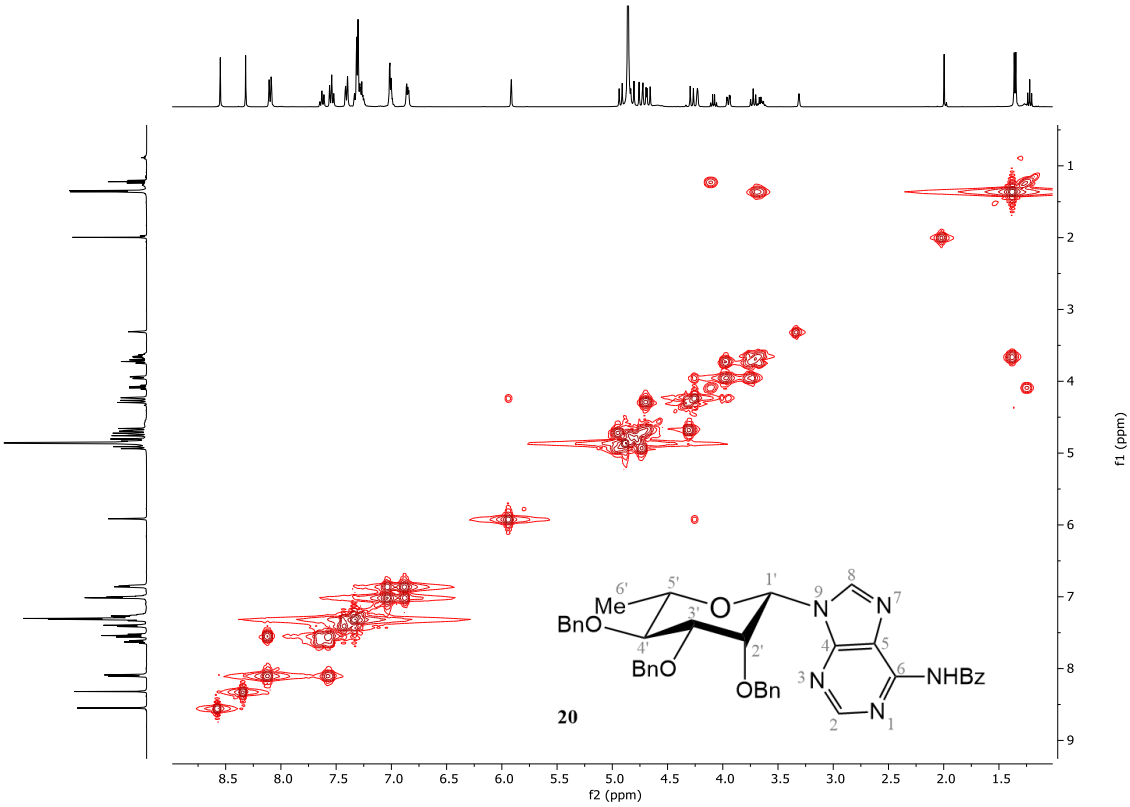

Figure 4.29. COSY spectrum for compound **20**

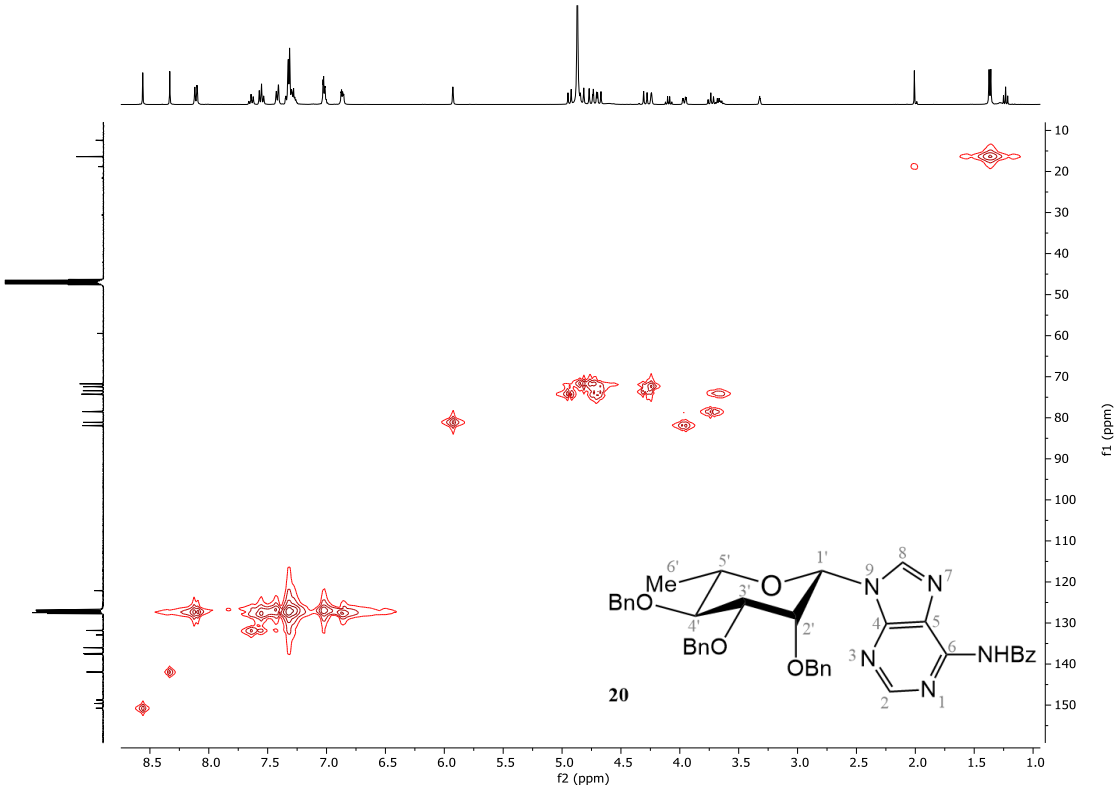

Figure 4.30. HSQC spectrum for compound **20**

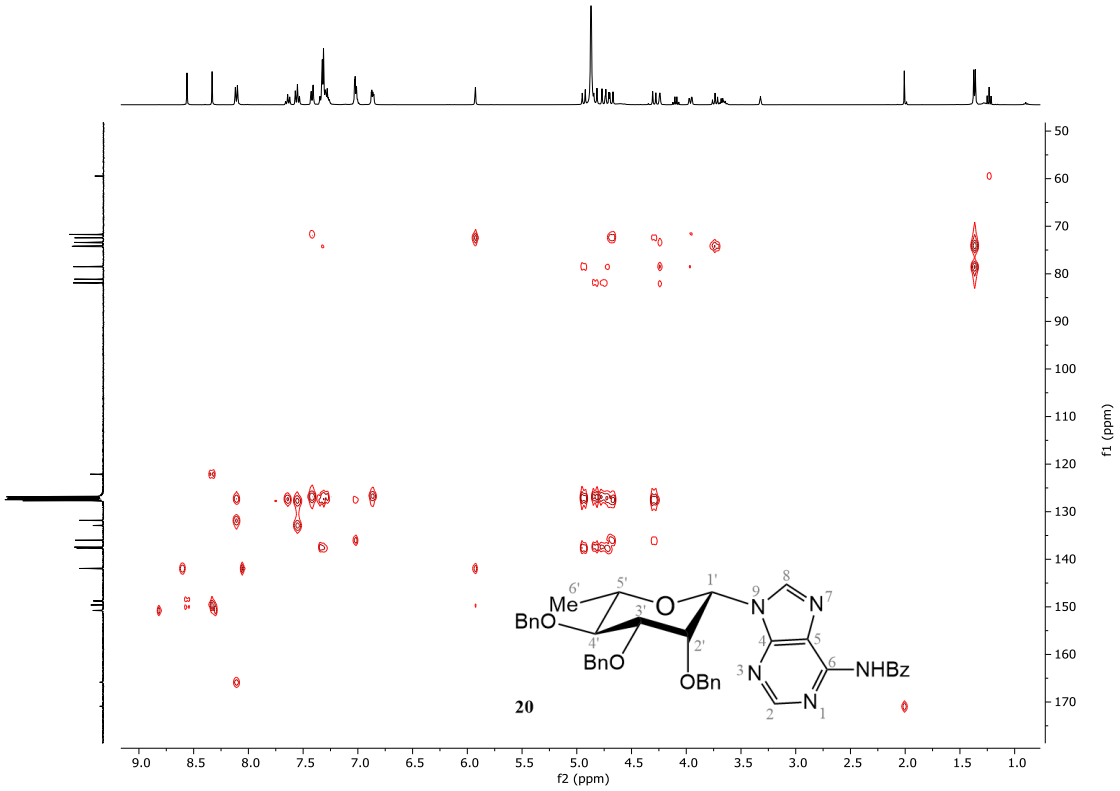

Figure 4.31. HMBC spectrum for compound **20**

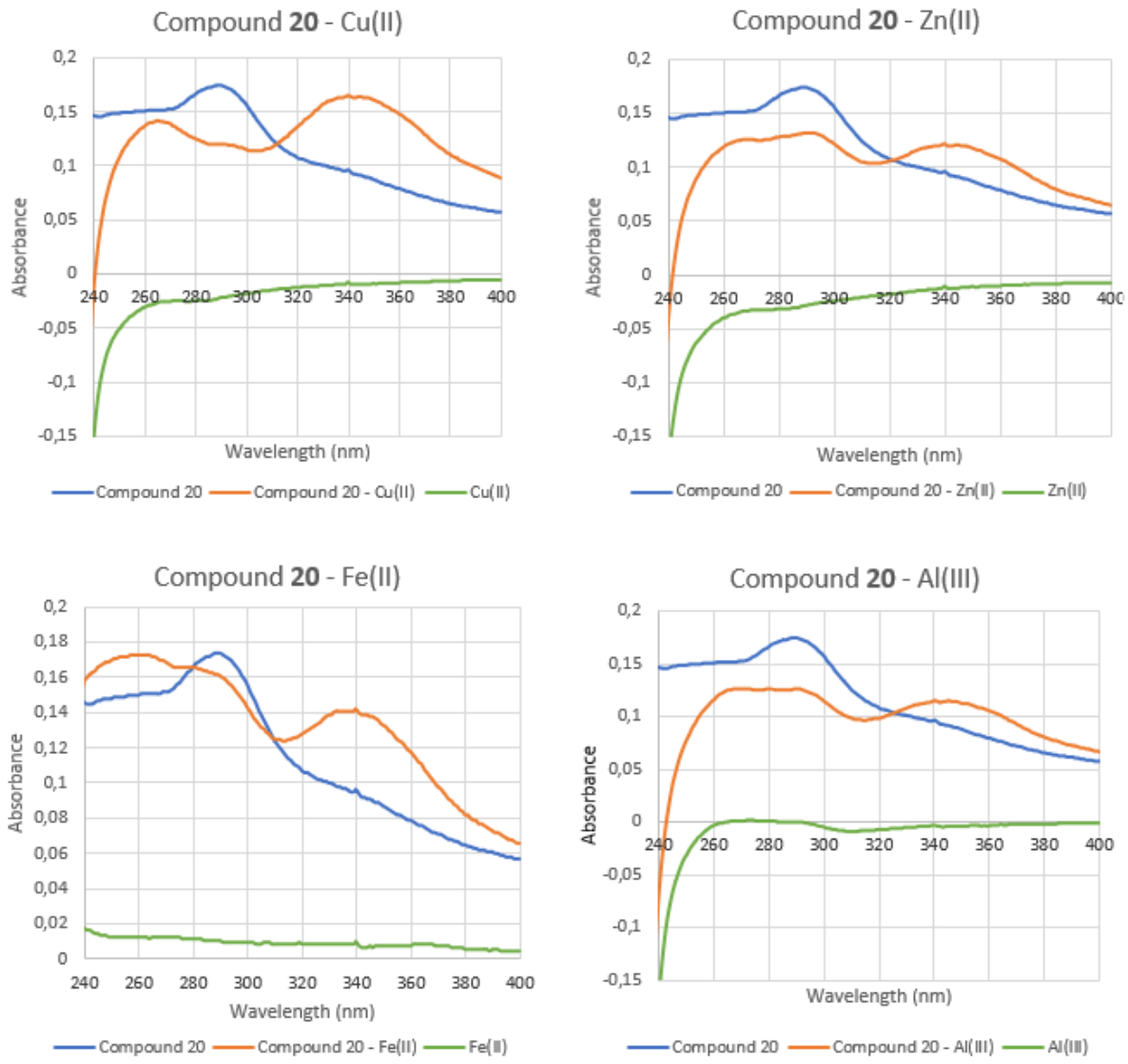

Figure 4.32. Interaction between compound **20** and metal ions

A.7 NMR and UV-Vis spectra for compound 2 [*N*-6-benzamido-9-(2,3,4,6-tetra-*O*-benzyl-α-D-mannopyranosyl)purine]

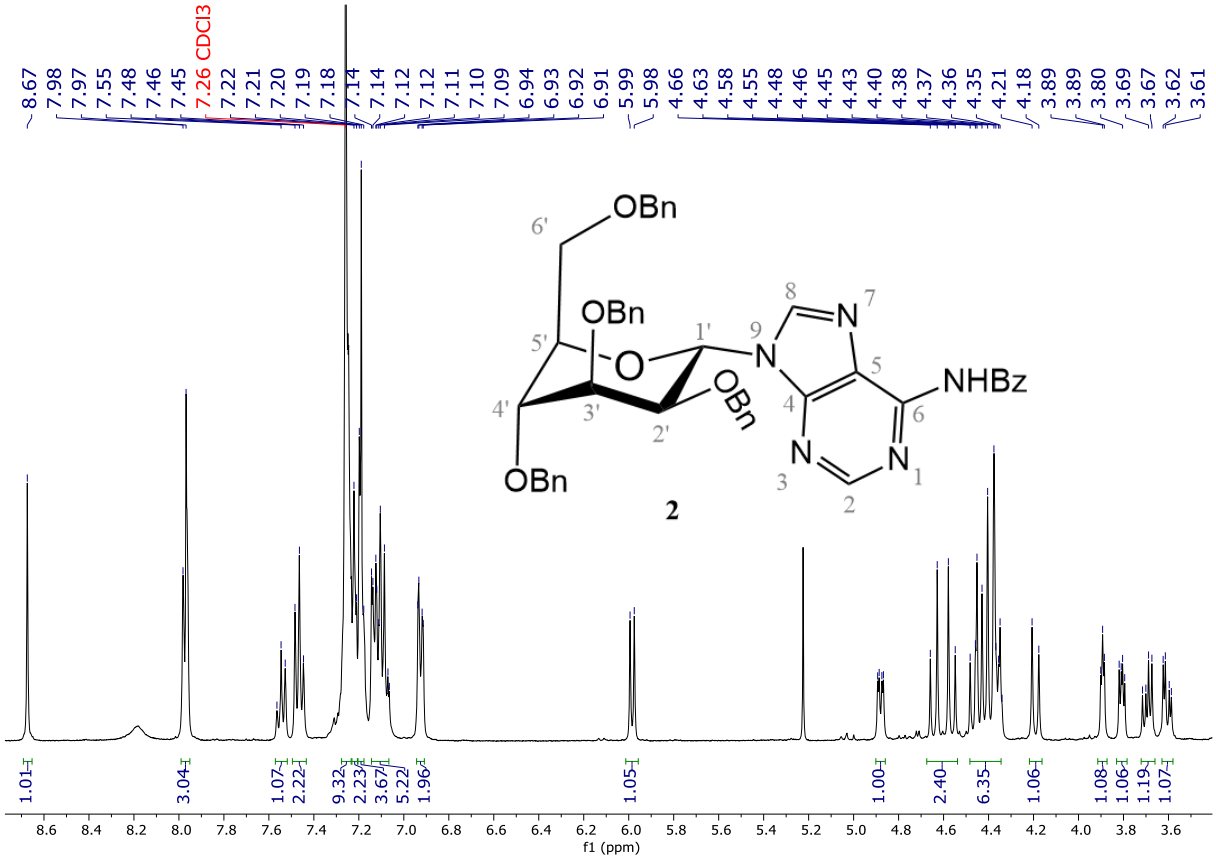

Figure 4.33. ^{1}H NMR spectrum for compound **2** (400 MHz, $CDCl_3$)

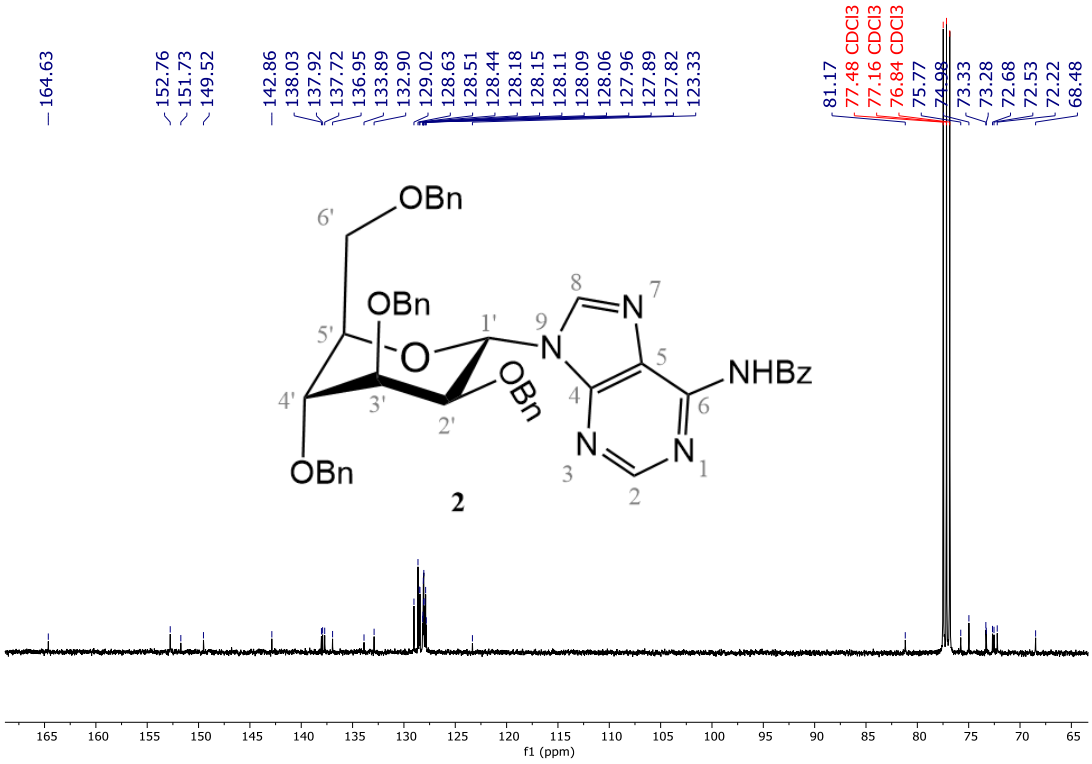

Figure 4.34. ^{13}C NMR spectrum for compound **2** (101 MHz, $CDCl_3$)

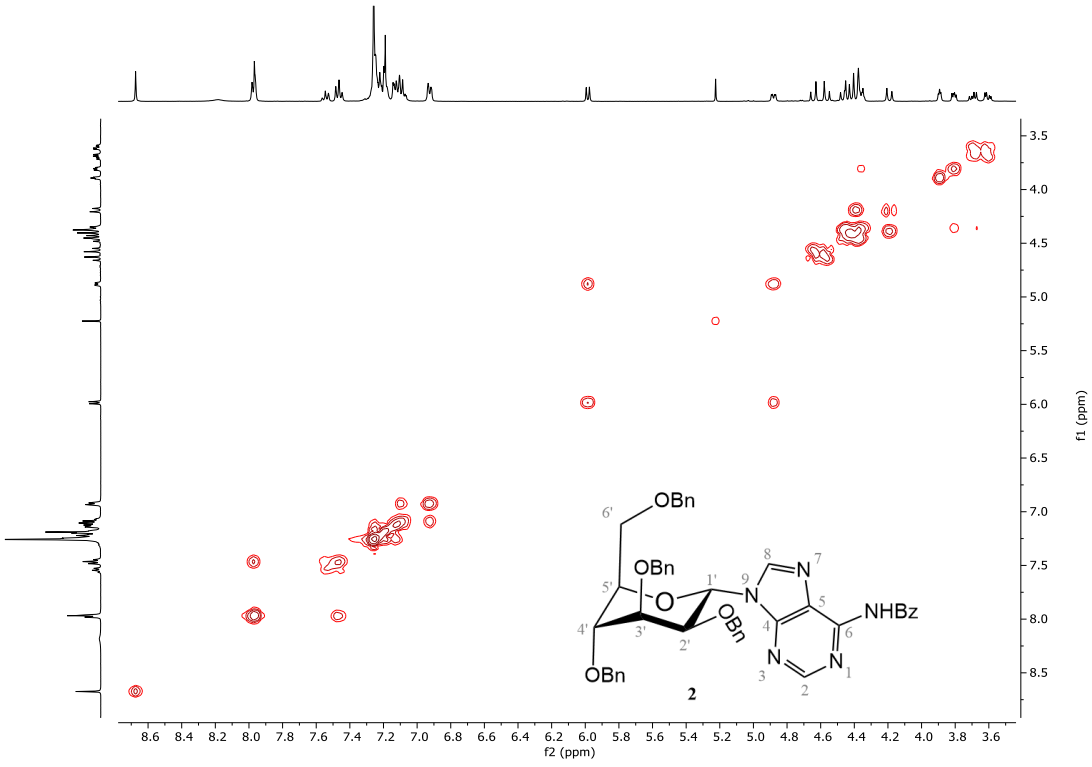

Figure 4.35. COSY spectrum for compound **2**

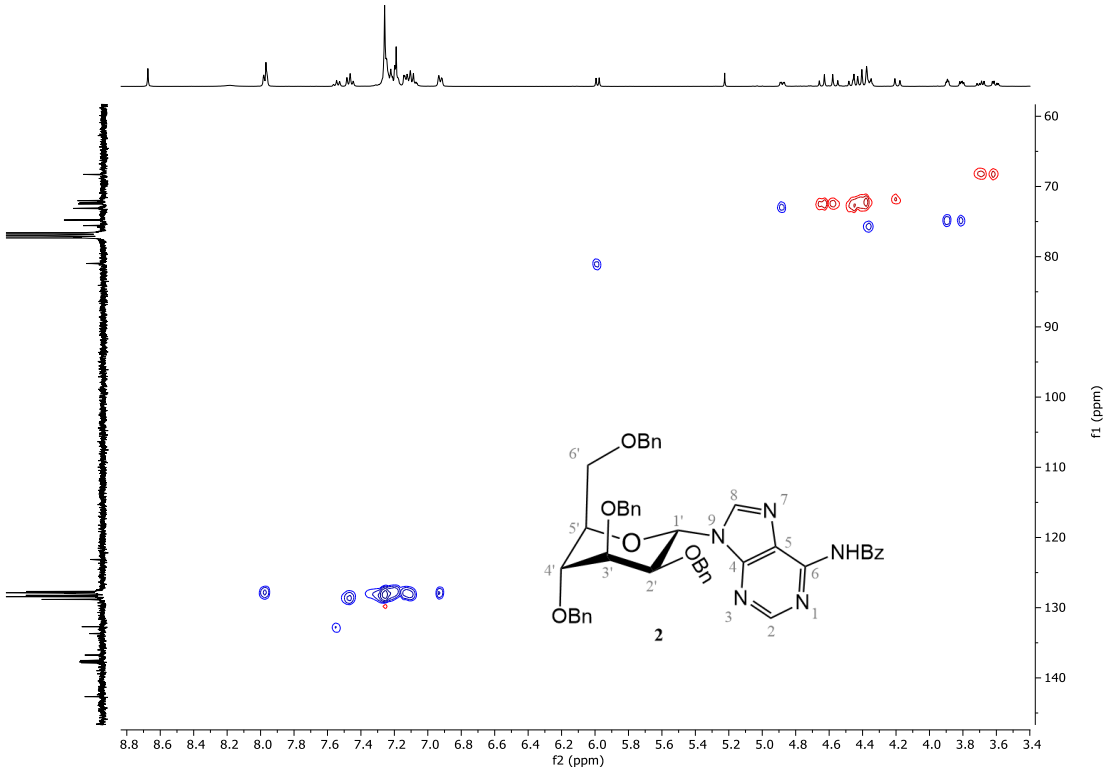

Figure 4.36. HSQC spectrum for compound **2**

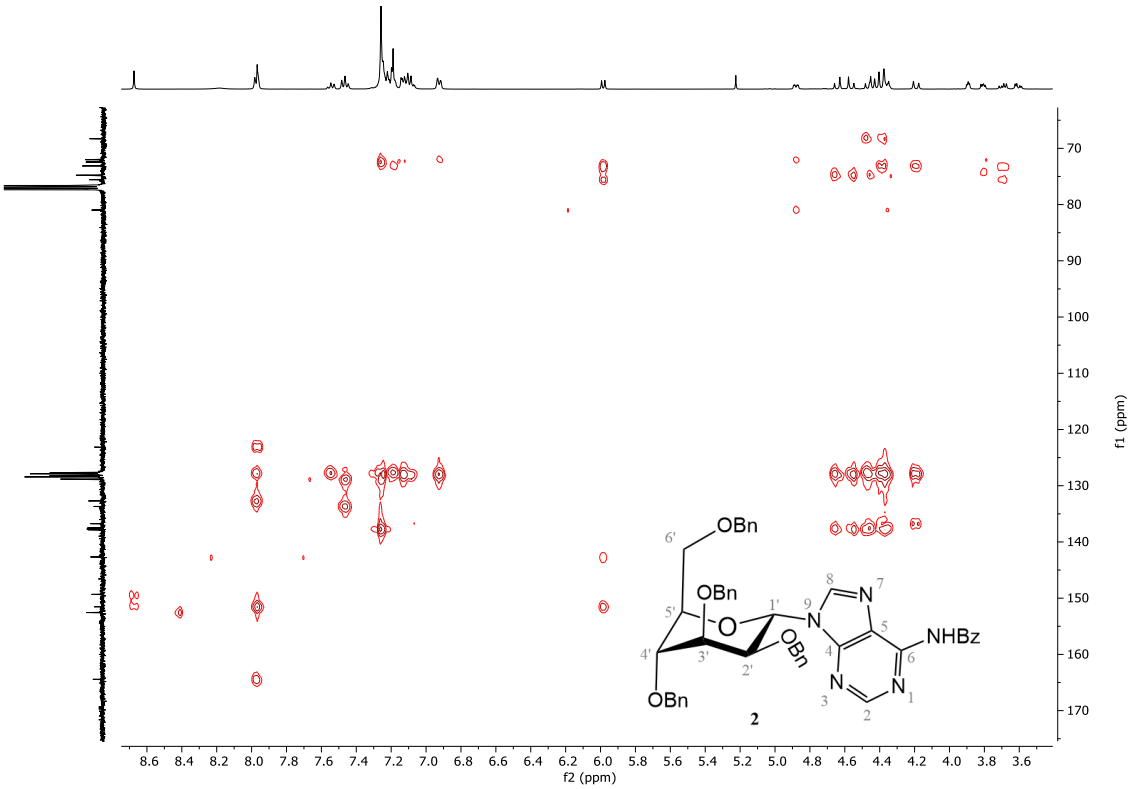

Figure 4.37. HMBC spectrum for compound **2**

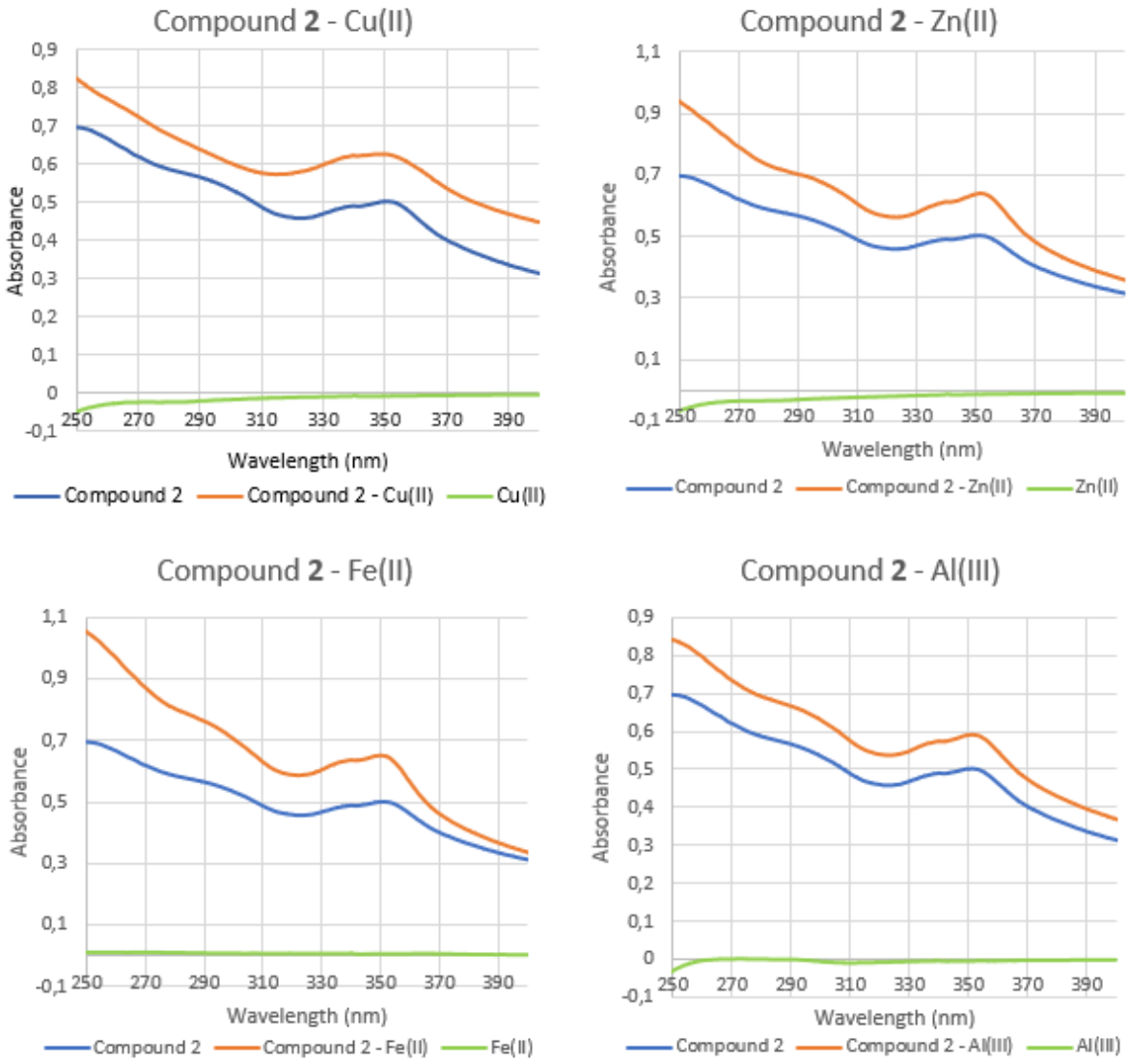

Figure 4.38. Interaction between compound **2** and metal ions

A.8 NMR and UV-Vis spectra for compound 21 [*N*-6-benzamido-9-(2,3,4,6-tetra-*O*-benzyl-β-D-mannopyranosyl)purine]

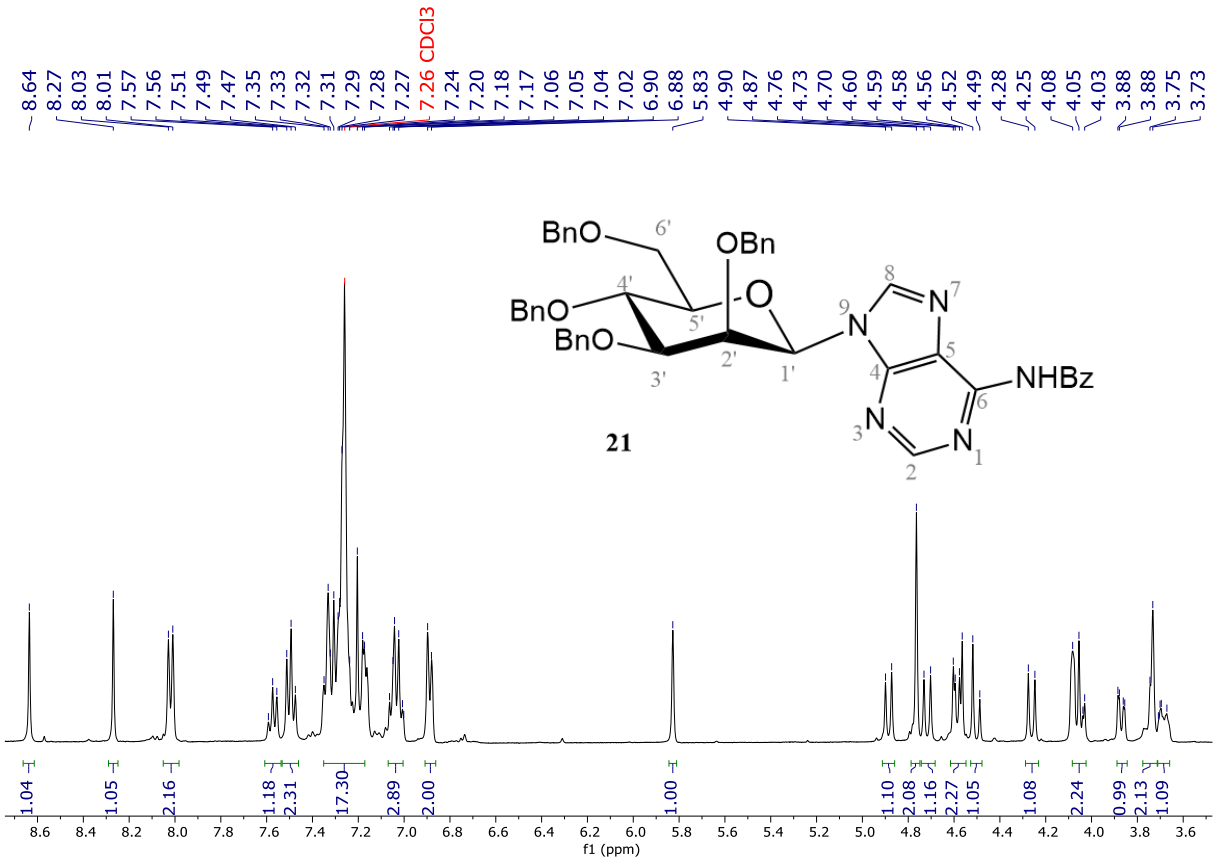

Figure 4.39. ^{1}H NMR spectrum for compound **21** (400 MHz, $CDCl_3$)

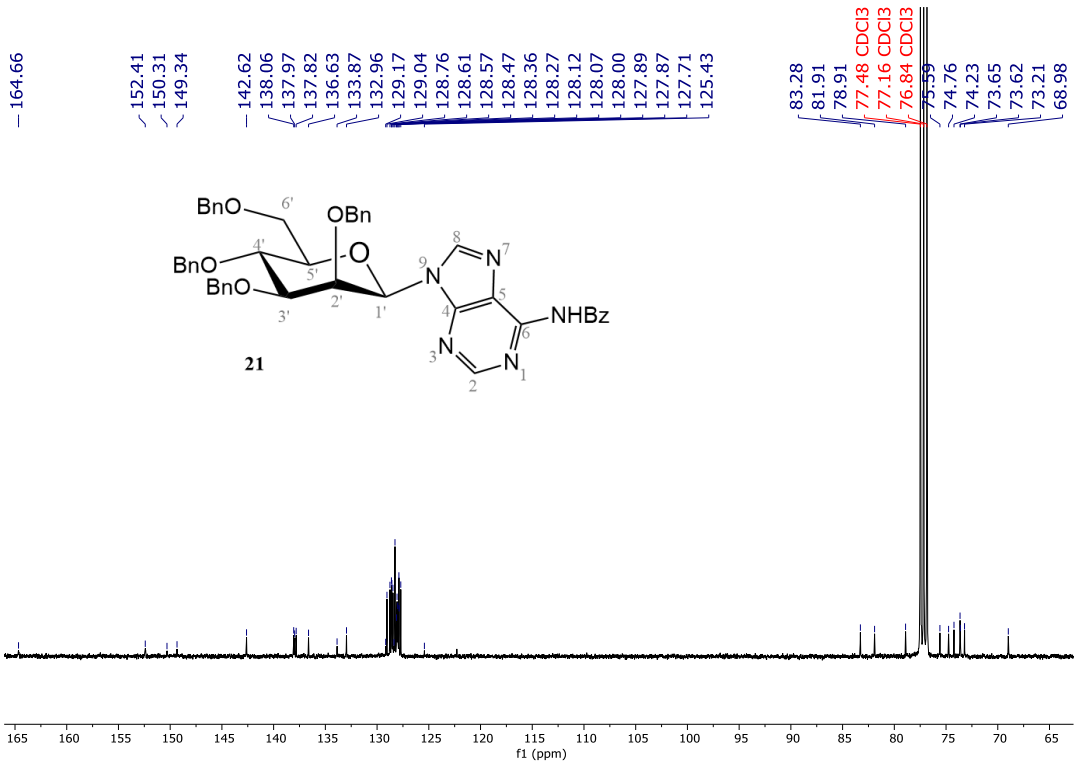

Figure 4.40. ^{13}C NMR spectrum for compound **21** (101 MHz, $CDCl_3$)

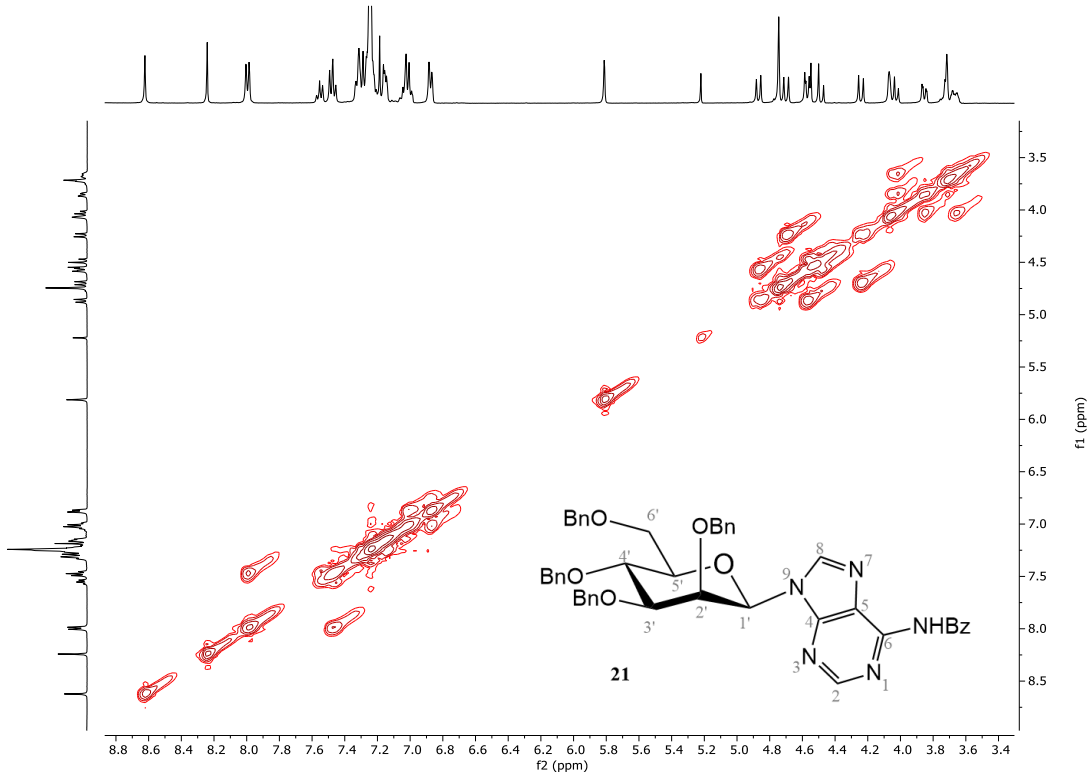

Figure 4.41. COSY spectrum for compound **21**

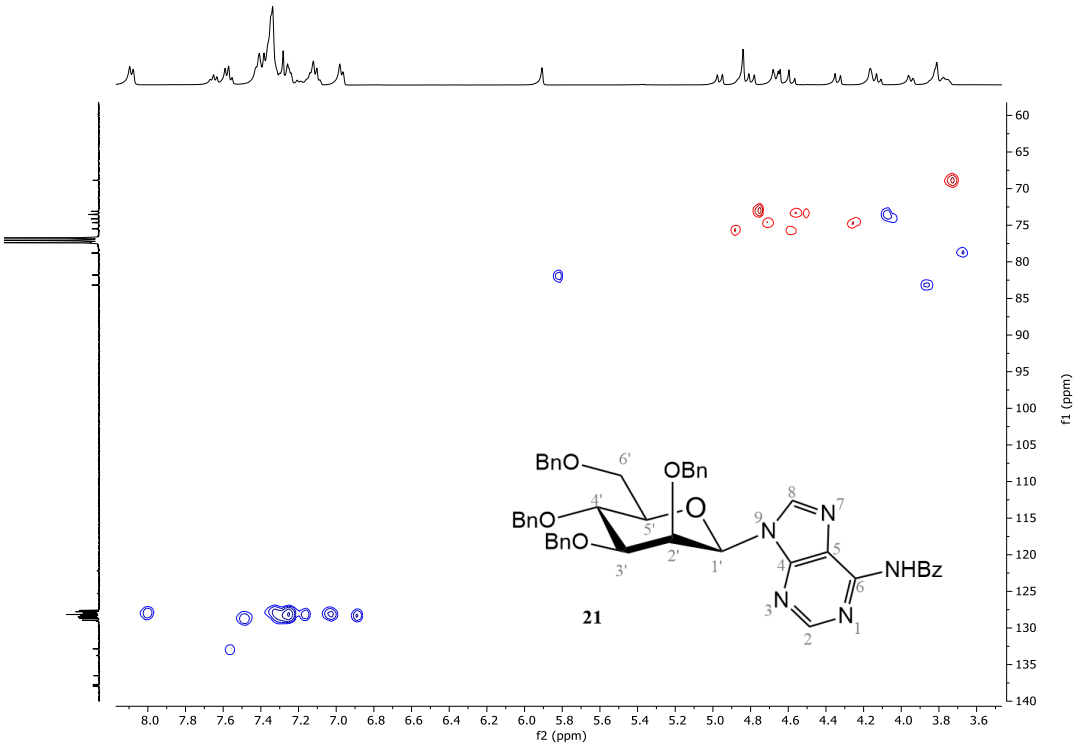

Figure 4.42. HSQC spectrum for compound **21**

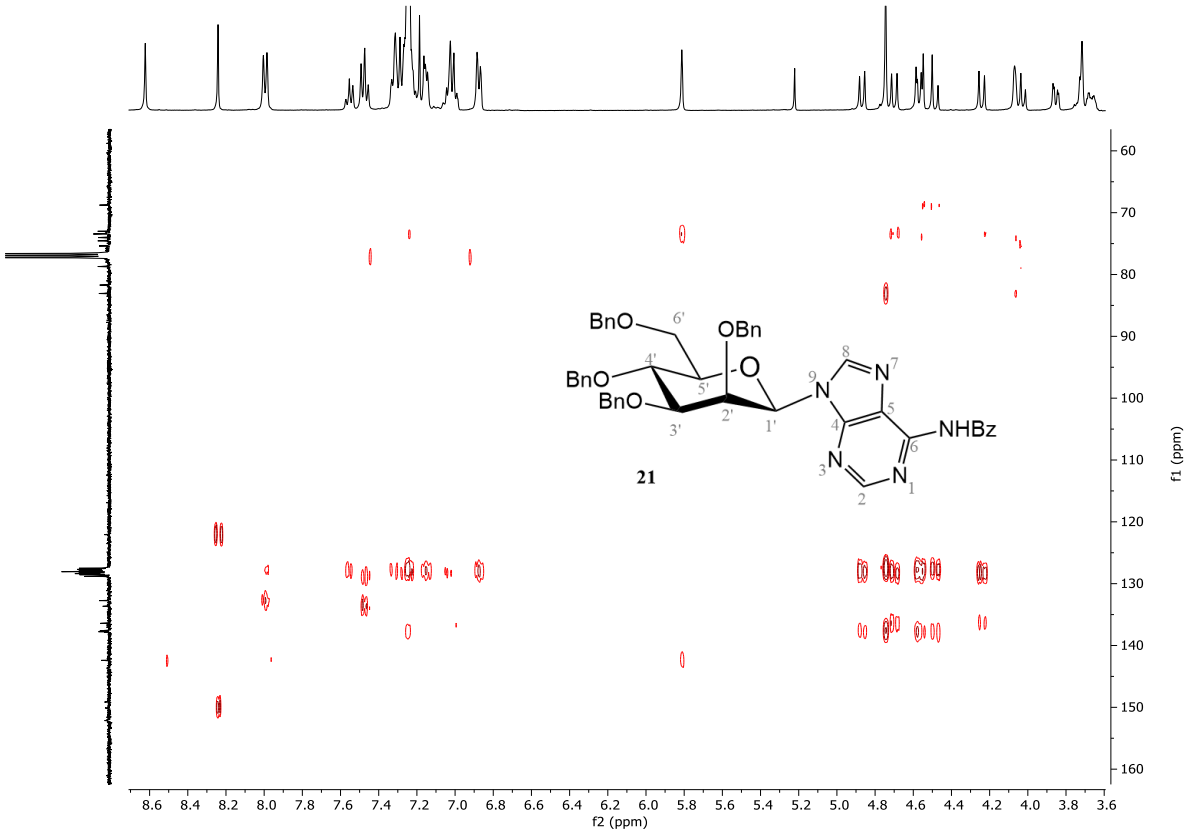

Figure 4.43. HMBC spectrum for compound **21**

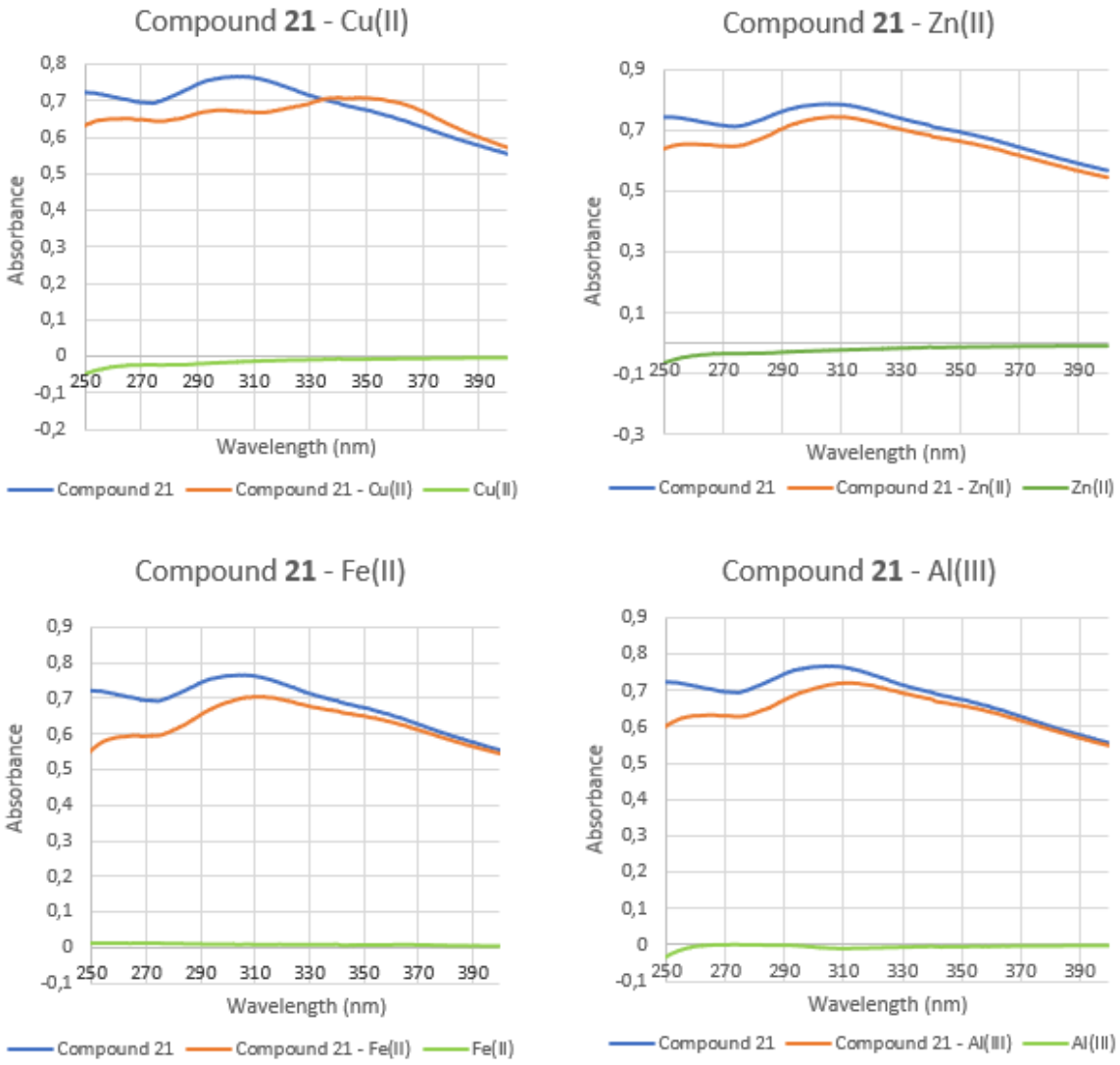

Figure 4.44. Interaction between compound **21** and metal ions

A.9 NMR spectra for the compounds 22 [*N*-6-benzamido-9-(2,3,4-tri-*O*-benzoyl-α-L-rhamnopyranosyl)purine] and 23 [*N*-6-benzamido-9-(2,3,4-tri-*O*-benzoyl-β-L-rhamnopyranosyl)purine] mixture

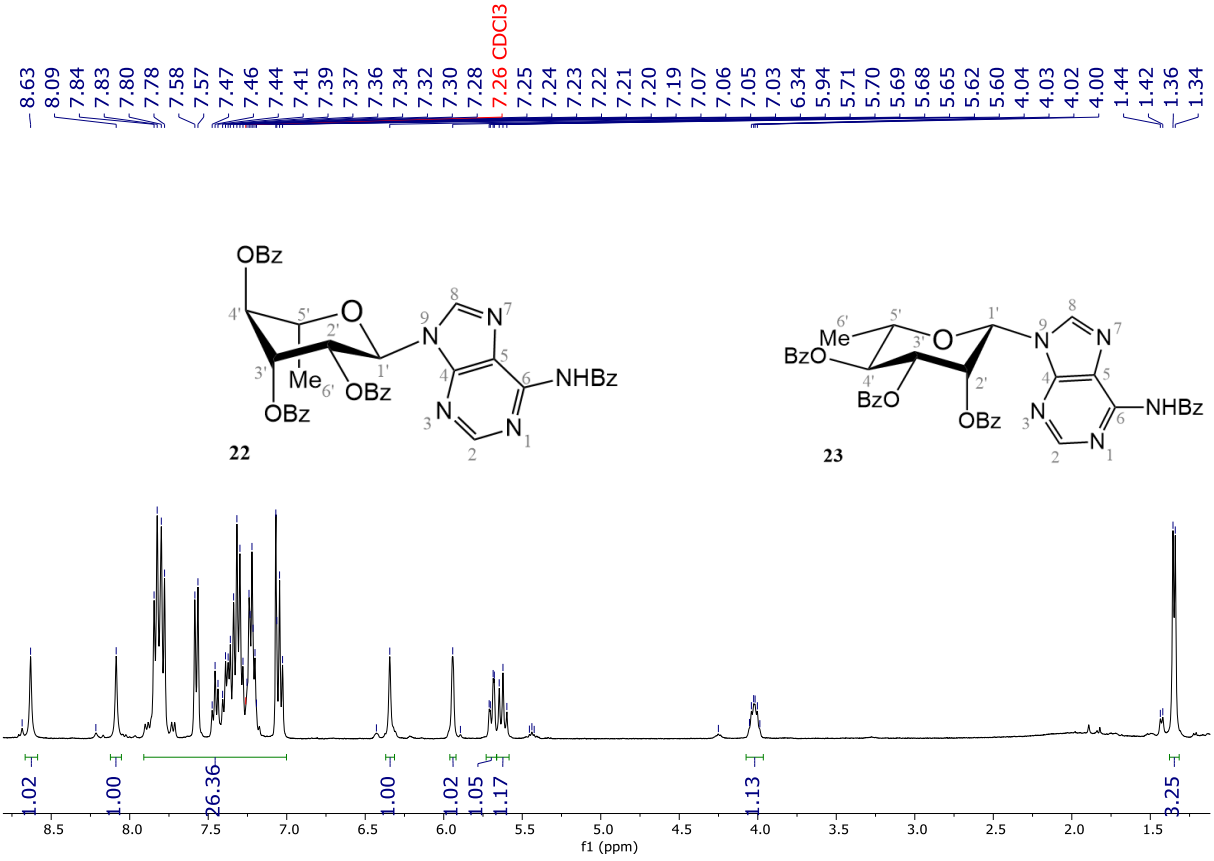

Figure 4.45. ^{1}H NMR spectrum for compounds **22** and **23** mixture (400 MHz, $CDCl_3$)

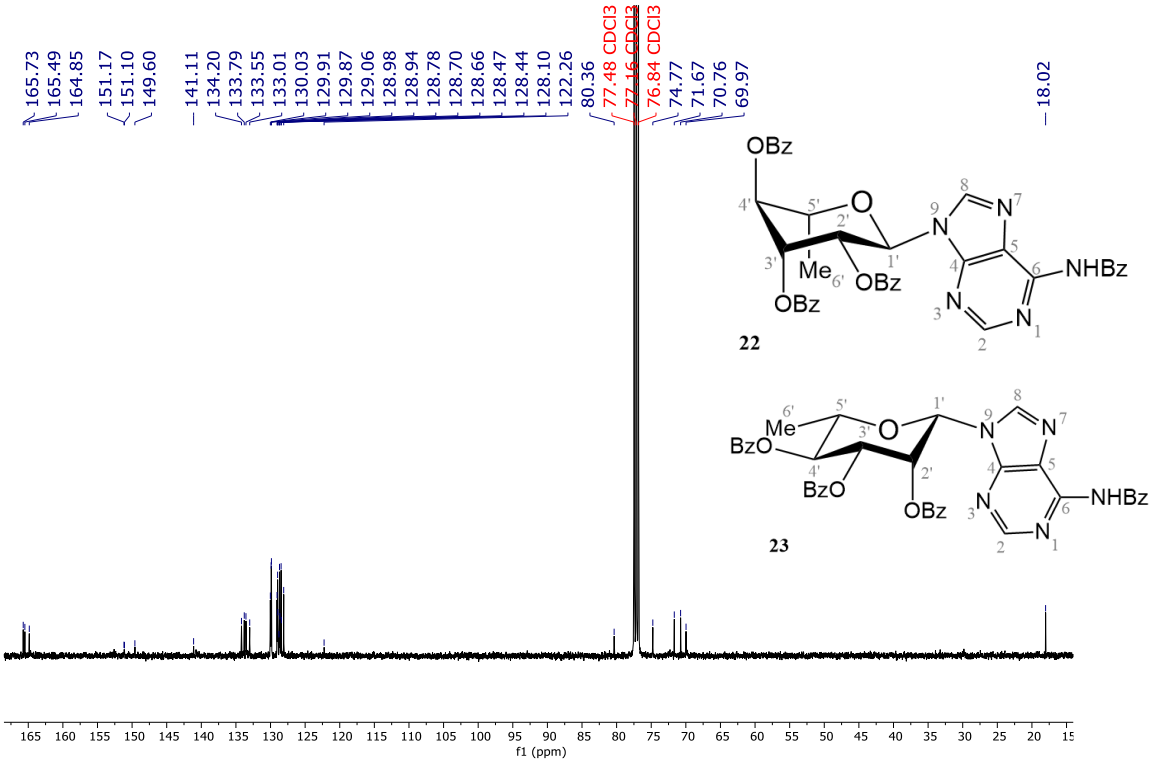

Figure 4.46. ^{1}H NMR spectrum for compounds **22** and **23** mixture (101 MHz, $CDCl_3$)

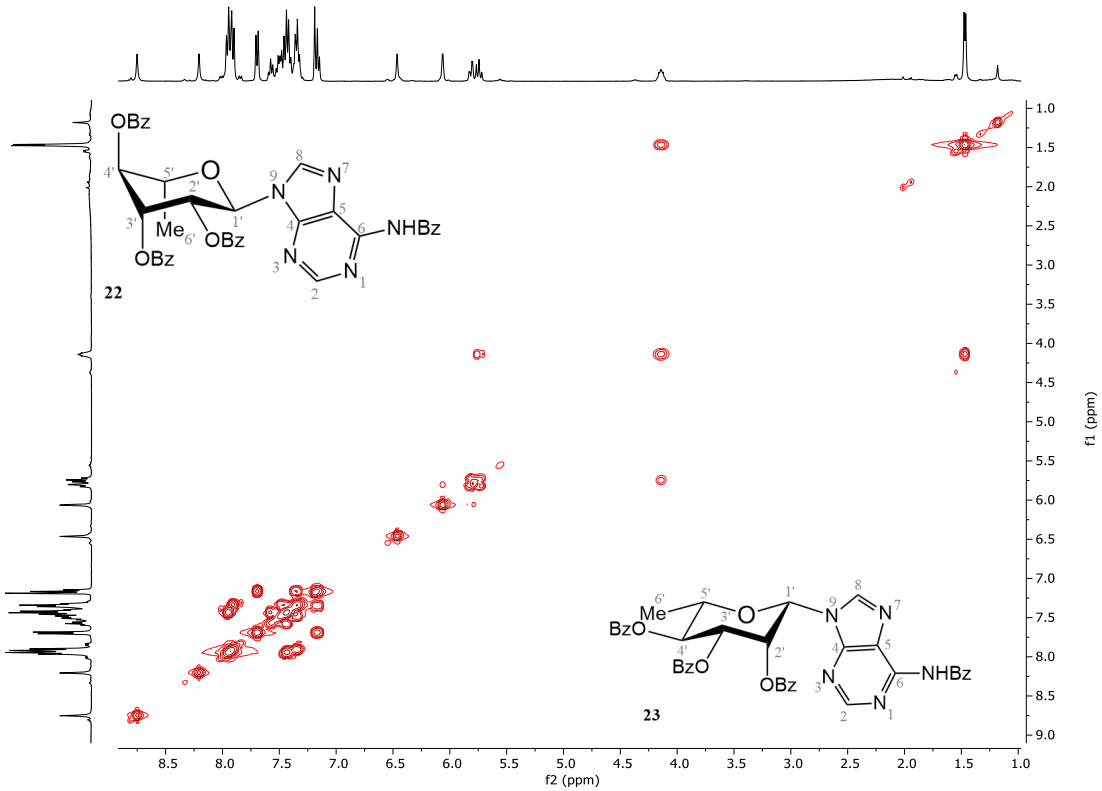

Figure 4.47. COSY spectrum for compounds **22** and **23** mixture

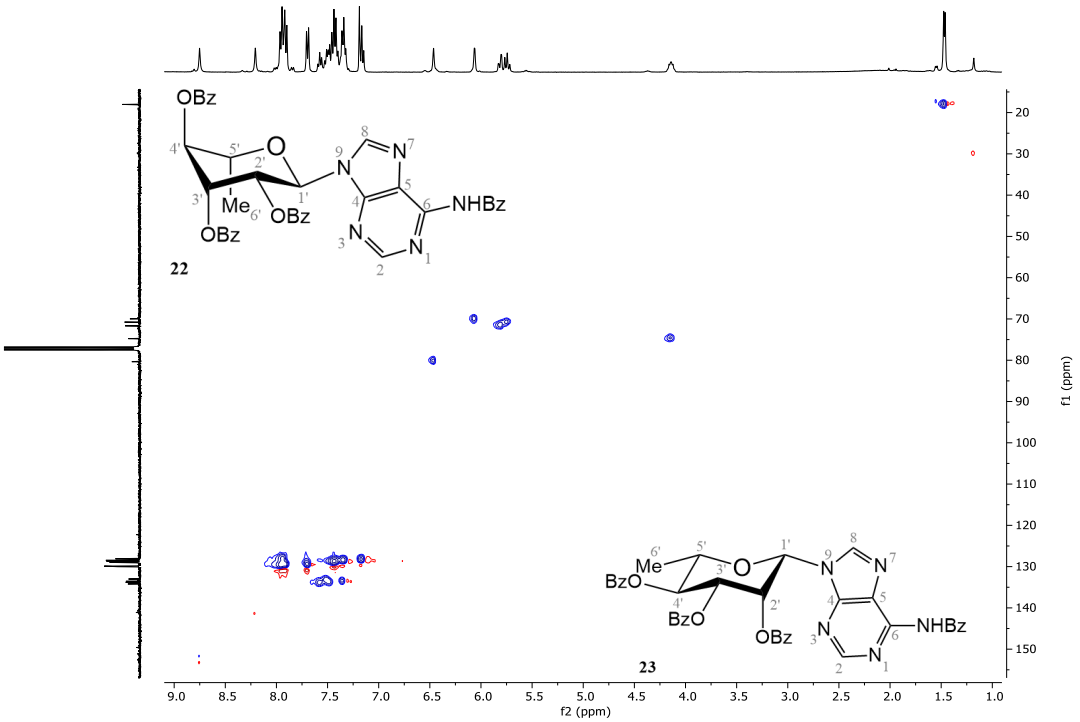

Figure 4.48. HSQC spectrum for compounds **22** and **23** mixture

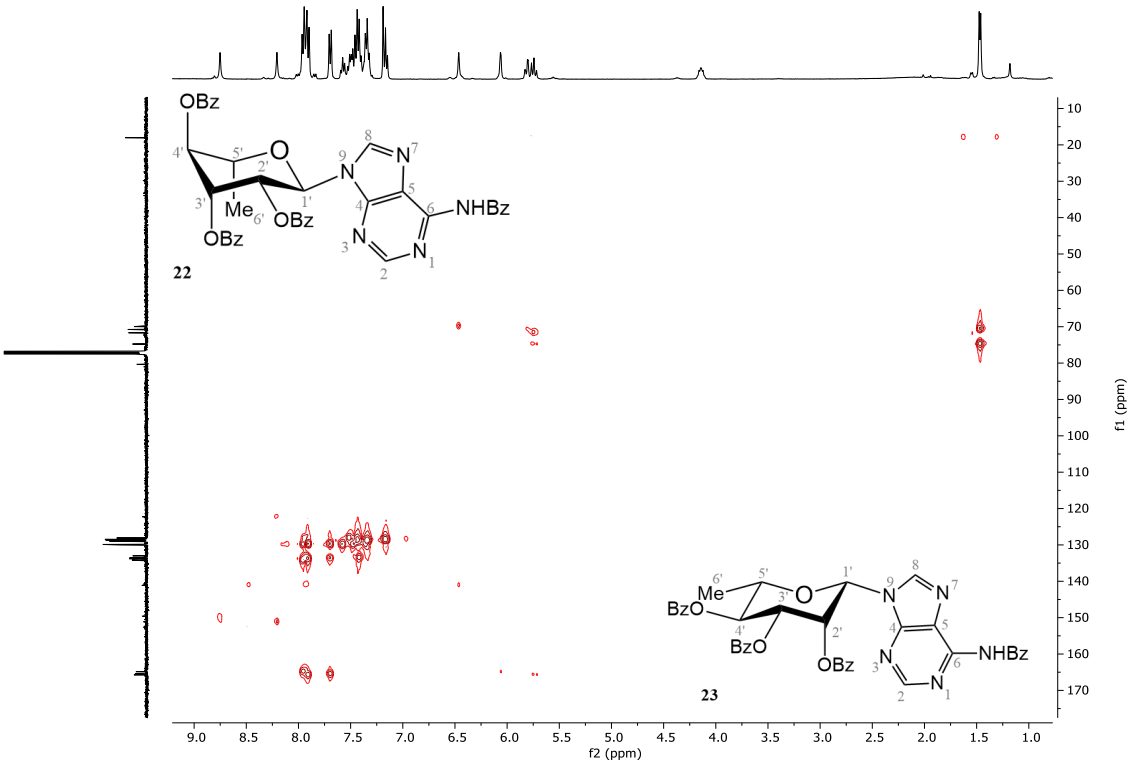

Figure 4.49. HMBC spectrum for compounds **22** and **23** mixture

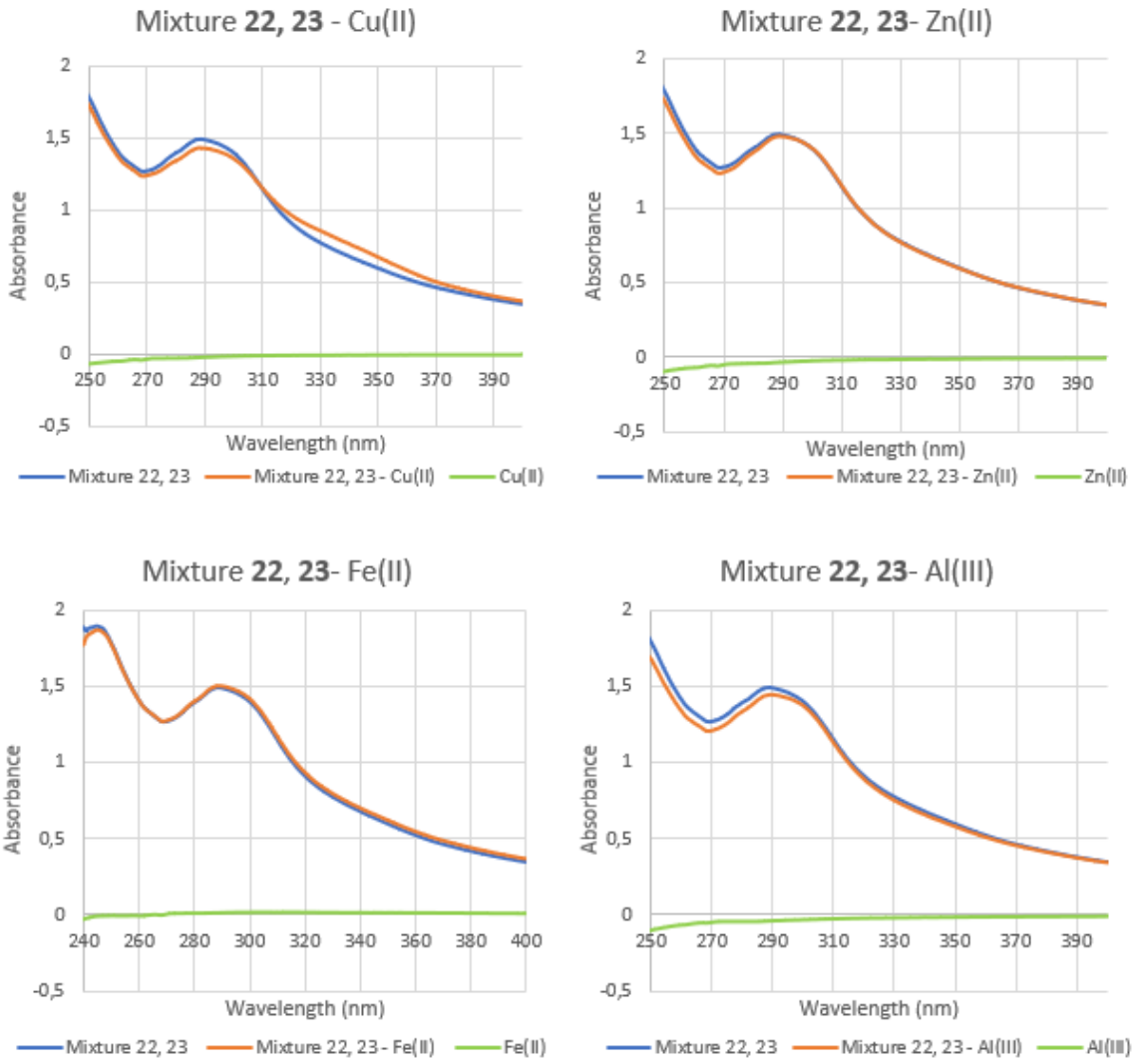

Figure 4.50. Interaction between mixture **22**, **23** and metal ions

A.10 NMR and UV-Vis spectra for compound 24 [2-acetamido-6-chloropurine-9-(2,3,4,6-tetra-*O*-benzyl-α-D-mannono-pyranosyl)purine]

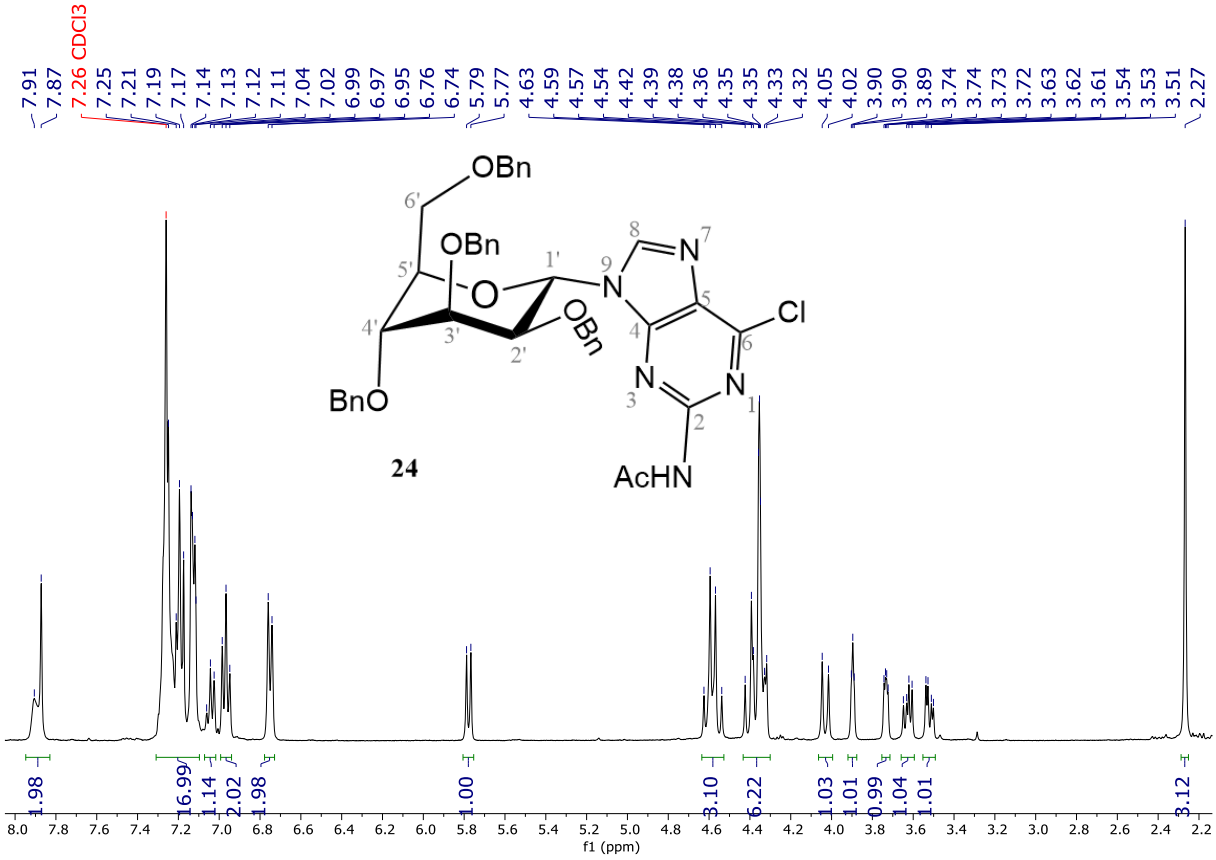

Figure 4.51. ^{1}H NMR spectrum for compound **24** (400 MHz, $CDCl_3$)

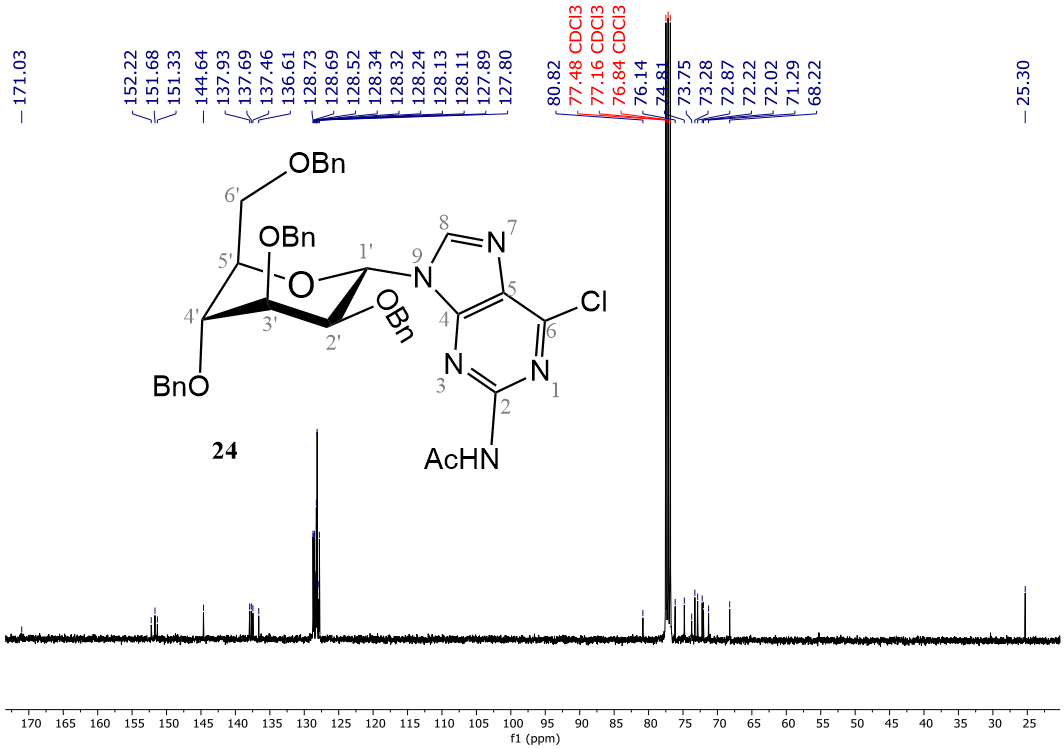

Figure 4.52. ^{13}C NMR spectrum for compound **24** ($CDCl_3$)

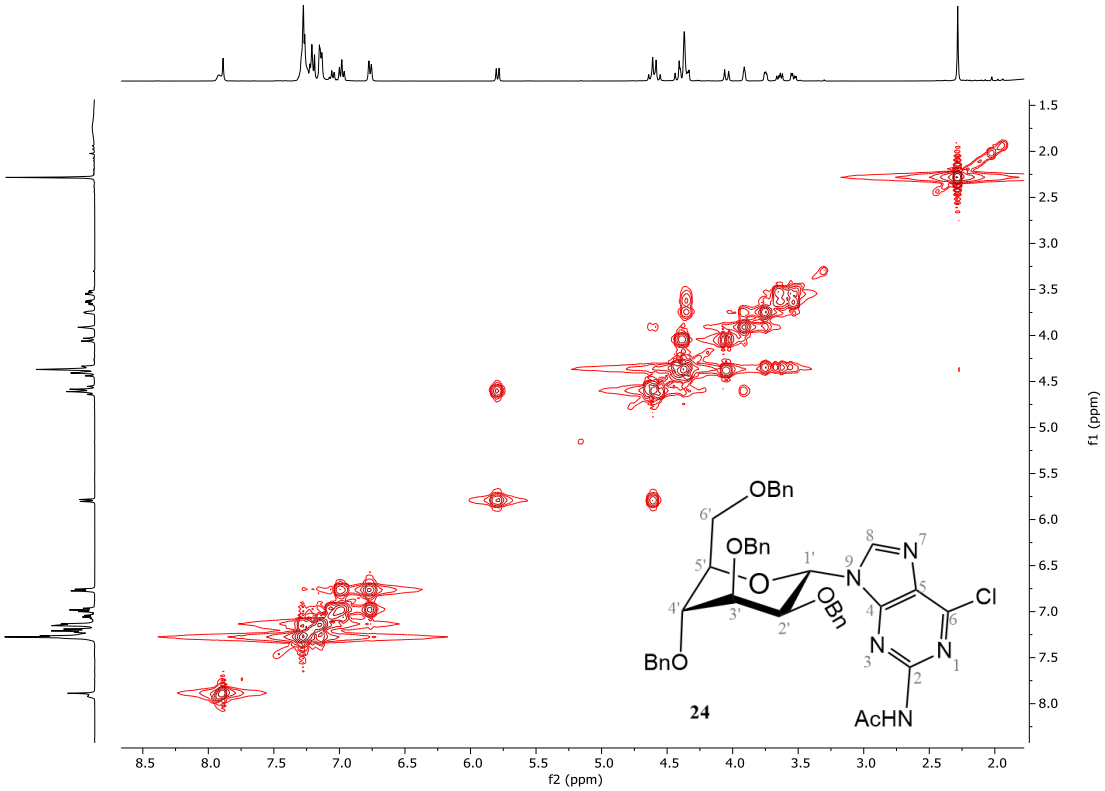

Figure 4.53. COSY spectrum for compound **24**

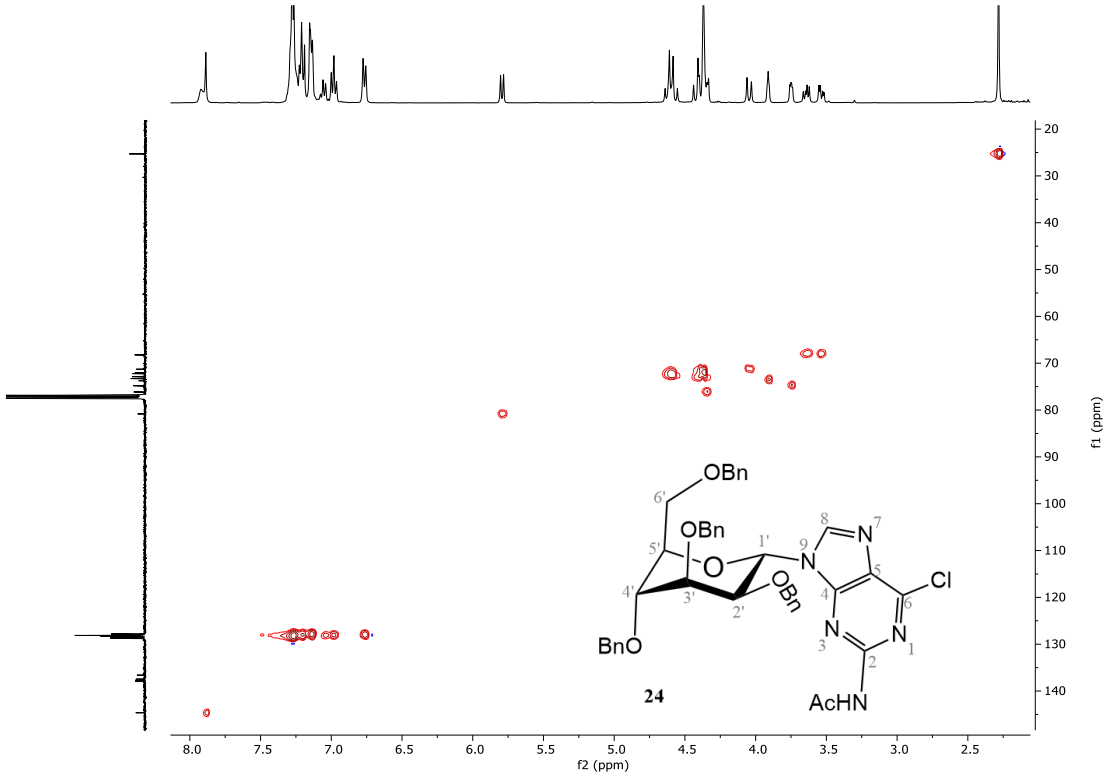

Figure 4.54. HSQC spectrum for compound **24**

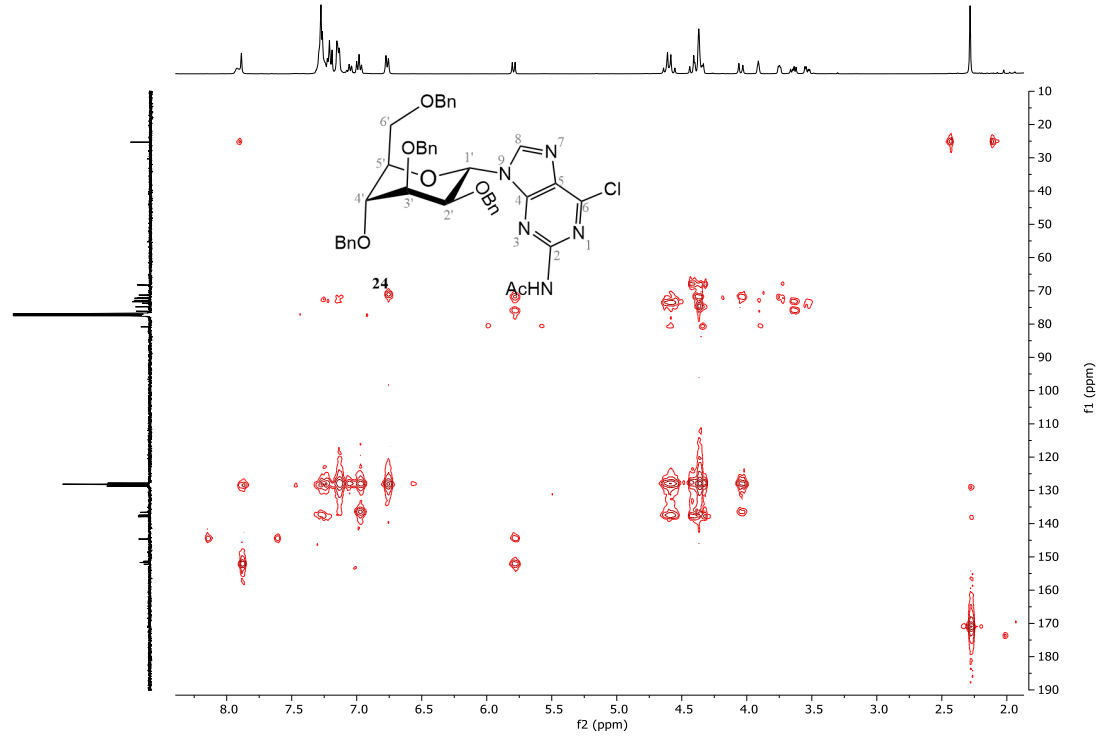

Figure 4.55. HMBC spectrum for compound **24**

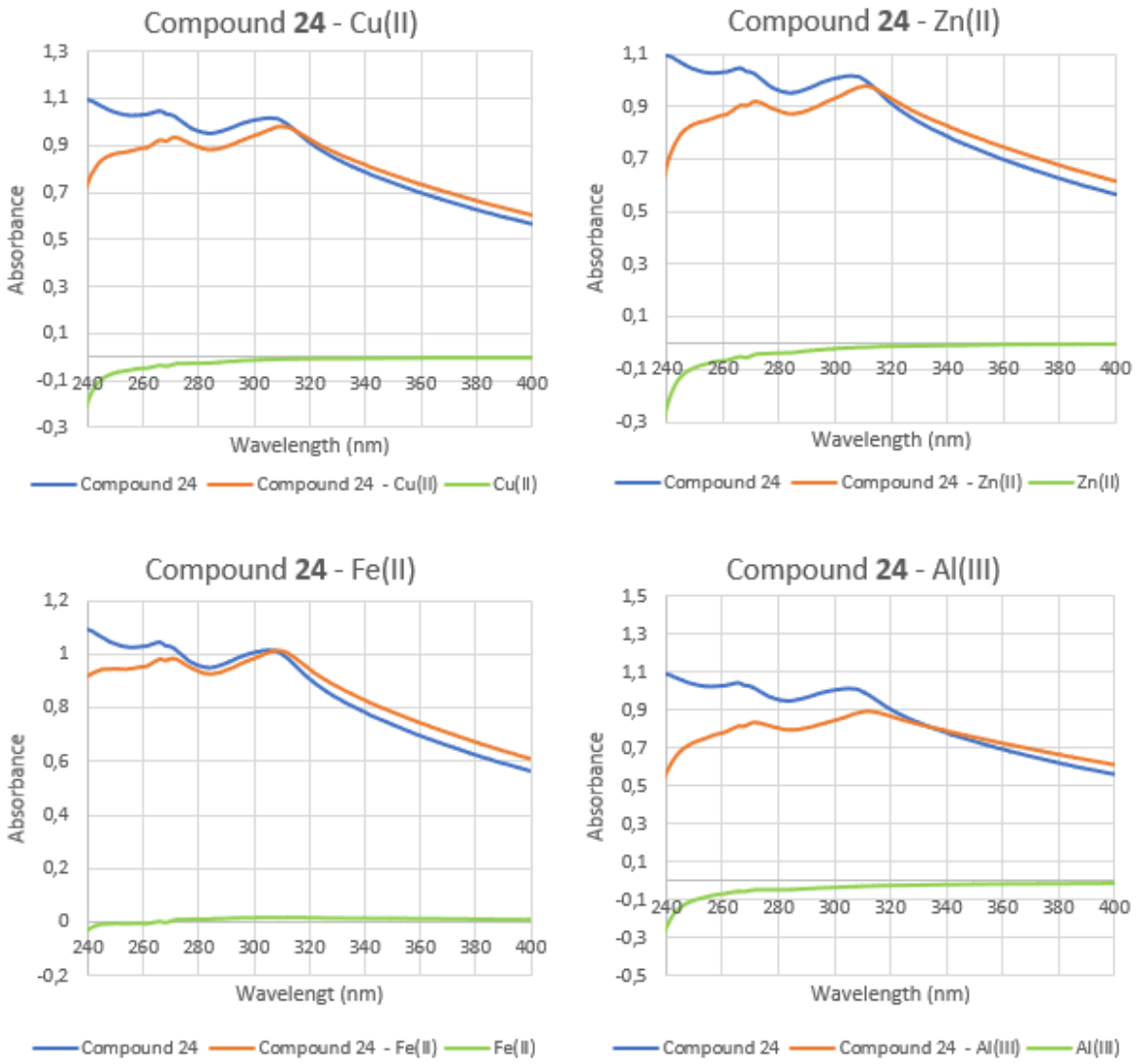

Figure 4.56. Interaction between compound **24** and metal ions

A.11 Structures of all synthesized compounds

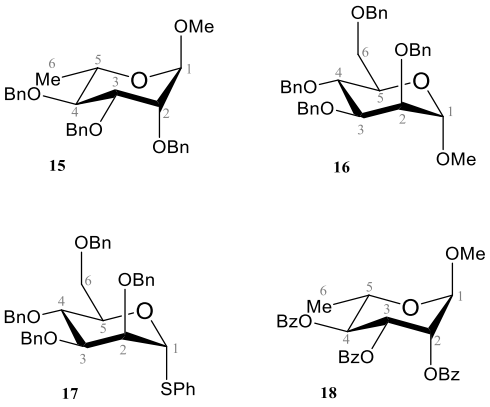

Figure 4.57. Structures of the synthesized intermediates

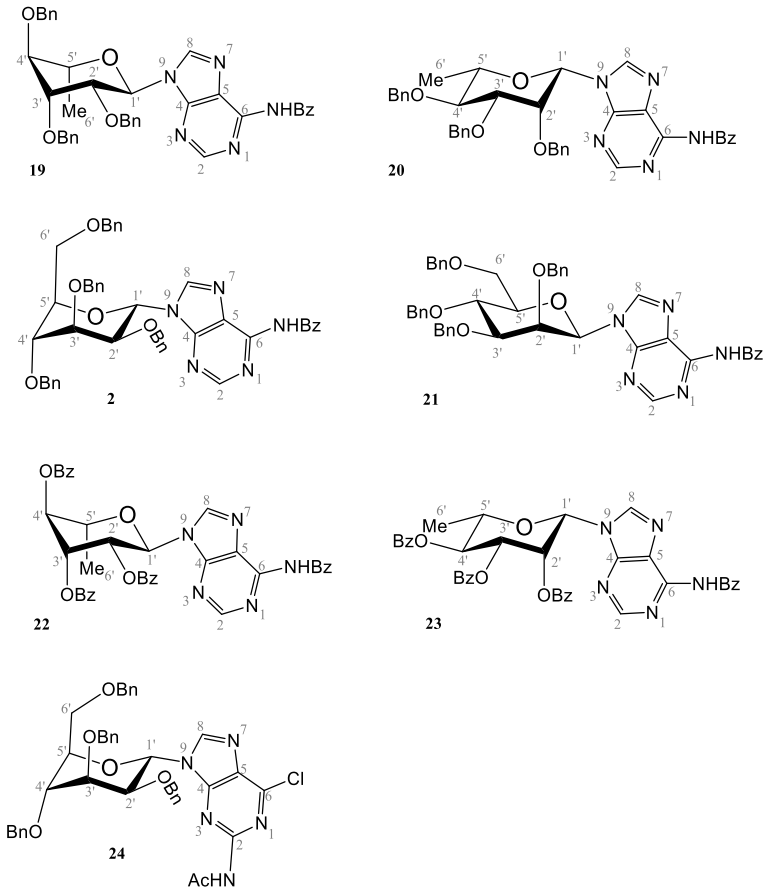

Figure 4.58. Strcutures of the synthesized nucleosides

2022 CATARINA MARIA

EXPLORING SYNTHETIC APPROACHES OF PURINE NUCLEOSIDES AS POTENTIAL COPPER CHELATORS AND CHOLINESTERASE INHIBITORS

NOVA SCHOOL OF SCIENCE & TECHNOLOGY